Defence Research and Development Canada
Recherche et développement pour la défense Canada

DEFENCE R&D DÉFENSE

Investigation of Gasless Detonation

Julian J. Lee
Defence R&D Canada – Suffield

Defence R&D Canada
Technical Report
DRDC Suffield TR 2012-142
December 2012

Canada

Investigation of Gasless Detonation

Julian J. Lee
Defence R&D Canada – Suffield

Defence R&D Canada – Suffield

Technical Report

DRDC Suffield TR 2012-142

December 2012

Principal Author

J.J. Lee

Approved by

C.J. Anderson
Head/MES

Approved for release by

R.G. Clewley
Head/Document Review Panel

Abstract

This report describes the body of work produced in the Technology Investment Fund (TIF) project titled "Gasless Detonation - A Novel System For Energy Release And Terminal Effects". The main objectives of the project were to establish the properties and explosive performance of a new mode of energy release known as gasless detonation. Theoretical and experimental studies were performed on gasless reactive mixtures to investigate shock-initiated reactions in these systems. Ultimately, gasless detonation was not achieved in this project, however several practical and scientific results were produced as a result of the increased understanding of gasless reactive systems. On the theoretical side, a rigorous assessment of the conditions for gasless detonation and an estimation of its explosive performance was performed. This assessment included the new use of Calculation of Phase Diagrams (CALPHAD) techniques for performing thermo-chemical calculations of detonation properties in low-gas reactive mixtures. On the experimental side, there were many outcomes. The Russian claims of gasless detonation were disproved through attempts to duplicate their experiments. The limits of shock-initiated combustion were found for many gasless reactive systems, as well as their dependence on mixture reactivity and morphology. Mechanisms of reactive wave propagation were elucidated, and a dual propagation mode was observed where a small portion of the mixture reacts rapidly within microseconds, followed by a slower bulk reaction where the remaining majority of the energy is released. A back-up hypothesis to achieve gasless detonation was also investigated. This effort involved developing methods to synthesize very dense gasless reactive mixtures by combining the Arrested-Milling (ARM) technique with Cold-Gas Dynamic Spray (CGDS) deposition. A new reactive nano-composite material mixed down to a nano-scale level was achieved with nearly 100% Theoretical Maximum Density. This synthesis method was developed for a number of reactive mixtures, and accelerated flame speeds were observed for the new materials. This approach yielded promising results and constitutes a future research direction in the advanced energetics program.

Résumé

Le présent rapport décrit le travail effectué dans le cadre du projet du Fonds d'investissement technologique (FIT) intitulé « Gasless Detonation - A Novel System For Energy Release And Terminal Effects ». Les principaux objectifs de ce projet étaient d'établir les propriétés et le rendement explosif d'un nouveau mode de libération d'énergie appelé « détonation sans dégagement de gaz ». Des études théoriques et expérimentales ont été effectuées sur des mélanges réactifs sans gaz, afin d'étudier les réactions produites par des chocs dans ces systèmes. Finalement, aucune détonation sans dégagement de gaz n'a été produite dans le cadre du projet, mais un certain nombre de résultats pratiques et scientifiques ont été obtenus grâce à la compréhension accrue des systèmes réactifs sans gaz. Sur le plan théorique, une évaluation rigoureuse des conditions pour une détonation sans dégagement de gaz et une estimation de son rendement explosif a été effectuée. Cette évaluation comprenait la nouvelle utilisation de techniques de calcul de diagrammes de phase (CALPHAD) pour effectuer des calculs thermochimiques des propriétés de détonation dans des mélanges réactifs à faible taux de gaz. Sur le plan expérimental, il y a eu un de nombreux résultats. Les allégations russes de réussite de détonations sans dégagement de gaz ont été réfutées au moyen de tentatives de reproduction des expériences russes. Les limites de combustion produite par des chocs ont été découvertes pour un certain nombre de systèmes réactifs sans gaz, ainsi que leur dépendance à la réactivité et à la morphologie du mélange. Des mécanismes de propagation d'ondes réactives ont été élucidés, et un mode de double propagation a été observé. Dans ce mode, une petite partie du mélange réagit rapidement en quelques microsecondes, ce qui est suivi par une réaction en masse plus lente où la majorité restante de l'énergie est libérée. Une autre hypothèse a également été étudiée relativement à l'obtention d'une détonation sans dégagement de gaz. Cet effort comprenait la mise au point de méthodes visant à synthétiser des mélanges réactifs sans gaz très denses en combinant le procédé ARM (de l'anglais « Arrested-Milling ») avec un dépôt par pulvérisation dynamique à froid en phase gazeuse (CGDS). Une nouvelle matière nanocomposite réactive mélangée jusqu'à une échelle nanométrique a été obtenue avec une densité théorique maximale de près de 100 %. Cette méthode de synthèse a été mise au point pour un certain nombre de mélanges réactifs, et des vitesses de flamme accélérées ont été observées pour les nouvelles matières. Cette approche a produit des résultats prometteurs et constitue une orientation future des recherches dans le cadre du programme de matières énergétiques avancées.

Executive summary

Investigation of Gasless Detonation

Julian J. Lee; DRDC Suffield TR 2012-142 Defence R&D Canada – Suffield;
December 2012

Background: The original motivation of this Technology Investment Fund (TIF) project was to investigate a new mode of energy release called gasless detonation. High explosives generate a high-pressure gaseous fireball that causes extensive damage and injury to the nearby surroundings due to the powerful blast wave. At much further distances, the blast wave is still strong enough to cause injury to personnel. Gasless detonation is a reported but unconfirmed explosive phenomenon that does not produce a gaseous fireball. Instead, significant amounts of energy is released, but the combustion takes place exclusively in a solid or liquid state. As a result, only a negligible blast wave is produced. It is hypothesized that a gasless detonation could be used for a focused-energy device that causes very localized damage without the risk of collateral damage from a blast wave.

Principal results: Theoretically, a new method of calculating detonation performance was developed. A method of calculating the thermodynamic states of solids and liquids known as Calculation of Phase Diagrams (CALPHAD) was combined with Chapman-Jouguet detonation theory to assess whether gasless detonation is possible in a given reactive mixture, and estimate its explosive performance.

Experimentally, careful reproduction of the Russian experiments first claiming gasless detonation showed these results to be likely a mis-interpretation of statistical scatter of separate shock velocity measurements due to small variations in the initial conditions of the reactive mixtures.

The mechanisms of shock-initiated reaction in several gasless reactive mixtures was investigated. While microsecond reactions were observed in a small fraction of the material, most of it was found to react at much slower flame speeds, consistent with diffusion-driven combustion. This small level of reaction was found to be insufficient to support gasless detonation.

Finally, attempts to increase the burning rate led to the discovery of a novel method of producing densely-packed reactive metals mixed at a nanometer scale. This technique involves a two-step process of Arrested Ball-Milling and Cold-gas Spray Deposition. In preliminary experiments, this approach was found to produce a finely-mixed microstructure for inter-metallic and thermite mixtures, and an increase in the reaction rate by a factor of nearly six.

Significance of results: Although gasless detonation was not achieved in this project, several significant advances have been made to elucidate a phenomenon that has periodically piqued interest over the last fifty years. Past claims of gasless detonation were refuted in

this project. A theoretical approach for predicting detonation properties in gasless reactive mixtures has been developed, and may be useful for other energetic materials that contain large proportions of solid or liquid products such as metallized explosives. A deeper understanding of the mechanisms of shock-induced reaction has been achieved. Finally, novel techniques of pre-mixing reactive metals down to a nanometer-scale in a densely-packed configuration have been developed, leading to a new type of reactive material.

Future work: The optimization of dense reactive nano-composite materials presents a promising avenue of research with many possible applications, from very localized and controlled pressure wave generation to novel energy production. Further developing the techniques of Arrested-Milling and Cold-gas Spray Deposition would further improve methods of generating a new class of reactive materials. Combined with accurate solid-state reaction calculations using CALPHAD methods for screening of systems to find those with the desired properties, the stage is set for a fertile area of research and technology.

Sommaire

Investigation of Gasless Detonation

Julian J. Lee ; DRDC Suffield TR 2012-142 ; R & D pour la défense Canada – Suffield ; décembre 2012.

Contexte : Le motif initial de ce projet du FIT était d'étudier un nouveau mode de libération d'énergie appelé « détonation sans dégagement de gaz ». Les explosifs détonants produisent une boule de feu gazeuse à haute pression qui cause des dommages importants à proximité et des blessures aux personnes à proximité en raison de la puissante onde de souffle créée. À de bien plus grandes distances, l'onde de souffle est tout de même assez puissante pour causer des blessures au personnel. Les détonations sans dégagement de gaz sont un phénomène explosif observé, mais non confirmé, qui ne produit pas de boule de feu gazeuse. Il libère plutôt de grandes quantités d'énergie, mais la combustion se produit exclusivement à l'état solide ou liquide. Par conséquent, seul un souffle négligeable est produit. Selon certaines hypothèses, une détonation sans dégagement de gaz pourrait être utilisée pour un dispositif à concentration d'énergie qui cause des dommages très localisés sans les risques de dommages collatéraux d'une onde de souffle.

Principaux résultats : Théoriquement, une nouvelle méthode de calcul du rendement de détonation a été mise au point. Une méthode de calcul de l'état thermodynamique des solides et des liquides appelée « calcul de diagrammes de phase » (CALPHAD) a été combinée à la théorie de détonation Chapman-Jouguet, afin de déterminer si une détonation sans dégagement de gaz est possible dans un mélange réactif donné, et afin d'en estimer le rendement explosif. Sur le plan expérimental, les expériences russes qui ont entraîné les premières allégations de possibilité de détonations sans dégagement de gaz ont été reproduites avec soin. Les expériences reproduites ont démontré que les résultats des expériences russes étaient probablement une interprétation erronée de la dispersion statistique des mesures distinctes de vitesse des chocs, en raison des faibles variations des conditions initiales des mélanges réactifs. Les mécanismes de réactions produites par des chocs dans un certain nombre de mélanges réactifs sans gaz ont été étudiés. Même si des réactions de seulement quelques microsecondes ont été observées dans une petite partie de la matière, la majorité a réagi à des vitesses de flammes beaucoup plus faibles, ce qui concorde avec la combustion par diffusion. Ce faible niveau de réaction est insuffisant pour permettre une détonation sans dégagement de gaz. Finalement, les tentatives d'augmenter le taux de combustion ont entraîné la découverte d'une nouvelle méthode de production de métaux réactifs à densité élevée mélangés à une échelle nanométrique. Cette technique consiste en deux étapes : un procédé ARM et un dépôt par pulvérisation dynamique à froid en phase gazeuse. Lors des expériences préliminaires, cette approche a produit une microstructure à mélange fin pour des mélanges intermétalliques et des mélanges de thermite, ainsi qu'une augmentation du taux de réaction par un facteur de presque six.

Importance des résultats : Même si aucune détonation sans dégagement de gaz n'a été produite dans le cadre du projet, un certain nombre de progrès importants ont été réalisés afin d'élucider un phénomène qui a périodiquement suscité l'intérêt au cours des 50 dernières années. Les allégations antérieures de détonations sans dégagement de gaz ont été réfutées dans le cadre du projet. Une approche théorique pour la prédiction des propriétés de détonation dans des mélanges réactifs sans gaz a été mise au point, et elle pourrait être utile pour d'autres matières énergétiques qui contiennent des proportions importantes de produits solides ou liquides, comme les explosifs métallisés. Une compréhension plus approfondie des mécanismes de réactions produites par des chocs a été obtenue. Finalement, des nouvelles techniques de pré-mélange de métaux réactifs jusqu'à une échelle nanométrique dans une configuration à densité élevée ont été mises au point, ce qui a créé un nouveau type de matière réactive.

Travaux futurs : L'optimisation de matières nanocomposites réactives denses présente un axe de recherche prometteur avec de nombreuses applications possibles, allant de la production d'une onde de pression très localisée et contrôlée à une nouvelle production d'énergie. L'amélioration du procédé ARM et de la technique de dépôt par pulvérisation dynamique à froid en phase gazeuse améliorerait les méthodes de création d'une nouvelle classe de matières réactives. Avec des calculs exacts de réactions à l'état solide à l'aide des méthodes de calcul de diagrammes de phase (CALPHAD) permettant d'évaluer des systèmes afin de déterminer lesquels présentent les propriétés souhaitées, tout est en place pour un environnement fertile de recherche et de technologie.

Table of contents

List of figures

This page intentionally left blank.

1 Introduction

The present TIF research project focussed on two essential properties of gasless detonation: the absence of gases during the energetic reaction, and the mechanisms of shock-driven chemical reaction in condensed phases. The first property requires that the components of the energetic mixture remain in a solid or liquid phase throughout the entire reaction, i.e. the starting reactants release energy in the form of heat, pressure, or kinetic energy while forming only solid or liquid combustion products. In the absence of gaseous products, the chemical energy is released essentially without the formation of a blast wave in the surrounding air, resulting in a stealthy or very localized explosion. The second property requires the process be a detonation, and therefore consisting of a supersonic reactive wave comprising a steady-state shock closely coupled to a driving reaction zone. Detonation is often considered the most powerful mode of chemical reaction as it produces shock waves that can result in high pressures and impulses conducive to strong terminal effects. Because the chemical energy must be rapidly released behind the shock in a detonation, the focus of the research was on rapid reaction mechanisms on a microsecond time-scale. The primary hypothesis was that gasless reactions could occur in powder mixtures through 'shock-induced' [1] inter-particle interactions. Although the exact nature of these reactions is unclear, but they have been called 'ultrafast', 'super diffusion', or 'ballotechnic' reactions [2, 3, 4] and are presumably related to high plastic deformation and shear. The secondary hypothesis considered in this project was that gasless reactions occur through conventional mass and heat diffusion, but that the process could be greatly accelerated through nano-scale mixing of the reactants. The theoretical and experimental efforts investigated in this research project were conceived to confirm the existence of gasless detonations, determine the energy partition (and potential applications), and finally, identify and understand the underlying mechanisms.

The theoretical studies started with a fundamental look at the equilibrium thermodynamics of detonations in condensed phase. To accomplish this, theoretical calculations of the Hugoniot, Chapman-Jouguet (CJ), and isentrope properties of gasless systems were first performed for select systems using the CERV code developed in Canada by the University of Toronto Institute for Aerospace Studies (UTIAS)[5]. This code is capable of thermochemical equilibrium calculations when no gases are present at equilibrium. However, to accurately calculate detonation properties, an equilibrium code must include liquid and solid compressibility through appropriate equations of state. Efforts to implement this capability in CERV were ultimately unsuccessful, and another code called FACTSAGE [6, 7] was chosen to perform the equilibrium calculations. This code uses Calculation of Phase Diagram (CALPHAD)[8] techniques designed specifically for calculation of equilibrium phases of condensed states, particularly for metals, and is well suited to the reactive systems of interest for gasless detonation. FACTSAGE was enhanced by implementing new models to allow calculations at the high pressures and temperatures relevant for detonation, and was used to predict gasless detonation properties for a number of inter-metallic and thermite mixtures. Preliminary performance calculations were also performed using Hugoniot analysis and impedance matching to estimate shock transmission from gasless reactive mixtures into target materials such as steel, aluminum, and tungsten.

The experimental studies started with a verification of the Russian experiments claiming observation of gasless detonation. In conjunction with this effort, several studies were conducted on the shock-induced chemical reaction in gasless mixtures. In an effort to screen various reactive mixtures for their suitability to support gasless detonation, a simple donor-acceptor arrangement was used. The donor charge used to generate the strong shocks was a high explosive, which resulted in the transmission of a shock into an acceptor section several charge diameters long containing a candidate gasless reactive powder mixture. Due to the length of the acceptor section, it was possible to observe the progression of the reactive wave over distance sufficiently long to reach a steady-state detonation. Studies of shock initiation mechanisms were also performed in a recovery capsule experiment to establish the ignition limits and burning properties for select mixtures including reactive micron-size powders, powders of different shape, and ball-milled powders. Diagnostic techniques for the capsules included shock pins, thermocouples, and light detection. In these experiments, it was possible to establish the minimum shock strength required to ignite the test mixture, as well as the ignition delay of bulk reaction when the majority of the reaction energy is released. Different powder mixtures were tested to investigate the effects mixture sensitivity and burning rate, mixing methods i.e. ball-milled v.s. loose packed powders, and particle morphology i.e. round particles compared to irregular shaped.

In parallel with these studies on powder mixtures, a secondary research effort was also performed based on the hypothesis that rapid gasless reactions could be obtained through nano-scale mixing of the reactants. The main mechanism driving the chemical reaction would be conventional heat and mass diffusion at the interfaces between the reactants as in a 'shock-assisted reaction' [1] rather than a 'shock-induced reaction'. Thanks to the drastic increase in the contact surface between reactants due to nano-scale mixing, a very rapid reaction could ensue. In this research effort, the nano-scale mixing was accomplished through a relatively new technique known as Arrested Milling (ARM)[9]. Studies on the effect of packing density on diffusion-driven flames in gasless reactive powders were performed, and a novel method of increasing the packing density to nearly 100% was developed using cold-gas spray deposition.

This report presents the theoretical and experimental studies on a set of gasless detonation mixtures chosen from the scientific literature and through experimental screening tests. A secondary study is also presented on the synthesis and combustion of gasless ARM powders. The results of these topics are assessed in the framework of gasless detonation.

2 Background

In April 2006, a Technology Investment Fund (TIF) project titled "Gasless Detonation - A Novel System For Energy Release And Terminal Effects" was started at DRDC Suffield with the present author as the principal investigator. The original motivation of the project was to investigate and develop a novel mode of explosive energy release without a blast wave or fireball that could lead to a highly-focused kinetic energy device or useful tool for close proximity operations with little risk of injury to personnel. The physical process at the

basis of this energy release was gasless detonation, a reported but not widely-accepted phenomenon consisting of a highly energetic explosion process where a stable supersonic wave reacts exclusively in the solid phase. The main objectives of the project were to establish the properties and explosive performance of gasless detonation.

Supporting evidence for gasless detonation was found mainly in a large body of work from the former Soviet Union[10] and in a number of theoretical studies predicting its properties based on Hugoniot analysis. Literature reviews by Frost [11] and Radulescu [12] have shown the evidence to be scant and speculative, but compelling. The phenomenon is related to a number of condensed-phase energetic reactions: exothermic inter-metallic reactions, exothermic reactions between a metal and a chalcogenide such as manganese and sulphur, thermite reactions between a metal and an oxide, Self-propagating High-temperature Synthesis (SHS) describing synthesis of ceramic-like materials through a combustion wave, Structural Bond Energy Reactions (SBER) which includes phase transition waves, and shock synthesis describing the creation of new materials through a reactive shock compaction. These processes were initially considered within the framework of gasless detonation as they all contain some relevant features of gasless detonation such as a strong energy release, energetic processes occurring in the solid or liquid phase, or shock-induced chemical reactions. Of these processes, SBER was removed from consideration early in the project as the amount of energy released in these processes was generally found to be lower than in chemical reactions. The ignition of chemical reactions by shock wave was considered a key phenomenon as shock-induced reaction is an essential mechanism in detonation.

The use of shock compression for the modification and synthesis of materials has been studied extensively over the past several decades. Summaries of work on 'shock synthesis' can be found in the reviews by Graham and co-workers at Sandia National Laboratory ([13, 14, 15, 16, 17]) as well as in the more recent review by Thadhani [18] and Eakins [19] The various processes that are being developed for the shock processing of powders include shock-induced solid-state polymorphic phase transformations, shock compaction (for consolidating powders), shock modifications (of defects and grain size), shock-enhanced sintering, and shock-induced reaction synthesis.

Investigations of shock-compressed reactive powder mixtures have resulted in two categories of chemical reactions being observed[1]: (i) 'shock-induced reactions' which occur on microsecond timescales and are largely due to non-equilibirum shock interactions, and (ii) 'shock-assisted reactions' which occur much slower at millisecond timescales and are controlled mainly by mass and heat diffusion. Shock-induced reactions are initiated within the shock pulse due to the processes occurring during crush-up of the powders to their full density.

The formation of reaction products immediately or following the shock front influences the equilibrium shock state. These 'ultrafast chemical reactions' [2, 3, 4] which are influenced by the thermal effects of the shock wave, are primarily driven by mechanical effects such as plastic deformation, turbulent mixing and interparticle shear. As a result, these mechanisms have been called 'mechano-chemical' reactions. These fast reactions have been shown to occur on a timescale of 100 μs just after the shock front and have been called 'ballotechnic

reactions' by Graham [17] to emphasize the close connection between the shock pressure and the chemical reaction. They have also been referred to as 'super-diffusion' [10] for lack of a definitive explanation for the process. In contrast, shock-assisted chemical reactions [18, 1] are influenced by the high-pressure shock wave, but occur largely after the high pressure pulse has relaxed. These reactions rely on the shock to mix, compact, and heat the reactants both locally through generation of hot spots and globally by increasing the bulk temperature. The bulk of the energy release, however, occurs long after the shock and seems to be dominated by thermally-controlled reaction mechanisms such as mass diffusion.

Experimental observations of gasless detonation have been scarce and preliminary to date. Recent papers report quasi-steady shock-coupled reactions in the Mn-S system [20], the Zn-S system [21] and the Zn-Te system [22]. In these studies, wave velocities between 1-2 km/s were observed. However, due to the limited charge size and limited diagnostic measurements, the stability and even the nature of these waves could not be established.

The main expected outcomes of the TIF project were a fuller understanding of gasless detonation phenomena and an estimate of the performance in terms of explosive energy release for performing useful work (e.g. target damage, terminal effects). As a secondary outcome, it was also expected that the research would increase the DRDC capabilities in experimental high energy research through development of state-of-the-art, ultra-high pressure diagnostic techniques and facilities.

The work performed in this project is presented starting with a theoretical study consisting of thermo-chemical equilibrium calculations of the detonation properties as well as calculations of shock transmission into target materials to estimate the work potential of gasless detonation. The body of experimental work is described next, consisting of experimental verification of Russian gasless detonation claims, screening of gasless systems, and shock initiation studies. The final section of this report presents preliminary efforts to develop and test a new reactive nano-composite materials through Arrested Milling and Cold-gas Spray Deposition techniques.

3 Theoretical Study

3.1 Introduction

Equilibrium thermodynamic calculations can provide estimates of the blast and brisance performance [23] of gasless detonation as well as insight on the reaction process through composition phase diagrams. To perform these calculations, a chemical equilibrium code capable of providing results for systems with no gaseous products is required. Codes such as the Russia-based THERMO [24, 25] and the Finland-based HSC [26] are capable of certain calculations in systems with little or no gas. Of particular interest is the CERV code developed in Canada by UTIAS [5], which comprises a unique solution approach that allows for highly accurate calculation of equilibrium composition and thermo-chemical properties when no gases are present at equilibrium. By performing enhancements on the code to include shock and detonation calculations, CERV was expected to provide

supporting calculations for gasless detonation processes.

As with most theoretical studies involving detonation, the main theoretical steps to model the phenomena include:

1. shock propagation properties in a mixture without chemical reaction,
2. properties for constant volume combustion and detonation,
3. isentropic Taylor wave expansion,
4. steady state ZND profile,
5. detonation initiation process.

The first three items provide the information required to estimate the energy partition. For high-explosive and fuel-air explosives, most of this data can usually be obtained using a chemical equilibrium code such as CEA, for Fuel-Air Explosions, or Cheetah [27], for high explosives. Unfortunately, codes with similar capabilities are not yet available to calculate gasless detonation properties. A suitable code for this purpose would require not only suitable thermodynamic databases but would also need to include equations of state for condensed combustion products. Codes such as HSC [26] and THERMO [24, 25] provide material databases and some combustion analysis capabilities, but need to be enhanced to treat high-pressure condensed phases.

With additional assumptions, data and calculations, the databases and output from these codes can be used to determine whether an explosive is a likely candidate to support gasless detonation based on its exothermicity and volume expansion after combustion. This information can also be used to construct approximate product Hugoniots, which combined with Rayleigh line calculations, can be used to estimate detonation properties using methods similar to those used by Bennett and Horie [28]. A more accurate analysis could be performed by incorporating the Hugoniot calculations directly in the chemical equilibrium calculations. The CERV code developed by UTIAS for DRDC Valcartier [5] was deemed to be a suitable candidate not only due to its ability to include condensed products, but also due to the availability of the source code allowing for direct implementation of the necessary enhancements.

Once CJ, constant volume (CV) and isentrope properties can be calculated, some estimates of the energy partition can be made by calculating the available work though the change in internal energy along the isentrope. This information can be used to estimate the blast performance and brisance properties [23] of the gasless explosive. For blast performance, the change in internal energy under the entire isentrope (down to atmospheric pressure) is usually used to estimate the TNT equivalency factor. For brisance properties of high explosives, only the initial part of the isentrope behind the reflected detonation contributes to the process.

Since gasless detonations involve minimal expansion of the combustion products, it is anticipated that the work energy available for blast will be relatively small. On the other hand, for detonation pressures comparable to those of high explosives, the brisance may still be significant, provided that the initial slope of the Taylor wave is not too steep. An

explosive with reasonable brisance properties with minimal air blast could have benefits for applications requiring low collateral damage.

Equilibrium calculations for gasless detonation present a unique challenge in that all codes are designed for systems that produce large quantities of gas to perform post-combustion work. Although condensed-phase products are allowed in small amounts, the bulk of the work is performed by volumetric expansion of the gaseous reaction components. Consequently, the thermodynamic treatment of condensed-phase species is usually incomplete because they have a negligible influence on the overall work capacity of the products. In contrast with most explosives, systems that detonate gaslessly perform all the work by thermal expansion or phase changes of the condensed-phase products. Two approaches to the problem were adopted: the first was to start with a thermo-chemical equilibrium code capable of detonation calculations of gas-producing reactants and modify the code to include detailed equations-of-states to address condensed-phase changes of state, and the second approach was to start with a code capable of calculating detailed phase transformations and thermodynamic equilibrium states in the condensed phase and modify the code to calculate detonation states. CERV was chosen amongst codes such as CHEETAH [27] or CEA [29] for the first approach, and FACTSAGE [6, 7] was selected amongst codes such as JMatPro [30] for the second approach.

3.2 Performance Calculation

Preliminary performance calculations were performed through analysis of the wave transmission properties into selected target materials [31]. A sample gasless reactive mixture consisting of Aluminum and Nickel was used, producing $AlNi_3$ as a main product. The detonation Hugoniots were approximated using the isentrope-shifting method described by Bennett and Horie [28], and impedance matching by equating the pressure and particle velocity at the material interface was performed to obtain the transmission diagrams shown in Figure 1.

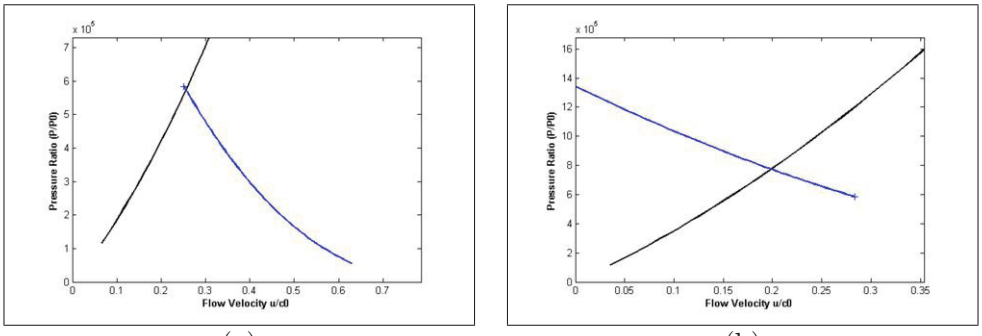

(a) (b)

Figure 1: *Wave transmission for detonation in Al-Ni into a) steel and b) tungsten targets.*

Due to the high density and sound speed of the condensed detonation products, the transmitted wave pressure in the target is high, as shown by the substantial pressure ratios.

Estimated CJ detonation pressures of several gigapascal [28] are comparable with conventional high explosives such as C4 and TNT, however impulses are much lower due to the small volumetric expansion of the products. Another factor of importance is the distension factor, which corresponds to porosity in the reactive mixtures. Theoretical Maximum Density (TMD) corresponds to a distension factor of one, which increases with increasing porosity. Figure 2 shows that optimum pressure transmission into the target occurs at a distension factor of one, indicating that porosity is undesirable for energy transmission into a target.

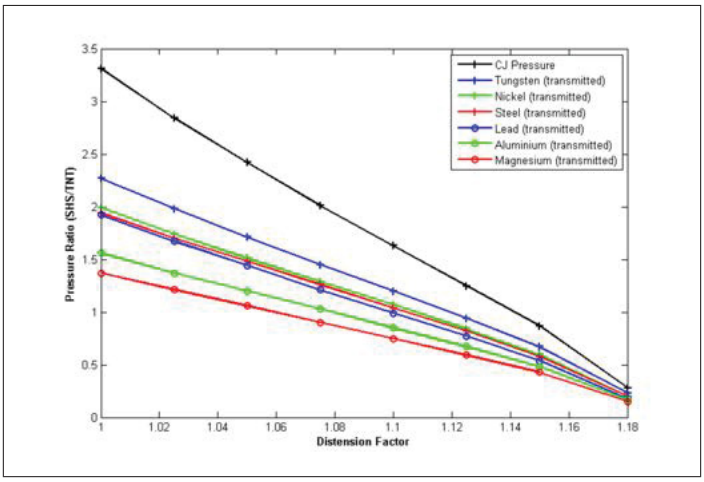

Figure 2: *Dependence of transmission pressure ratio on target material and distension factor.*

3.3 CERV Equilibrium Code Developments

A number of features were added to the CERV code to enhance its equilibrium calculations capability [32]. CERV [5] is capable of calculating the following thermodynamic points and processes: Thermodynamic Points:

- Temperature-Pressure (TP)
- Temperature-Volume (TV)
- Pressure-Volume (PV)

Processes:

- Constant pressure (CP) combustion
- Constant volume (CV) combustion
- Detonation
- Isentrope

A driver program was written to perform various P-V plane calculations. The results of these calculations are then graphically displayed through a post-processing program. The plots generated include colour contours of various thermodynamic quantities and species concentrations as a function of pressure and volume. They also include a display of the Rayleigh line and Hugoniot curve with constant pressure, constant volume and detonation

combustion points. The physical models included in CERV currently minimize the Gibbs energy based on:

1. NASA polynomials for the thermodynamic properties,
2. Virial equation of state (EOS) for gases,
3. Incompressible solids and liquids.

In spite of the enhancements, CERV currently has certain limitations which prevent it from treating completely gasless systems. For gas-phase equations of state, the third-order virial EOS, used in CERV, is suited to rocket applications where the pressures are of the order of 0.01 GPa. It may therefore not be accurate for condensed explosives and SHS systems where the detonation pressures are of the order of 5-50 GPa. Moreover, CERV does not currently include corrections for non-ideal mixtures.

For condensed-phase species, CERV also has a number of limitations. It does not include an EOS that accounts for volume change due to compression or thermal expansion. In addition, specific volumes of condensed species do not differ between the liquid and solid phases and are often set to a default value of 2 g/cc. The effect of pressure on the melting temperature is also not considered. No solution rule (ideal or non-ideal) is included, resulting in separate melting temperatures are assigned to co-existing condensed species. Finally, phase diagram topologies (eg. eutectic point) are therefore not modelled.

3.3.1 Conclusions and Outcomes

From performance calculations, it was found that in a gasless detonation, the volume expansion of the condensed-phase products is very low, typically on the order of only a few percent. There are several key implications resulting from this realization. Assuming that a positive volume change (i.e. expansion) of the products is necessary to couple the chemical energy release to the leading shock in a detonation wave, the existence of gasless detonation depends on a property that is only marginally positive, making the phenomenon inherently difficult to achieve. In addition, thermo-chemical equilibrium calculations of detonation states must be highly accurate in order to assess the ability of a mixture to support gasless detonation. Furthermore, gasless reactive mixtures typically consist of highly porous beds of packed powder mixtures, and the porosity may effectively counteract or even nullify the volume expansion resulting from the chemical reaction. This implies that gasless detonation mixtures can only tolerate a very low porosity. Finally, although the shock pressure can be efficiently transmitted to a solid material thanks to the high density of the detonation products, very little expansion work will be performed on a target. This can be a feature when the absence of a blast wave is desired during a stealthy explosive application, however it is a reminder that the range of action of a gasless detonation is very short.

Regarding enhancements to CERV to treat gasless products, attempts to implement condensed-phase equations of state into the code were ultimately unsuccessful. To perform gasless reactive calculations, CERV must be further improved to contain gaseous equations of state, mixture rules, equations of state for condensed species to treat cold compression and phase changes. With its current limitations, it is unable to perform gasless detonation equilibrium calculations.

3.4 The Use of CALPHAD Techniques in Detonation Calculations

3.4.1 Introduction

This section presents the development of CALPHAD-based (Calculation of phase diagram) calculation methods for gasless reactive systems, in particular for detonation processes. This work was performed in collaboration with A.E. Gheribi at the Polytechnique de Montréal, and a future journal publication is planned [33].

FACTSAGE [6, 7] was found to be a suitable code for gasless detonation studies as it treats the detailed phase space of condensed species. However, enhancements were required to allow for calculations of detonation states, as most the phase diagrams were only established for ambient conditions. FACTSAGE software is a CALPHAD-type [8] thermodynamic software that is particularly suited for the thermodynamic description of condensed phases. This is in contrast with codes that are commonly used for the equilibrium detonation calculations such as CEA [29] or CHEETAH [27], which generally lack this capability as they are designed to treat common high explosives and detonable gaseous mixtures where the reaction products are predominantly in the gas phase. Equilibrium calculations of the condensed-phase detonation products of gasless detonation require detailed treatment of the complex condensed-phase states for solid and liquid phases of metals, salts, and oxides.

FACTSAGE lacks the ability to calculate very high-pressure and temperature states for detonation products, but a number of methods were used to achieve detonation equilibrium calculations. Using equilibrium calculations for ambient conditions from FACTSAGE, detonation states were then calculated through a shock physics method based on formal derivations of the shock Hugoniots and equations of state. These two steps are described in the following sections.

3.4.2 CALPHAD Equilibrium Thermodynamics For Gasless Systems

The CALPHAD method is based on the fact that a phase diagram is a representation of the thermodynamic properties of a system [8] . The thermodynamic properties of a system are represented by thermodynamic functions derived from all available experimental data. The thermodynamic functions are expressed as polynomials of temperature and chemical composition. The numerical values of the polynomial coefficients are obtained using numerical optimization techniques. Experimentally-determined phase diagrams, however, are usually available for binary systems only, and to some extent, for ternary systems, and very rarely for higher-order systems. This is where the CALPHAD method is useful. If the thermodynamic properties are known, it is possible to calculate the multi-component phase diagrams. Thermodynamic descriptions of lower-order systems are done by the Gibbs energy (G) of each phase. The Gibbs energy of a phase is described by a model that contains a relatively small number of experimentally-optimized variable coefficients: melting and other transformation temperatures, solubilities. The Gibbs energy is also described by thermodynamic properties such as heat capacities, enthalpies of formation, and activities.

Figure 3 is a flowchart of the Calphad method. The first step of the thermodynamic optimization of a phase diagram is collecting and categorizing experimental information.

All constitutional and thermochemical data must be extracted from primary sources. The second step involves the critical evaluation of the collected data. The third step is the choice of the Gibbs energy model and the optimization process to obtain the values of the model parameters for each phase. In general, the simplest model was chosen to obtain reasonable extrapolation characteristics in the higher-order systems. The last step involves merging all the state models to form a coherent thermodynamic database for the system. After an assessment of the unary, binary and ternary systems (if available), the main purpose is to assemble all these data to obtain a single dataset for performing calculations on the whole complex system.

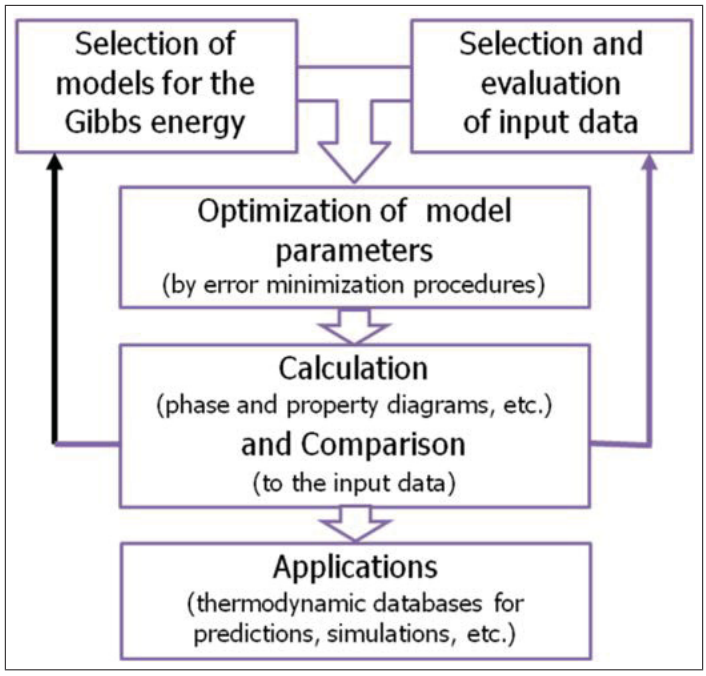

Figure 3: *Flowchart of the CALPHAD method.*

In the CALPHAD approach, the Gibbs energy of a phase φ at standard pressure depends on composition $x\underline{x} = (x_1, x_2, x_3, ..)$, and temperature. It is expressed as follow:

$$G_m^{\varphi}(\underline{x}, T) = G_m^0(\underline{x}, T) + G_m^{ideal}(\underline{x}, T) + G_m^{excess}(\underline{x}, T) + G_m^{mag}(\underline{x}, T) \quad (1)$$

The first term $G_m^0 = \sum_i x_i G_i^0$ is the Gibbs energy of a mechanical mixture of the constituent phases where G_i^0 is the Gibbs energy of constituent elements. $G_m^{ideal} RT = \sum_i x_i ln x_i$ is the ideal Gibbs energy term derived from the entropy of mixing of an ideal solution, G_m^{excess} corresponds to the excess Gibbs energy of mixing, and G_m^{mag} is the contribution due to the magnetic ordering. The Gibbs energy of a non-magmatic solid can be represented by:

$$G_i^0(T, P_0) = G_i^{ref}, +3RTln(1 - e^{\theta_E/T}) - \frac{1}{2}aT^2 - \frac{1}{6}bT^3 + ce^{-E_{Vac}/RT} \quad (2)$$

where $G_i^{ref} = E_0 + 3R\theta_E/2$ is the reference molar Gibbs energy of the element at 0 K, the term $3R\theta_E/2$ is the total energy of the element at 0 K, and the term $3R\theta_E/2$ is the

energy of zero point lattice vibration. The second term describes the contribution from the harmonic lattice vibration and θ_E is the Einstein temperature. Both parameters a and b are adjustable although they can be related to physical properties: a consists of contributions from the electronic excitation and first order anharmonic vibration, and b is from the second order anharmonic vibration. The last term of this equation describes the contribution from vacancies: E_{Vac} is the formation energy of a mol of vacancy, and $c = (E_{Vac}/R)e^{S_{Vac}/RT}$ where S_{Vac} is an entropy related to changes in the vibrational spectrum of the lattice. Generally, the previous expression is approximated as a polynomial of temperature expressed as:

$$G_i^0(T, P_0) = a + bT + cTlnT + dT^2 + eT^3 + \frac{f}{T} + \frac{g}{T^2} \tag{3}$$

ΔG_m^{mag} , the magnetic contribution to the molar Gibbs energy, is described by the Inden model. It is based on the expression:

$$G_m^{mag}(\underline{x}, T) = RTln[\beta_0(\underline{x}) + 1]g[\tau(\underline{x}, T)] \tag{4}$$

where $\tau = T/T_c$ is the reduced temperature with T_c being the critical temperature of magnetic ordering (i.e. Curie temperature, T_c is the ferromagnetic and Neel temperature, T_N is the antiferromagnetic, and β_0 is the average spin magnetic moment per atom and related to the total magnetic entropy as follows $\Delta S_m^{mag,tot} = Rln(\beta_0 + 1)$ and $g(\tau)$ is characteristic function for the magnetic ordering.

In the database used in this work, the excess Gibbs energy of the liquid phase is described by the Modified Quasichemical Model in the Pair Approximation. This model takes into account the effect of short-range order (SRO) on the configuration contribution to the mixing entropy of the solution as a function of the change in the Gibbs energy of the quasichemical first-nearest-neighbor pair reaction: $(A-A)_{pair}+(B-B)_{pair} = 2(A-B)_{pair}$. The non-configurational Gibbs-energy change for the formation of 2 moles of (A-B) pairs is Δg_{AB}. A negative value of Δg_{AB} for reaction indicates that the equilibrium is shifted to the right resulting in SRO. On the other hand, a positive value of Δg_{AB} implies that A-A and B-B pairs are favoured. This is usually expressed as a polynomial expansion in terms of the pair fractions. The Gibbs energies are then extrapolated to the higher order system using the Toop or Toop-Kholer model of interpolation by considering the optimized parameters for the binaries subsystems.

The compound energy formalism (C.E.F) is used to describe the excess Gibbs energy of solid solutions. This model can address interactions among multiple sublattices in the ordered phase using the element site fraction in each sublattice. In the case of crystalline solid solutions thermodynamic sublattices may correspond to crystallographic sublattices. The Gibbs energy is expressed as a function of the site fractions and the mole fractions of each component in the sublattice.

The Gibbs energy of a stoichiometric compound $A_U B_V C_W ..$ is related to the Gibbs energy of the pure components:

$$G_m^{A_U B_V C_W ..}(T) = \frac{u}{u+v+w}G_m^A(T) + \frac{u}{u+v+w}G_m^B(T) + \frac{W}{u+v+w}G_m^C(T) + \Delta^{form}G^{A_U B_V C_W ..} \tag{5}$$

where $\Delta^{form}G^{A_U B_V C_W \cdot\cdot}(T) = A^{A_U B_V C_W \cdot\cdot} + B^{A_U B_V C_W \cdot\cdot}T + C^{A_U B_V C_W \cdot\cdot}ln(T)$ is enthalpy of formation of the compound. The addition of a magnetic term may be necessary for compounds showing magnetic ordering.

For thermite mixtures, the CALPHAD thermodynamic databases in FACTSAGE generally do not extend to high pressures required for detonation. For a number of select systems of interest, the databases were extended by adding a pressure-dependent term to the Gibbs energy expressions (Eqs. 1, 2, 3, and 4). This was done using a variety of experimentally-valided models such as ab initio calculations, quasi-harmonic approximations, molecular dynamics, analytical models (e.g. Brewer, Miedema), hard sphere models, and Eyring partition functions. The compounds of interest were treated on a case-by-case basis, and the appropriate methods were used to extend the thermodynamic database of each compound to high pressure. For certain cases, this was not possible due to the instability of certain compounds. For example the compounds involved in the thermite reaction: αAl+Fe_2O_3+δAl_2O_3 are particularly unstable and show many pressure-dependent phase transitions in the pressure range of interest. In these cases, assumptions were made on the state and composition of the reaction products at high pressure.

3.4.3 Theoretical Shock Physics Approach to Calculate Gasless Detonation Properties

To calculate detonation parameters based on FACTSAGE equilibrium calculations, a formal shock physics approach was formulated based on a derivation of the conservation equations at the Chapman Jouguet (CJ) detonation state for condensed phases. The approach was developed by calculating the detonation parameters using the classical Jouguet–Zeldovich theory, in which the hydrodynamic equations describe the state of the medium in the Jouguet plane, where the chemical reaction is terminated. The state parameters behind the leading shock can be determined by a system of equations comprising: the conservation equations for mass, momentum, and energy fluxes, the relation of product sound speed, the product equation of state, and the Chapman–Jouguet (CJ) condition, which states that the shock velocity is equal to the sum of the particle velocity and local sound speed. By simultaneously solving this system of equations, the state parameters of the reaction products behind the shock can be calculated from the initial state of the reactants and the heat of the reaction of the shock-initiated exothermic reaction producing the volume expansion.

Based on classical detonation theory of Zeldovich, von Neuman, and Doering (ZND), the conditions for detonation in a reactive medium can be stated qualitatively as [34]:

1. an exothermic chemical reaction or process,
2. expansion of the reaction products as they relax to the initial pressure,
3. sufficiently high reaction rate.

For gasless detonation, Gordopolov et al. [35] reformulated a necessary but non-sufficient condition for existence. Stated formally, the exothermic reaction must proceed with positive

volume change at constant pressure P and enthalpy H:

$$\Delta V_{P,H} > 0 \tag{6}$$

or a positive coefficient of thermal expansion is a non-zero isobaric-isochoric thermal effect of reaction:

$$Q_{P,V} > 0 \tag{7}$$

Calculations of the Hugoniot equations for the reactants and products mixture using the constant-pressure scheme can indicate the possibility of a self-sustained reaction (detonation) in the condensed state. The shock wave travels at velocity U_s through the solid, accelerates its atoms from rest to velocity U_p and changes its density, atomic volume, pressure, and internal energy per atom from ρ_0, V_0, P_0 and E_0 to ρ_0, V, P_H and E. Assuming thermal equilibrium before and after the shock, these quantities must satisfy the Rankine-Hugoniot relations, derived from considerations of mass, momentum, and energy conservation:

$$\begin{array}{l} \rho_0 U_S = \rho(U_S - U_P), \\ P = \rho_0 U_S U_P), \\ E - E_0 = \frac{1}{2} P(V_0 - V) \end{array} \tag{8}$$

From the measurement of U_s and U_p the Hugoniot equation of state $P_H(\mathrm{V})$ is obtained by solving these equations. A valuable relationship can be obtained by eliminating U_p from Eqs. 8, establishing $P = K^2 V_0$ where $K = U_S/V_0$ is a constant with respect to a steady state wave. This line in the P-V plane is called the Raleigh line.

The detonation process can be viewed as a shock moving through an explosive. The shock compresses and heats the explosive, which initiates the chemical reaction. The energy feeds the shock and drives it forward. The shock front, chemical reaction, and the leading edge of the rarefaction are in equilibrium. Under this equilibrium, the detonation wave exhibits a picture of the steady propagation in the explosive. According to CJ theory, the velocity of the shock front has a minimum value at equilibrium. Figure 4 shows a conceptual sketch for the Chapman-Jouguet detonation model.

Letting $R_{He}(V)$ be the Raleigh line function of pressure for reacted powder; $P_{He}(V)$ and $P_{HP}(V)$ are the Hugoniot equation of state of the reacted powder and products of detonation respectively. B_{HP} is the Hugoniot bulk modulus i.e. $B_H(V) = -V(\partial P_H/\partial V)_H$. V_{OR} and V_{0P} are the equilibrium volume of reacted powder and detonation products. V_{CJ} And V_{NS} are the Chapman-Jouget point and Von Neumann point. A set of equations describing the Raleigh line for reacted powder can be derived:

$$\begin{cases} \frac{V_{CJ}}{V_{OR}-V_{CJ}} = \frac{B_{HP}(V_{CJ})}{P_{CJ}} \\ \\ \frac{V_{OR}-V_{NS}}{V_{OR}-V_{CJ}} = \frac{P_{NS}}{P_{CJ}} \end{cases} \tag{9}$$

where $P_{CJ} = P_{HP}(V_{CJ})$ and $P_{NS} = P_{HR}(V_{NS})$. Eqs. 9 show that only the equation of state of the detonation product and the initial volume of reacted powder are necessary to

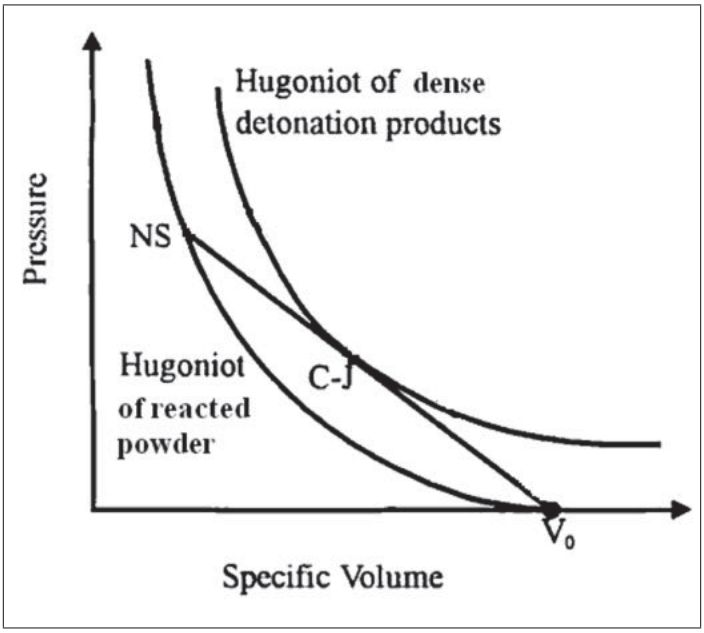

Figure 4: *Chapman-Jouguet detonation model represented on the reactant and product Hugoniots.*

calculate the Chapman-Jouget pressure and verify the existence or the non-existence of an ideal detonation. The second condition is the existence of the Von Neumann State (NS) point. According to the second equation of Eqs. 9 it is clear that if the CJ point exists then the NS point also exists.

For most condensed matter, it has been recognized that kinematic parameters can be measured in shock wave experiments where U_s and U_p can be empirically described in a region where no substantial phase change in the material occurs. An expression for the shock velocity of the form:

$$U_s(T) = C_0(T) + S(T)U_p(T) \tag{10}$$

can be used, where C_0 is the shock velocity at infinitesimally small particle velocity or the sound speed at ambient pressure, at a given temperature (T) which is given by:

$$C_0(T) = \sqrt{(B_{SOT}/\rho_{OT})} \tag{11}$$

where B_{OT} and rho_{OT} are the bulk modulus and density respectively. The bulk modulus is in turn given by:

$$B_{SOT} = B_S(T, \rho_{OT}) = B_S(T, P_O) \tag{12}$$

where the adiabatic bulk modulus is defined as:

$$B_S(V) = -V(\partial P/\partial V)_S \tag{13}$$

and the density ρ_{OT} at temperature T defined as:

$$\rho_{OT} = \rho(T_0, P_0)e^{-\int_{\tau_0}^{\tau} \alpha(T,P_0)dT} \tag{14}$$

where the thermal expansion coefficient is defined as:

$$\alpha = (1/V)(\partial V/\partial T)_P \tag{15}$$

The parameter S in Eq. 10 is linked to the first pressure derivative of adiabatic bulk modulus and can be written:

$$S(T) = \frac{1}{4}[(\partial B_{SOT}/\partial P)_T + 1 \tag{16}$$

Combining the conservation equations, the temperature dependent Hugoniot equation of state can be derived for the pressure P_H and the bulk modulus B_{HP} along the Hugoniot is:

$$B_{HP}(T,\rho) = \rho_{OT}C_{OP}^2(T)\frac{[1 + S_{OP}(T)\eta(T,\rho)]}{[1 - S_{OP}(T)\eta(T,\rho)]^3} \tag{17}$$

According to these, the expression for P_{CJ}, the pair (P_{CJ},V_{CJ}) can be expressed as:

$$\frac{[1 - S_{OP}(T)\eta_{P_{CJ}}}{\eta_{P_{CJ}}^{-1} + S_{OP}(T)} = \frac{V_{OR}}{V_{CJ}} - 1 \tag{18}$$

where $\eta_{P_{CJ}} = 1 - \frac{V_{CJ}}{V_{POT}}$, $\eta_{P_{RCJ}} = 1 - \frac{V_{CJ}}{V_{POT}}$ and $\eta_{P_{CJ}} = 1 - \frac{V_{NS}}{V_{POT}}$.

The detonation velocity is also an important parameter for establishing gasless detonation. By considering the energy flux conservation, the Chapman-Jouguet condition $D_{CJ} = U_S - U_P$, and the the continuity equation, at CJ condition the energy flux conservation are written as:

$$V_{ROT}D_{CJ}^2\eta_{RCJ} + \frac{(\Delta q + H_0)}{1 - \eta_{RCJ}/2} = P_{CJ} \tag{19}$$

When $\Delta q = 0$ (i.e for adiabatic reaction) the relation becomes:

$$D_{CJ} = V_{ROT} + \sqrt{\frac{P_{CJ}}{V_{ROT} - V_{CJ}}} \tag{20}$$

Since the detonation is a supersonic process, the minimum of gasless detonation must be greater than the sound velocity in initial mixture ($C_{OR}(T)$):

$$D_{min} = C_{OR}(T) \tag{21}$$

Thus, if U_s is a linear function of U_p for both equation of state of reactants and products, the detonation parameters: P_{CJ}/B_{SPO}, V_{CJ}/V_{OR}, and D_{CJ}/C_{P0} are functions of the ratio V_{OP}/V_{OR} and the parameters S_{0P}. The Hugoniot equation of state of initial reacted powder is not necessary to calculate the CJ parameters and it is thus not necessary to consider the equation of state of the reactants as a function of porosity. The linear behaviour U_s with respect to U_p is a reasonable assumption for most of transition metals and oxides in solid or liquid state at least up to P_H $\tilde{5}$0-100GPa.

For many solids and liquids, one needs a realistic model to extrapolate the temperature dependence of the Hugoniot equation equation of state. Assuming that the Gruneisen parameter γ depends linearly on volume, it can be shown that:

$$C_0(T) = C_0 \frac{[1-\theta(T)]^2}{[1-S_0\theta(T)]^3}[1+(S_0-\gamma_0)\theta(T)] \tag{22}$$

For most liquids (metal, non metal and slags), the sound velocity depends linearly on temperature. This corresponds to an approximation of the previous expression by the first order Taylor series:

$$C_0(T) \approx C_0 1 - \alpha_0[4S_0 - \gamma_0 - 2](T - T_0) \tag{23}$$

When S is not available one can assume that for $\gamma_0 = 2S - 1$, the previous approximation becomes:

$$C_0(T) \approx C_0 1 - \alpha_0(T - T_0) \tag{24}$$

Assuming also that Gruneisen parameter depends linearly on volume it is shown that S depends on temperature according to the following expression:

$$S_0(T) = [1-\theta(T)] \frac{\left\{\theta(T)S_0^2[2-\theta(T)\gamma_0] - \gamma_0^2\theta(T) + S_0[4 - 2\theta(T)\gamma_0 + \theta(T)\gamma_0]\right.}{4[1-S_0\theta(T)][1+(S_0-\gamma_0)\theta(T)]} \tag{25}$$

This last equation can approximated by a first order Taylor series:

$$S_0(T) \approx S_0 \left\{1 + \alpha_0 \left[1 - \frac{1}{2}S_0 + \frac{\gamma_0^2}{4S_0} - \frac{1}{2}\gamma_0\right](T - T_0)\right\} \tag{26}$$

Assuming $\gamma_0 = 2S - 1$, this last equation becomes

$$S_0(T) \approx S_0 \left\{1 + \frac{\alpha_0}{8}(3 - \gamma_0^2(T - T_0)\right\} \tag{27}$$

Finally, the mixture rule considered in this work are based on mass fraction averages. This method has been used in the study of shock included chemical reaction. The equation of state parameters ρ_{OT}, C_{0T}, and S_{0T} of the mixture are given by:

$$\begin{aligned} \rho_{OT}(\underline{x}, T) &= \textstyle\sum i\theta_p \rho_{OTi}(\underline{x}, T) \\ C_{OT}(\underline{x}, T) &= \textstyle\sum i\theta_p C_{OTi}(\underline{x}, T) \\ S_{OT}(\underline{x}, T) &= \textstyle\sum i\theta_p S_{OTi}(\underline{x}, T) \end{aligned} \tag{28}$$

where $\underline{x} = (x_1, x_2, x_3, ..)$ is the composition vector, and $\theta = M_i/M_{total}$ is the mass fraction.

Using the mixture rules (Eq. 2) and the equations for the detonation parameters (Eqs. 14, 19, and 20), the detonation parameters can be calculated from the results of constant pressure combustion calculations using FACTSAGE.

3.4.4 Sample Calculation with a Thermite Mixture

In this section the possibility of gasless detonation is investigated in an aluminum–iron thermite mixture: αAl+Fe_2O_3+δAl_2O_3. The thermite is diluted with alumina in order to maintain the gaslessness at the adiabatic flame temperature. The minimal ratio of alumina to reactants was sought for achieving the higher possible adiabatic temperature without formation of gaseous phases. The combustion reaction is given by:

$$\alpha Al + Fe_2O_3 + \delta Al_2O_3(\Delta V, \Delta H) 2Fe_{Lig} + (\alpha + \delta) Al_2O_3 \tag{29}$$

where ΔH and ΔV are the enthalpy and the volume change associated to the reaction, respectively. However this reaction is not realistic, because it does not take into account all possible solutions. Indeed, the effect of mixing rules on adiabatic flame temperature and volume change can be non-negligible and have a significant consequence on the calculation of the detonation parameters. In fact, combustion reaction is:

$$\alpha Al + Fe_2O_3 + \delta Al_2O_3(\Delta V, \Delta H)(Fe, Al)_{Met-Lig} + (Al_2O_3, FeO, Fe_2O_3)_{Slag-Liq} \tag{30}$$

The parenthesis in the last equation denotes a solution. The thermodynamic calculations were performed using the FTlite (metallic phases) and the FToxid (oxide phases) databases from the FACTSAGE thermochemical software [6, 7]. The results are expected to be reasonably accurate since the Al-Fe and Al_2O_3-FeO-Fe_2O_3 systems have been optimized and both databases are fully compatible.

The density is assumed to be a linear function of temperature and obey the following equation: $\rho(T) = |rho(T_m) + \rho'(T - T_m)$. This allows extrapolation above the range of temperature where experimental data on the density is available.

For the extrapolation of the sound velocity, a linear dependence with temperature is assumed: $C_0(T) = C_0(T_m) + C_0'(T - T_m)$. The parameters S is available in literature only for liquid iron but it is a calculated value. For the other compounds, S and its temperature dependence were estimated according to: $S_0(T) = S(T_m) + S'(T - T_m)$. For Fe_2O_3 a phase transition occurs at P_H=43.5 GPa, and below this pressure, the linear behaviour of Us-Up is valid. Since the range of CJ pressures is lower than 22 GPa the phase transition of hematite was not treated.

The pressure dependence of the chemical reaction and Gibbs free energy has generally not been treated in the present calculations due to the complicated phase transitions of the products and lack of high-pressure data to validate the thermodynamic estimates. The Chapman Jouguet detonation properties have therefore been calculated based on the assumption of frozen reaction products and independence of the Gibbs energy on pressure.

These assumptions can be relaxed for a more rigorous treatment of gasless detonation if a simpler system (e.g. Ti-B_2) with more stable products and more high-pressure data on the reaction and phase transitions is used.

Using the FACTSAGE and shock physics approach, the state surfaces for the non-dimensional detonation pressure, volume, and speed ($P_{CJ/}B_{SP0}$, V_{CJ} and D_{CJ}/C_{P0}) are calculated and shown in Figure 5 as a function of initial volume (V_{0P}/V_{0R}) and and the shock Hugoniot parameter S_{0P}. It can be seen that the detonation pressure (P_{CJ}) (and respectively, D_{CJ})

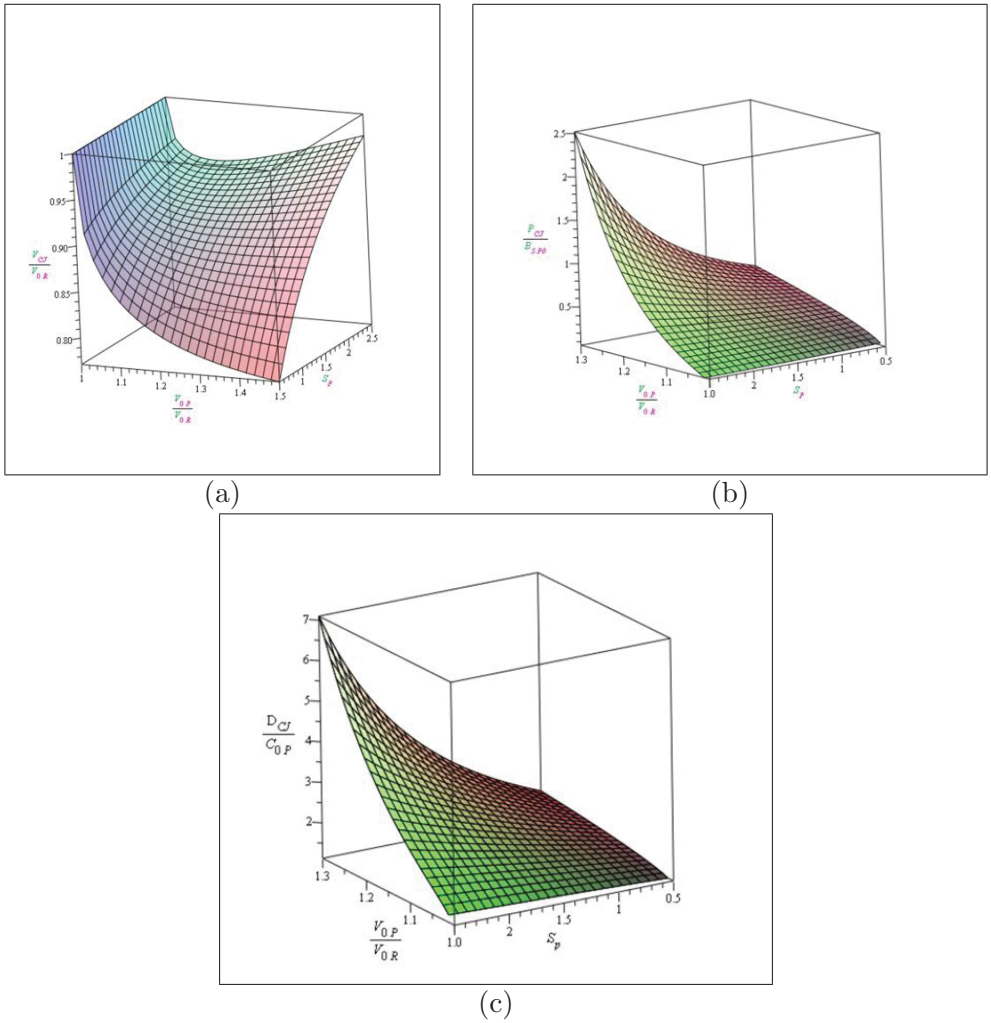

Figure 5: *State surfaces representing Chapman-Jouguet a) pressure (P_{CJ}), b) volume (V_{CJ}), and velocity (D_{CJ}).*

increases with S_{0P} and V_{0P}/V_{0R}, therefore to maximize P_{CJ} (and respectively D_{CJ}) one must first identify mixtures with high adiabatic bulk modulus of products reaction, a very large volume expansion, and with good mechanical properties: the adiabatic bulk modulus should increase fairly quickly as the pressure increases.

For non-diluted thermite i.e. α Al+Fe_2O_3, the moles of gaseous phases produced by the combustion reaction were calculated (Fig. 6a). The maximum amount of gas occurs at $\alpha \approx 3.6$, and the gaseous products consist mostly of Fe and a few percent of FeO. For $1.83 < \alpha < 6.05$ the combustion reaction is therefore not gasless. A method of rendering the reaction gasless within this range of mole fractions of aluminum is to dilute the thermite with alumina (Al_2O_3). The minimum amount of Al_2O_3 necessary to avoid gaseous phases in the combustion reaction is shown in Figure 6b. When the mole fraction of alumina is 0.227 ($\delta = 0.227$), the thermite reaction is gasless for all aluminum mole fractions.

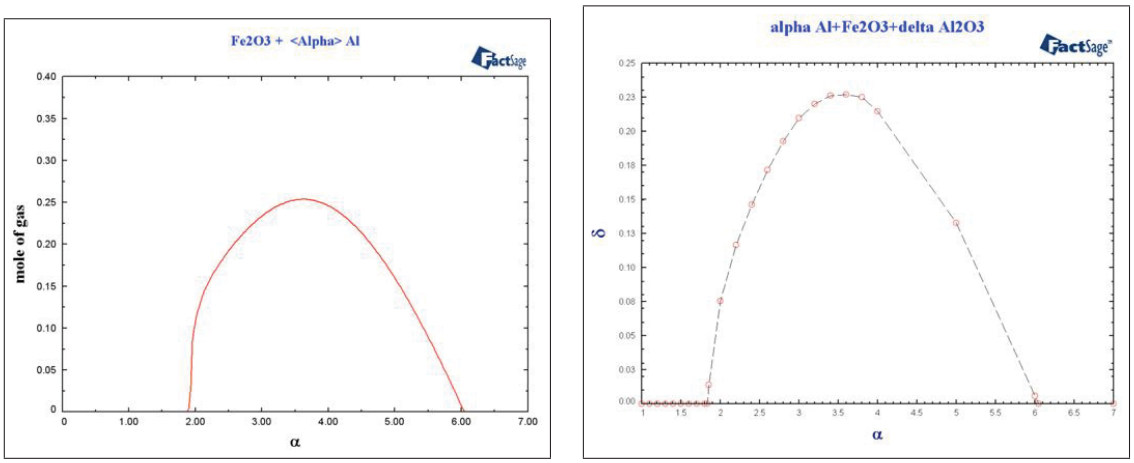

(a) (b)

Figure 6: *Composition plots showing the moles of a) gas produced by the thermite reaction $\alpha Al + Fe_2O_3$, and b) Al_2O_3 necessary to render the $\alpha Al + Fe_2O_3 + \delta Al_2O_3$ gasless..*

The adiabatic flame temperature T_{ad}, the liquidus temperature T_{liq}, (ignition temperature), and the condensation temperature T_{gas} for gasless thermite combustion in non-dilute thermite and dilute thermite are shown in Table 1. Two of the conditions which favor detonation are: 1) high adiabatic flame temperature 2) high volume expansion. For these reasons, non-dilute mixtures were considered: the aluminum-lean mixture with α=1.83, and the aluminum-rich mixture at δ=6.05. For this composition, the maximal adiabatic flame temperature and the maximal volume change were calculated. The dilute thermite with α=3.6 and δ=0.227 was also considered because this composition is the best compromise between a maximum adiabatic flame temperature and volume change. For the three compositions, the equilibrium composition of the system is calculated at adiabatic temperature, i.e.T_{ad}, T_{liq}, T_{gas} and ΔV. (Fig. 7).

The results of gasless detonation calculations for select thermite mixtures are summarized in Table 2. For the lean non-dilute mixture (α=1.83) the CJ velocity is very close to the sound speed of the initial reactant mixture (D_{min}), and therefore barely meets the criterion of a supersonic wave. Given the uncertainty caused by different approximations and experimental results used in the calculations, this mixture appears marginal in supporting a detonation. The fuel-rich non-dilute mixture (α=6.05) and the dilute mixture (α=3.6 ,

Table 1: *Adiabatic combustion temperatures for thermite.*

α	δ	T_{ad}	T_{liq}	T_{gas}	ΔV
		(K)	(K)	(K)	(%)
1.83	0	3130	1810	3131	13.75
6.05	0	2582	1431	2583	23.00
3.60	0.227	2748	1586	2748	18.50

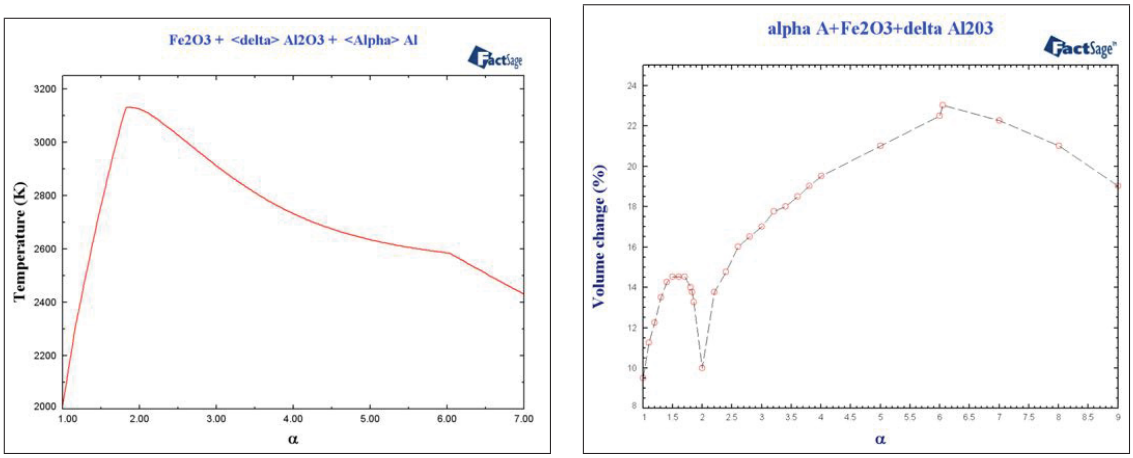

(a) (b)

Figure 7: *The adiabatic flame temperature (a) and volume expansion (b) dependence on moles of Al (α) for a non-dilute thermite mixture with 0.227 moles (δ) of Al_2O_3.*

δ=0.227), however, appear to be promising candidates for gasless detonation systems.

Table 2: *Detonation parameters for thermite.*

α	δ	P_{CJ}	D_{CJ}	D_{min}
		(GPa)	(m/s)	(m/s)
1.83	0	6.35±4	5526±750	5621
6.05	0	22.70	7309	5073
3.60	0.227	19.58	6472	5116

3.4.5 CALPHAD Equilibrium Calculations with Other Reactive Mixtures

Using the CALPHAD method, equilibrium calculations for the temperature and volume change were performed for a number of other systems. Since a positive volume change is an essential criterion for supporting detonation, this parameter is shown. These are summarized in Table 3.

Table 3: *Equilibrium calculations for gasless reactive mixtures.*

Mixture	**Type**	**Temperature** (K)	**Volume Change** (%)
2Al+ MoO_3+0.18143Al_2O_3 → Mo(liq) +1.18143Al_2O_3(liq)	thermite	3794	8.14
3Si + 5Ti→0.888 Si_3Ti_5 + 0.89597 Liq	intermetallic	2390	*-9.2*
Ni+Al→Ni(liq)+Al(liq)	intermetallic	1950	11.28
Zn+S→ZnS	metal-chalcogenide	1906	2.72

The temperatures in Table 3 refer to the adiabatic flame temperature or liquid temperature in the case of reaction products in the liquid phase. All mixtures showed a small volume expansion on the order of a few percent with the exception of the Ti-Si which showed a volume decrease. Based on volume expansion, these additional mixtures are therefore viable candidates for gasless detonation with the exception of Ti-Si. The relatively small expansion values emphasize the importance of minimizing porosity in the mixture, since porosity exceeding the volume expansion would effectively negate the expansion work produced by the reaction and eliminate the mechanism for the reaction to feed energy back into driving the leading shock wave.

3.5 Conclusions and Outcomes

Enhanced CALPHAD techniques were implemented in the FACTSAGE code to treat high-pressure compounds, and together with a rigorous shock physics approach to calculating CJ detonation parameters, a new method of performing detonation calculations for gasless systems was developed, addressing a deficiency of all previous thermochemical equilibrium codes. The shock physics approach produces convenient equations that permit optimization of desirable detonation parameters such as minimizing gas production, or maximizing shock velocity, volume expansion, and pressure. The composition of a gasless reactive mixture can thus be optimized for specific applications. For example, the composition-gas generation plots (Fig. 6) show the range of compositions that result in gasless reactions. Combined with plots of the volume expansion (Fig. 7), mixtures most likely capable of supporting gasless detonation can be found from a purely equilibrium point of view, although reaction kinetics remain another important factor. Conversely, mixtures that can theoretically not support a detonation wave, e.g. with negative volume expansion, can be eliminated from consideration.

The sample calculations performed for several reactive mixtures show a number of viable candidates for gasless detonation (Table 3). Since the reaction occurs entirely in the solid or liquid phase, the expansion is predictably small, however this further emphasizes the importance of low porosity in the mixtures. The results suggest that gasless detonation can only be obtained with packing densities above approximately 90% TMD.

The new mixture optimizing algorithms and CALPHAD techniques developed in this project provide the first accurate equilibrium calculations for Chapman-Jouguet detonations with no gaseous products. However to further increase the accuracy, additional work remains to include the pressure dependence of the phases, and composition changes along the product Hugoniot. Indeed, the biggest limitation of the present approach remains the lack of thermo-chemical data and solid state models for particularly complex systems, particularly at high pressure,making it difficult to treat the pressure dependence of the Gibbs energy. For example, the Al-Fe_2O_3 thermite system involves reaction species and products that are unstable and have several phase transitions that are highly pressure dependent at gigapascal pressures. Though the present theoretical approach is sound, the lack of independent thermodynamic data and high-pressure models for relevant species, particularly at high pressure, may make the calculations inaccurate for certain systems.

Another application of these techniques is that other thermodynamic and material properties of condensed-phase substances such as metallic alloys can be optimized. For example, alloy composition can be optimized to maximize hardness or bulk modulus. The present techniques therefore extend beyond detonation applications and may have specialized military applications such as armour steel or low corrosion alloys used in naval vessels.

4 Experimental Verification of Gasless Detonation Phenomena

4.1 Introduction

This section documents attempts to repeat and confirm key published results on experimental evidence of gasless detonation. This work was performed in collaboration with Jetté et. al. at McGill University and has subsequently been published [36].

In the early 1990s, gasless detonation was examined theoretically by Boslough [38] and Bennett & Horie [28] using equilibrium thermodynamics and shock physics methods to estimate the product Hugoniot for a shock wave in a reactive powder mixture, such as thermites and SHS (Self-propagating High-Temperature Synthesis) compositions. Although their methods did not implement CALPHAD techniques (section 3.4), they nevertheless found cases where the non-gaseous product Hugoniot curve lies above the initial unreacted powder state on the pressure-specific volume (p-v) plane. For these cases, a classical Chapman-Jouguet (CJ) detonation solution was found to exist [28] for the one-dimensional conservation laws of mass, momentum and energy. After performing a similar analysis, Merzhanov et al. [34] formalized the criteria for the existence of gasless detonation, and correctly pointed out that experimental difficulties stem from the fact that without knowledge of the kinetics of the reaction, the minimum charge diameter that could permit reactions to occur before lateral expansions reduced pressure and temperature cannot be estimated. Furthermore, the shock pressure and duration required to initiate reactions also depend on the kinetics. Experimental evidence of gasless detonation, however, remained sparse and inconclusive.

Early experimental investigations of gasless detonations were performed by Merzhanov et. al. [37] who conducted preliminary experiments with a 50-mm-diameter, 200-mm-long charge of compacted Ti+C+Al+paraffin (48:12:90:12 respectively, by weight %) initiated with a TNT charge. They observed shock deceleration followed by acceleration from 1.6 km/s to 2.5 km/s. In their tests, paraffin acted as a source of gas, so although what they observed was not entirely gasless, the authors believed that their results could be regarded as preliminary evidence of gasless detonation.

Jiang et al. [20] later measured the reaction front trajectory using ionization probes in quasi-solid (low-porosity) mixtures of Mn+S (25 mm diameter, 100 mm long) initiated by nitromethane charges sensitized with 15 wt% of diethylenetriamine. The Mn+S mixture appeared a promising candidate due to its large heat of reaction (for the Mn+S→MnS reaction, ΔH = -2.46 kJ/g) and gasless products at moderate pressures. In one experiment, they observed a re-acceleration of the reaction front in solid Mn+S from 1.8 km/s to 2.2 km/s after 40 mm of travel. Lee et al. [39, 40] repeated similar experiments with a similar diameter (25.4 mm) and longer tube (254 mm), with a stronger explosive initiating charge of C4 explosive (91% RDX). The shock wave was tracked with piezoelectric pins. Their results did not show any shock acceleration, instead, the shock decayed from over 4 km/s to 1.36 km/s in 50 mm of travel. In a relevant paper, Gurev et al. [22] suggested that shock acceleration should eventually be observed in the Mn+S system. Conversely, Batsanov and Gordopolov

[41] suggested that Mn+S may not be a good candidate for gasless detonation, arguing that Mn-S experiences an irreversible phase transition at high pressures which prevents the product density from being less than that of the starting mixture. This contraction could offset the volumetric dilation caused by the chemical energy release and prevent energy from being fed to the shock wave. Lending partial support to the experimental findings, Bolkhovitinov and Batsanov [42] estimated the theoretical detonation velocity in Mn+S to be approximately 2.77 km/s, which they compared to the 2.2 km/s reaction front of Jiang et al. [20].

The Zn-S mixture was further investigated experimentally by Gurev et al. [21], who measured the entrance and exit times of shock waves transmitted through Zn-S powder (3-5μm) mixtures with densities in the range 59.4-71.6% TMD. The powders were packed in cylindrical charges 16.5 mm in diameter and between 40 and 200 mm in length that were initiated by a TNT/RDX charge (height: 35 mm, diameter: 40 mm). The exothermicity of the Zn+S reaction is similar to that of Mn+S (for the Zn+S$\rightarrow$ZnS reaction, ΔH = -2.09 kJ/g). By comparing average shock speeds in charges of different lengths, they concluded that the shock initially decelerated to 1.3 km/s in samples shorter than 60 mm but then accelerated from 1.4 km/s to values oscillating near 2.2 km/s in charges longer than 100 mm. The apparent acceleration of the shock was "regarded as experimental evidence for the occurrence of solid-state detonation in the system under study" [21], providing perhaps the most direct claim of gasless detonation being observed.

In a re-examination of the average velocities in Zn-S reported by Gurev et al. [21], a position-time (x-t) diagram of the measured wave trajectories (Fig. 8) was made, and a statistical scatter in the data becomes apparent. Any systematic acceleration (concave curve) or deceleration (convex curve) of the wave cannot be concluded. The scatter in their data may be a result of large variations in their starting densities, or perhaps spurious signals from the contact gauges used, rather than due to an accelerating and oscillating shock front. Nevertheless, subsequent papers have attempted to correlate the observed shock velocity (2.2 km/s) with predicted detonation velocities (2.56 km/s in [42]) as well as to explain the oscillatory behavior of the shock velocity [41]. Lastly, Batsanov [43] estimated the sound speed of the powdered Zn+S mixture to be in the range 0.53-0.77 km/s, which led him to conclude that the measured 2.2 km/s wave was supersonic.

In the light of the uncertainty regarding claims of gasless detonation, an effort was made to reproduce the most compelling claims. While attempts to observe gasless detonation have been performed in gasless or low-gas production compositions such as Zn+Te [22] and Aluminum+Teflon [44, 45], the focus of the current effort was on the metal-sulfur systems. Part of the effort was dedicated to repeating the experiments of Gurev et al. [21] for low-density (porous Zn-S) mixtures. To increase the chances of observing detonation, additional experiments were performed on higher density (low porosity) samples of Mn+S and Zn+S, prepared using the same technique as in [20] and [46]. Larger diameter charges were also tried to help mitigate the effects of slow kinetics, and long charges of at least 200 mm were used to ensure that detonations could propagate over a sufficiently long distance to stabilize.

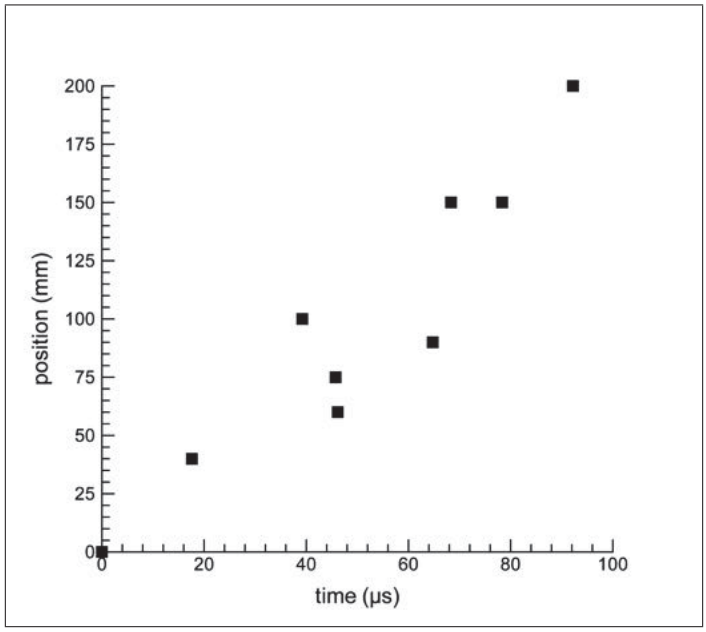

Figure 8: *Time of arrival data from Gurev[21].*

4.2 Experimental Details

The experimental setup is illustrated in Figure 9. Stoichiometric mixtures of Mn+S and Zn+S (1-5 μm metal, -100 mesh sublimed sulfur (<149 μm)) were prepared in cardboard tubes with an inside diameter of 50.8 mm. The high-density test samples were prepared as described in [47]. The metal and sulfur powders were thoroughly mixed in a roller mill and then heated until the sulfur began to melt. This mixture of metal powder suspended in melted sulfur was poured into the cardboard tube and left to solidify as it cooled. Using this method samples with density in the range 81-88% TMD were obtained. The low-density test samples were prepared by hand-compacting the well-mixed powder inside the cardboard tube. With this technique, sample densities of 59-66% TMD were produced. To ensure uniform density throughout the sample, the tube was filled in about 200-g increments, and compaction was performed using a plastic rod after each increment. All samples were filled from the bottom, in order to guarantee that the top surface was flat and uniform.

Piezoelectric shock pins (Dynasen CA-1135) were installed at various locations along the samples as shown in Figure 9. For low-density powder tests, the shock pins were inserted in the sample simply by pushing them into the sample. For the high-density tests, the shock pins were glued into position before the samples were cast. The shock pins were installed such that their tip containing the piezoelectric crystal would be at the centre of the charge, so as to measure the earliest appearance of the curved shock front at every given axial location. When inserted as shown, the shock pins produced a negative voltage signal when the shock reached their location. Since the PZT-5A piezoelectric crystal of the shock pin is shocked on its side, a slight decrease in sensitivity (by approximately a

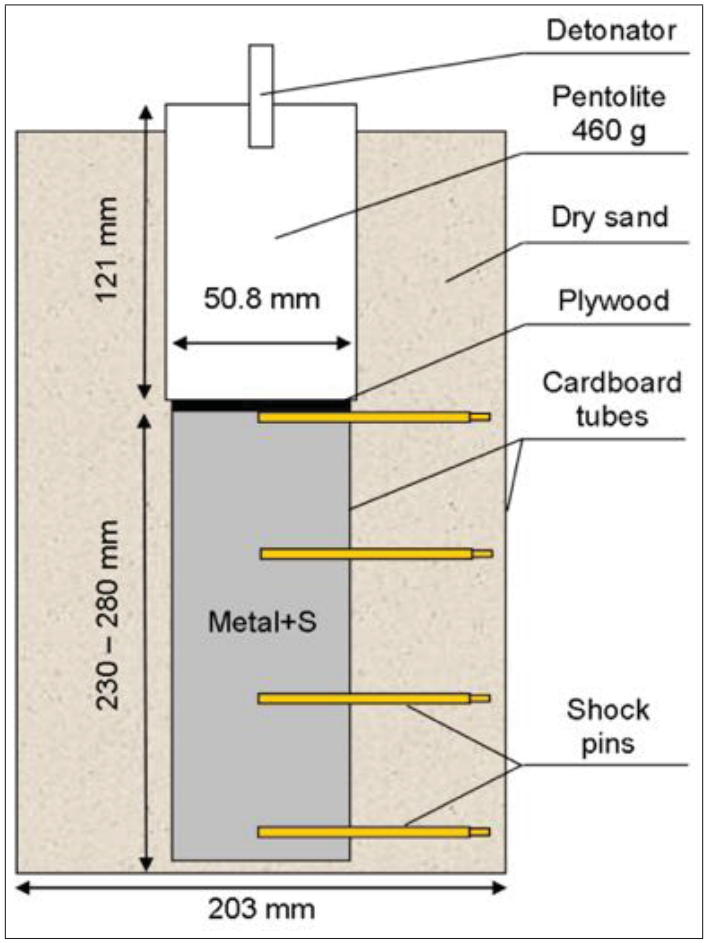

Figure 9: *Experimental arrangement used to test detonation propagation in powder samples showing donor explosive, acceptor test mixture, and diagnostic gauges.*

half) and a reversal of signal polarity occurs compared to a shock pin loaded on its tip [39]. In laboratory tests, the response of shock pins loaded sideways was found to be as fast as shock pins loaded on their tip in PMMA at pressures below 6.5GPa. Considering that those sensors are extremely sensitive, placing them sideways causes no significant loss in sensitivity and/or response time for the work performed here.

A 50.8 mm diameter, 121 mm long, 460 g charge of pentolite (50/50 TNT/PETN, Dynonobel D45) was placed on the test sample. A thin, 3-mm thick layer of plywood separated the two to prevent direct contact between the pentolite detonation products and the metal-sulfur sample. An electric detonator was used to detonate the pentolite charge. A fiber optic was inserted into the top of the pentolite charge and a photodiode monitored the onset of detonation. This photodiode signal was used to trigger all instrumentation (all data shown in the next section is referenced to this triggering time).

A cardboard tube with an inner diameter of 203 mm was placed such that the explosive/sam-

ple assembly was centrally located inside, and the empty space between the assembly and the cardboard tube was filled with sand. The sand provided a moderately strong confinement for the test samples, thus reducing the lateral pressure losses, which should reduce the rate of shock attenuation. Because of the low speed of sound in sand (see for instance [48]), no precursor waves could affect the shock propagation in the samples or disturb the sensors prior to the arrival of the shock in the test sample. Finally, the sand surrounding the explosive charge helped contain the detonation products, preventing them from damaging the coaxial cables used to carry the shock pin signals to the recording oscilloscopes (Lecroy Wavesurfer 424).

4.3 Results and Discussion

Sample voltage traces from the piezoelectric shock pins obtained in high-density samples of 81-88% TMD are shown in Figure 10. The traces are spread along the vertical axis with arbitrary amplitudes to display all signals in the same plot in a clear in distinguishable manner. Only the time-of-arrival information was inferred from the signals. Signals from broken gauges were truncated for presentation clarity. The very sharp signals like those at the bottom of Fig. 10a and Fig. 10b have been attenuated by a factor of 2 to 4 for displaying purposes. The vertical offset between the various signals represents the nominal distance between the shock pins, in inches. For example, in Fig. 10b, the first shock pin was located at 0 from the pentolite charge, while the others were located at 4 in. (101.6mm), 8 in. (203.2mm), and 11 in. (279.4mm), respectively, from the pentolite charge. At

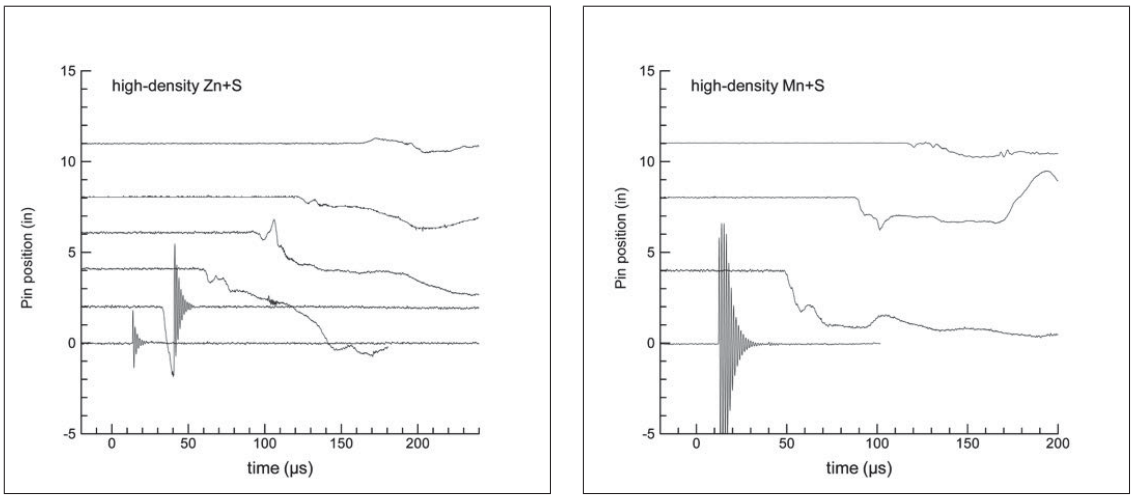

(a) (b)

Figure 10: *Sample signals from shock pins in high-density powder-filled tubes of a) Zn+S mixture, b) Mn+S mixture. The units on the vertical axes indicate the position of the gauge along the tube. The signal amplitudes are arbitrary.*

locations near the pentolite explosive, the shock wave caused a sharp signal spike typical for a piezoelectric crystal breaking under an intense shock. As the wave moved down the

sample, the signals became much more continuous, which implies that the shock pin crystal was not destroyed. Note that since these signals were less sharp, the error in determining the time of arrival of the wave is slightly greater for those signals than for sharper signals. The amplitude of the signals also decreased as the travel distance increased. This implies that the shock was decaying into an acoustic wave.

Sample traces from the piezoelectric shock pins obtained in low-density samples of 59-66% TMD are shown in Fig. 11. As done for Fig. 10, the very sharp signals have been attenuated by a factor of 2 to 4 for displaying purposes. Just as with the high-density samples, the shock quickly decayed into what appears to be an acoustic wave of decreasing amplitude. At the farthest shock pin from the pentolite donor (279.4 mm or 11 in.), the pressure had decayed below the level of detection of the transducer.

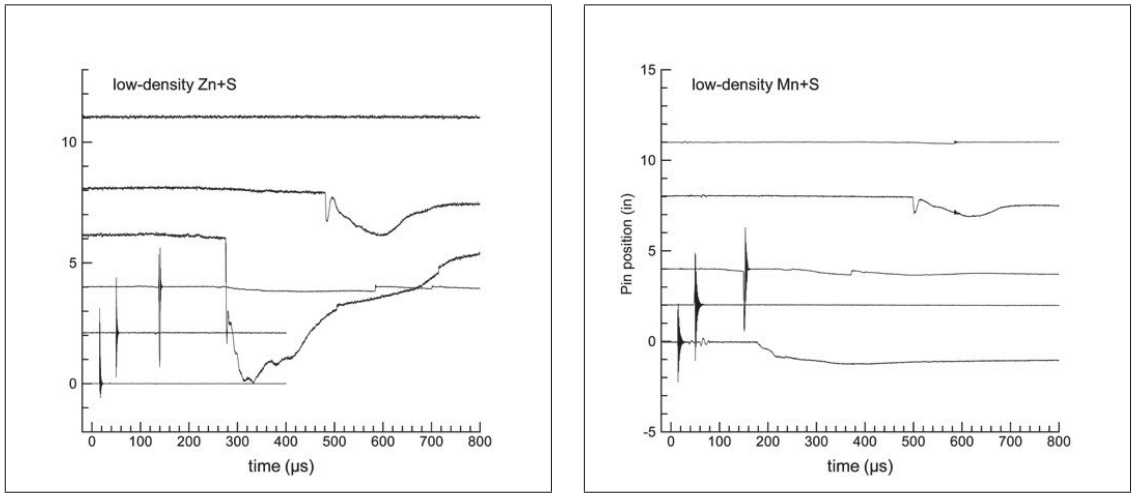

(a) (b)

Figure 11: *Sample signals from shock pins in the low-density powder-filled tubes of a) Zn+S mixture and b) Mn+S mixture.*

Figure 12 shows a summary of all the wave times of arrival for all the tests performed with high-density samples. As shown by the straight dashed lines drawn on the figure, the wave velocity appears to decay rapidly (i.e. in less than 150 mm of travel) to a steady value of about 2.5 km/s for the Mn+S mixtures and 1.8 km/s for the Zn+S mixtures. No re-acceleration of the wave was observed at positions beyond 150 mm.

If the inert shock Hugoniot of 100% TMD Mn+S is computed using the mixture method in [49] it is found that the intercept of the linear fit to the Hugoniot in the U_s-u_p plane (i.e. shock speed as a function of particle velocity) is 2.5 km/s. This intercept is usually close to the sound speed of the material. The wave velocity of the decayed shock in the experiments was also close to this value. For Zn+S mixtures, the sound speed estimated from the intercept is 2.16 km/s. This value is slightly greater than the 1.5 km/s obtained for the Zn+S experiments, but the test mixtures had a density slightly less than 100% TMD.

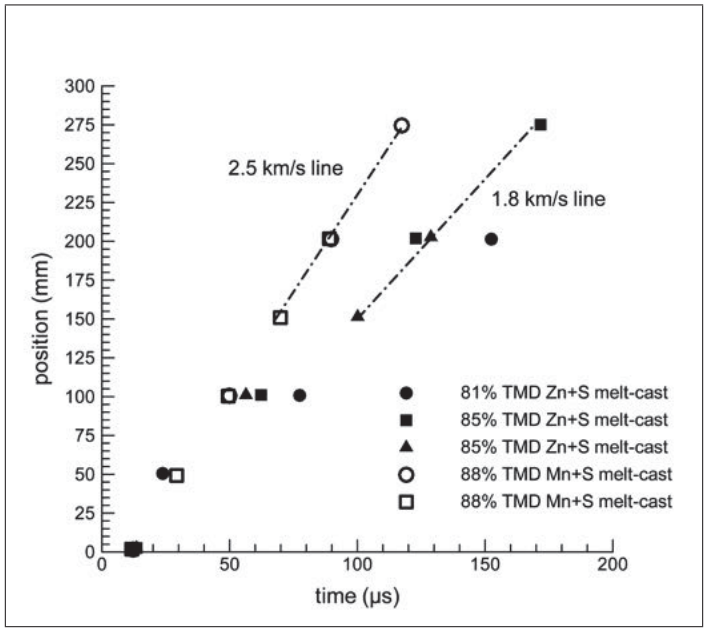

Figure 12: *Sample signals from shock pins in a a) low-density Zn+S powder-filled tube, and b) low-density Mn+S powder-filled tube.*

Overall, it appears that for both mixtures, the wave had decayed to an acoustic wave whose velocity was very close to that estimated from the intercept.

It is apparent from Fig. 12 that one Zn+S sample had a lower density than the other two that were tested. This sample exhibited a faster decay and a lower final velocity consistent with the expectation of a lower sound speed in a less dense mixture. This data also demonstrates that there could be large differences in the arrival times of waves in samples of varying densities.

Figure 13 shows a summary of all the wave times of arrival for all the tests performed with low-density (high-porosity) samples. As shown by the straight dashed line drawn on the figure, the wave velocity appears to decay to a steady value of about 0.22 km/s for both powder types. As with high-density charges, no re-acceleration was observed, in contrast with the results of Gurev et al. [21].

The final wave velocity measured in this work agrees with the theoretically-estimated sound speed of 0.53 km/s-0.77 km/s estimated by Batsanov [43] for 67% TMD Zn+S.

A section 50 mm to 160 mm in length from the bottom of the test sample was recovered intact and completely unreacted for each high density mixture tested. For samples that were 230 mm long, the last 50-90 mm of the sample were recovered, while for the 280 mm long charges, the last 80-160 mm were recovered. The decayed shock had thus become too weak to to initiate reactions. Unfortunately, for low-density mixtures, the samples could not be recovered after a test, as the cardboard and sand confinement failed to preserve the

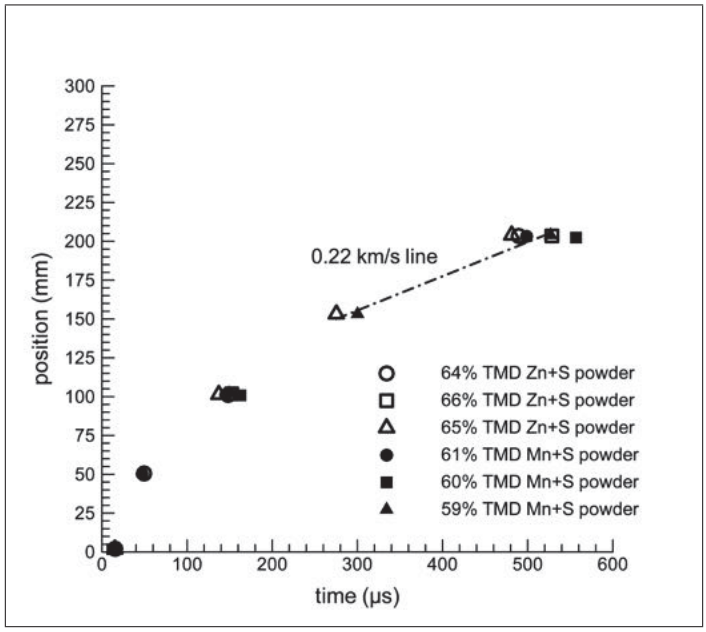

Figure 13: *Sample signals from shock pins in the low-density Mn+S powder-filled tube.*

sample material characteristics. It was thus not possible to determine the extent of reaction in these tests.

In recovery tests performed using explosively shocked ampoules in the laboratory [47], the high-density Mn+S mixture was found to be easily initiated by relatively weak shocks ($\sim$2 GPa). At the same time, it was also discovered that almost no exothermicity was observed via luminosity measurements in the first 100 μs following shock transmission into that same mixture [50]. Thus, from these results, it is believed that while reactions may be initiated locally by the shock wave which produces small hot spots at density discontinuities, the bulk of the reaction propagates as a classical thermo-diffusive flame. It is therefore postulated that in this test series, reactions may have been initiated locally near the pentolite explosive charge where the shock is strongest, and propagated slowly by a diffusive mechanism. As strong lateral expansions stretched the sample, the liquid reacting parts were blown off the unreacted parts, thus leaving an unreacted stump in the case of high-density samples or nothing at all in the case of the low-density samples. Had a stronger confinement been used, it is likely that one would have recovered reacted ZnS or MnS, as Gurev et al [21] reported.

4.4 Conclusions and Outcomes

In contrast with the results reported by Gurev et al. [21], shock acceleration was not observed in Zn+S mixtures, nor was it in Mn+S mixtures. The charges were weakly confined with a diameter of 50.8 mm. Instead, a decaying shock that rapidly stabilized near the sound velocity was observed in the material. This decayed wave became too weak to ignite

reactions near the base of the denser samples.

Since the sample diameter in our experiments was three times that in the experiments of Gurev et al., it should have been at least as likely, if not more, to observe detonation in the present tests since lateral expansion quenching was reduced. Since detonation was not observed, the new type of fast reaction or transport mechanism suggested by Gurev et al. [21] cannot be confirmed or supported.

A closer examination of the results of Gur'ev et. al. [21] shows a random scatter in the wave velocity (Fig. 8) rather than a systematic increase. In addition, the dependence of velocity on packing density, as observed in the present tests, suggest that variations in packing density may be partially responsible for misleading velocity fluctuations. Based on this re-examination and the results of the present investigation, it is premature to claim the existence of a well-established, steady-state gasless detonation by definition, and the observation of a new type of fast reaction or transport mechanism to drive the wave does not appear to be well-supported.

5 Screening of Gasless Reactive Mixtures

5.1 Introduction

This section documents shock initiation experiments on gasless reactive powders performed at DRDC Suffield by the present author. The two main objectives of this study were to study the propagation of reactive waves over long distances (up to ten charge diameters) in gasless reactive powders, and to experimentally screen a number of mixtures for potential as gasless detonation candidates. Portions of this work were published in [39, 40].

The screening of a number of mixtures was performed by performing measurements of the propagation of shocks into long tubes of powder mixtures to allow the observation of wave decay or acceleration as found by [21]. The reactive mixtures were composed of micron-size powders composed of mixtures of various reactive components. Using a high-explosive (C-4) booster, a shock was introduced into the powder mixture across a metal separator plate in a donor-acceptor configuration. It was expected that the shock would either propagate or accelerate in the more reactive mixtures or decay in the less reactive mixtures. This test is similar to a direct initiation experiment in gas phase detonations or a donor-acceptor shock sensitivity test for high explosives, and was chosen as a means to set up an overdriven detonation wave structure in a test mixture to observe whether the wave would decay to a steady-state stable detonation or decay and eventually extinguish itself. From the results, the most reactive mixtures could be selected as the best candidates for gasless detonation.

5.2 Experimental Details

5.2.1 Test Apparatus

The charges were made by filling steel tubes with the unreacted powder mixtures (Fig. 14a). The tubes had an inner diameter of 26.7 mm, and a length of 254 mm, i.e. ten charge

diameters. The wall thickness was 3.6 mm. A booster charge of C4 explosive composed of 91% RDX was placed on top of the tube to provide a strong initiating shock. The booster had a diameter identical to that of the steel tube, and a length of 127 mm, thus generating a nearly planar shock for initiation. A 0.5 mm thick steel plate was placed between the booster and the powder mixture to isolate the powder from the hot gaseous products from the high-explosive detonation in the early stages of shock transmission into the powder.

Diagnostic measurements were made using embedded gauges along the inner wall of the steel tubes to measure the time-of-arrival of the shock and reactive fronts (Fig.14b). PZT shock pins were used to measure the arrival of the shock, 66 μm glass core fiber-optic cables were used to measure the arrival of the luminous reactive front, and fine-wire thermocouple gauges (not shown in Fig. 14b) were used to measure the arrival of the heat front from the reaction. The thermocouple gauges consisting of 1.6 mm bead K-type thermocouples were used based the method described by Jetté et al. [51] as applied to recovery capsules. All cables entered the tubes from the bottom and were bonded to the inside wall.

(a) (b)

Figure 14: *a) Charge consisting of a steel tube filled with reactive powder and a booster charge on top (in white); b) arrangement of shock pins and fiber-optic cables.*

5.2.2 Reactive Systems

The reactive mixtures fell into three categories: metal-sulphur systems, inter-metallic systems, and thermite mixtures. For metal sulphur systems, Zn-S, Mn-S, Al-S, and Al-Mn-S were tested. For the inter-metallic systems, Ti-Si, Zr-Al, Zr-B, Ti-B, and Al-Ni were tested. For the thermite mixtures, Al-CuO, Mg-CuO, Al-MoO_3, Al-Fe_2O_3, and Al-Fe_2O_3-Al_2O_3 were tested. For the titanium (Ti), silicon (Si), amorphous boron (B), aluminum (Al),

copper oxide (CuO), and molybdenum trioxide (MoO_3), the purity of all powders exceeded 99% and particles were of irregular shape. A mixture porosity between 47% and 53% was obtained by tamping the powder into the charge container.

5.2.3 Size Distribution Measurements

A size distribution analysis was performed on the powders by laser light scattering with a Malvern system. The volume-weighted mean diameter of the Ti, Si, and Al powders was found to be 31 μm, 15 μm, 9 μm, respectively. Typical size distributions for titanium and silicon powder are shown in Figure 15.

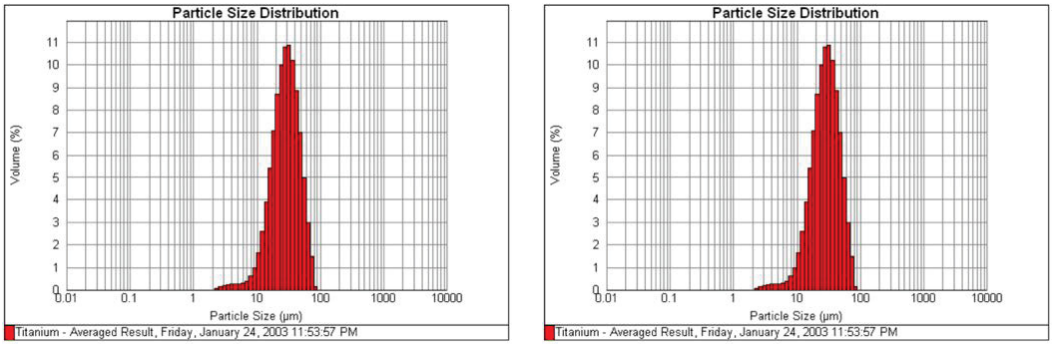

(a) (b)

Figure 15: *Size distribution measurements using a Malvern laser-scattering system for a) titanium powder, and b) silicon powder.*

The B, CuO, and MoO_3 powders did not yield reliable size distribution measurements, however all were found to pass a 45 μm sieve (325 ASTM designation).

5.3 Results and Discussion

The shock pin and fiber-optic gauges provided time-of arrival information for the shock and luminous fronts respectively. The general appearance of the signals was similar to that described by Lee and Zhang [39] and are shown in Figure 16.

The thermocouple gauges were found to respond to the passage of the shock by showing a small increase in voltage. Unlike recovery capsule tests [51] where the thermocouples were fixed to the end wall of the capsule cavity, the gauges were positioned along the side wall, which likely subjected them to additional shear stresses and consequently shortened the lifetime and duration of a useful recorded signal. The gauges were useful in identifying the initial temperature rise due to the shock, but unfortunately they did not survive long enough to show late burning effects several hundreds of milliseconds later.

As in previous work [39, 40], both shock and light signals were observed at the beginning of the charge, decreasing in amplitude after a propagation distance of up to about five

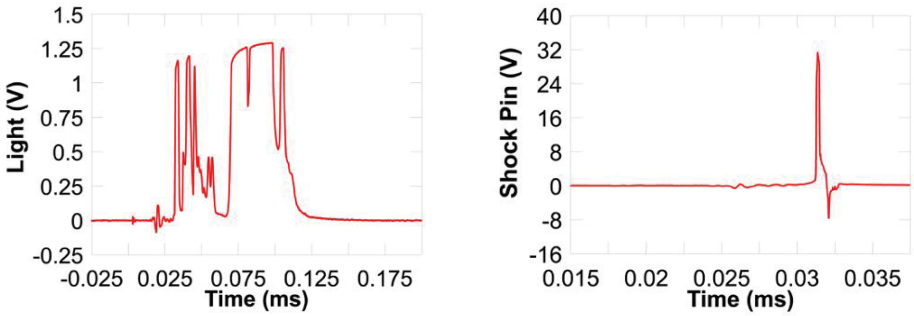

(a) (b)

Figure 16: *Time-of-arrival signals from a) fiber-optic gauges, and b) shock pins.*

tube diameters depending on the mixture. Typical time-distance diagrams for Ti-B and Al-CuO mixtures are shown in Figures 17 and 18, where the time-of-arrival signals from the optical fibers and shock pins are plotted as a function of propagation distance. For all mixtures, both the light and shock signals were found to initially coincide after the shock entered the powder mixture at about 4 km/s. After a certain propagation distance, the luminous zone appeared to decouple as the luminous front started to lag behind the shock wave. This behavior is similar to tests performed in manganese-sulfur mixtures where wave failure was also observed after a certain distance of propagation [20, 46], and emphasizes the necessity of sufficiently long charges to observe true self-sustained propagation rather than an initiation transient. The luminous front in the present tests with longer charges appeared to quickly decelerate and lag far behind the shock for the Ti-Si and Ti-B mixtures, while for the Al-MoO_3 and Al-CuO mixtures, the luminous front decelerated more gradually.

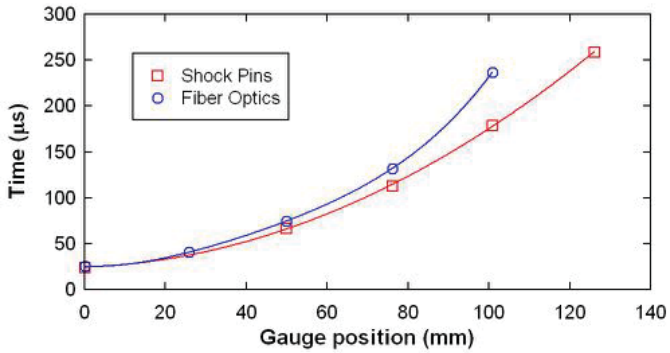

Figure 17: *Propagation of the reactive wave in a Ti-B mixture plotted as a time-distance diagram.*

Microscopic examination of the post-trial charges showed a complete change in powder morphology with indications of widespread melting, suggesting nearly complete reaction. Pre-

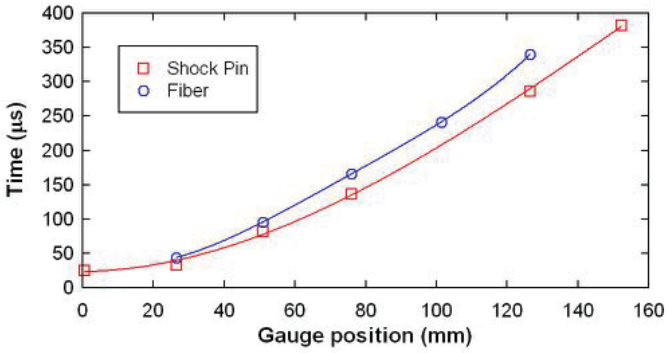

Figure 18: *Propagation of the reactive wave in a Al-CuO mixture plotted as a time-distance diagram.*

liminary X-ray diffraction (XRD) measurements of selected post-trial products confirmed the presence of reaction products. For example, the Ti-Si products showed the presence of Ti_5Si_3 (Fig. 19) as found by Thadhani et. al. [52], however the peak counts were extremely low, suggesting a highly textured microstructure or low phase composition. The peaks for Ti-Si products from a thermally-initiated sample which burned through a slow diffusion flame process are shown for comparison. These mixtures were ignited with an electric hot wire. The other curves show XRD of product samples taken near the high-explosive booster and at the other extremity of the tube furthest from the booster charge. The peak counts for the thermally-iniated sample were slightly higher but also very low. The peaks from the two shock-initated samples were nearly identical, indicating the reaction process was uniform throughout the charge. Further analysis is necessary to evaluate the composition and uniformity of the shock-initiated products.

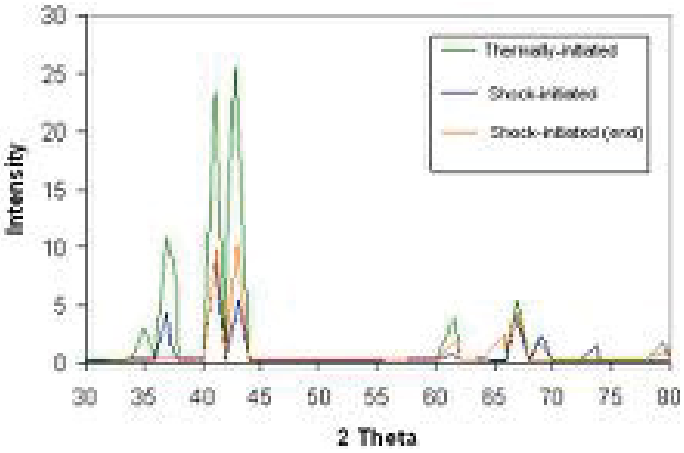

Figure 19: *XRD of post-trail products from thermally and shock-initiated Ti-Si powders.*

A significant portion of the reaction was found to occur long after passage of the shock front.

This was observed on video recordings of the experiment which showed a luminous flash burn of the wood at the base of the charge 2-3 seconds after initiation of the high-explosive booster (Fig. 20). The moment of flash burn occurred when the slow diffusion flame in the mixture reached the bottom of the charge and transferred temperatures of over 1500 K to the wooden base. Hot gases, presumably from air trapped in the inter-particle pores were also observed to exit the top of the charge from the moment of initiation. This clearly indicates that reaction did not reach completion in the shock timescale although the light signals from the fiber-optic gauges indicated at least partial reaction and coupling to the shock front.

Figure 20: *Late-time burning of a titanium-silicon mixture showing hot gases exiting both ends of the tube.*

These results suggests that two reaction mechanisms: shock-induced reaction and shock-assisted reaction as described by Eakins [1, 53] are occurring in sequence in the powder mixtures investigated in this study. The shock-induced reaction first occurs at microsecond timescales where a portion of the reactants burns behind the shock front. The mixture subsequently proceeds to completion at a much later time after shock unloading of the mixture. This bulk exothermicity constitutes a shock-assisted burn mechanism where the bulk of the energy release takes place as a slow diffusion flame. This late-time burning has been observed directly with temperature measurements in recovery capsules by Jetté et al. [51], where the bulk of the heat release was observed 50-200 ms after shock initiation in Ti-Si mixtures.

5.4 Conclusions and Outcomes

The shock-initiated solid-phase, i.e. gasless, reaction of several energetic powder mixtures has been observed. Embedded gauges were used to observe a sharp pressure front and a luminous front, suggesting shock-induced reactions at short microsecond timescales. A short coupled region is observed where the pressure and luminous fronts propagate close together, then decouple as the leading shock wave distances itself from the luminous front. In addition, a second shock-assisted portion of the reaction is also observed at a much longer timescales, on the order of seconds, as indicated by video recordings. Thus, two types of shock-initiated chemical reaction are observed, but the lack of a sustained supersonic wave indicates that the amount of energy released at short timescales is insufficient to support the leading shock.

From a gasless detonation perspective, none of the mixtures tested was able to support a supersonic reaction, however the densities of the packed powder mixtures may have been too low to allow the reaction energy to feed the leading shock (cf. 3.4).

6 Shock Initiation Limits

6.1 Introduction

The present section presents an investigation of shock initiation limits for gasless reactive systems. This work was performed in collaboration with F.X. Jetté et al. at McGill University, and portions are published in [55].

Although extensive research has been performed on the subject of shock initiation of energetic reactive powder mixtures, such as thermites, pyrotechnics, and Self-Propagating High-Temperature Synthesis (SHS) materials, the mechanism responsible for this initiation is still not well understood. Factors that have been found to influence the shock sensitivity of a sample include: power morphology and particle dimensions [56, 57, 58, 59, 51], stoichiometry [57], porosity of the mixture [58, 51, 60], and mechanical activating techniques such as arrested ball-milling [60, 61]. Although there appears to have been little systematic study on the effect of the relative impedance between the two components on their reactivity, it is usually considered that materials with similar impedances would mix more intimately (as both components would deform) and react more readily [53].

The importance of those factors, along with the fact that bulk shock heating in powders is typically well below the threshold for onset of thermal initiation of reactions, suggests that prompt initiation depends on the mechanical action of the shock wave. At material or density discontinuities, shock waves cause large local stress concentrations, which give rise to severe plastic deformations and material flow, material impacts, large temperatures, etc. It is unclear whether reactions are initiated directly via mechanical mixing on the shock pressure relaxation time scale (ns to μs), or via thermally-induced reactions that subsequently propagate from the locally heated region (or hot spot) to the remainder of the material on the temperature equilibration time scale (μs to ms).

In high explosives, the initiation process is dominated by the ignition and growth of hot spots. The volume of hot spots is typically very small compared to the total volume of explosive. The bulk of the explosive is therefore consumed by deflagration fronts originating at hot spots, whose velocity increases with increasing pressure.

In powder mixtures, deflagration velocities are typically independent of pressure (and relatively slow as a consequence) and limited by diffusive mixing of the components. If the hot spot ignition and growth mechanism were applicable to reactive powders, bulk reaction rates should be slower than in high explosives. However, if the mechanical action of the shock wave results in significantly enhanced mixing, much greater bulk reaction rates can be expected. In order to elucidate the initiation mechanism, the relative portions that are initiated directly by the shock and by the growth of hot spots must be quantified. The reaction rate of the overall reaction may provide important clues to solve this problem.

Various test methods have been used to study the reaction mechanism of powder mixtures: recovery experiments that preserve the shocked sample for post-shock analysis, pressure gauges, velocity interferometers, light detectors and pyrometers, high-speed cameras, and thermocouples.

The data published so far seems to suggest that initiation occurs via hot spots, and that the bulk of the material is consumed via propagating burning fronts over a relative long time on the order of milliseconds. The mechanical role of the shock may be limited to local effects at density discontinuities, such as producing high hot spot temperatures and good local mixing leading to fast reactions that prevent the hot spot from quenching.

However, there currently exists only limited published data encompassing the long time scales of diffusive/convective burning of the shocked samples. Light and temperature measurement techniques showed promise for directly observing the reaction buildup in reactive powders. Results of experiments using thermocouples on various mixtures, along with experiments that incorporate light detectors in addition to thermocouples, are presented in this chapter.

6.2 Background on Measurement Techniques

Various test methods have been used to study the reaction mechanism of powder mixtures: recovery experiments that preserve the shocked sample for post-shock analysis, pressure gauges, velocity interferometers, light detectors and pyrometers, high-speed cameras, and thermocouples. This section comprises a review of these experimental and diagnostic techniques.

6.2.1 Sample Recovery

The recovery method provides only limited information concerning the reaction mechanism or the reaction rate. Nevertheless, the evidence gathered using this technique suggests that the bulk of reactions occur via deflagrations, with the mechanical action of the shock being responsible only for initiation of the reactions in small zones (or hot spots).

In certain situations, a correlation between the threshold shock energy and autoignition enthalpy was observed [62, 63, 64], suggesting that temperature plays a key role in reaction initiation.

Evidence that products melted and subsequently re-solidified during the reaction process was also obtained; many pores were typically found in an otherwise homogeneous matrix of product [58, 65, 66]. In contrast, in samples that remained unreacted after being shocked near the threshold energy, no remaining porosity was observed. These findings indicate that once initiated, exothermic reactions and large temperatures usually spread to the entire sample.

In addition, although the Ti-Si mixture can be readily initiated at low shock pressures, virtually no mixing of the reactants occurs near the threshold shock pressure for initiation [59]. This suggests that few reactions and mixing are caused by the shock. Therefore, the bulk material must be consumed by a burning process rather than a mechanical initiation.

Past studies [67, 68] on Ni-Al powders suggest that reactions are initiated in very small hot spots, which then grow or quench depending on different factors. Sparse and localized reaction spots were observed in mostly unreacted zones whose bulk temperature (approximately 320°C) remained below alloying temperature. Thus, it appears that what the authors observed were quenched hot spots in the low-temperature regions of their samples.

6.2.2 Pressure and Material Velocity

In order to better observe the early stages of reaction onset and the overall reaction rate, in-situ observations are required. In-situ pressure measurements have revealed pressures slightly in excess of those expected for an inert shock in Ni-Al [69, 70]. In pyrotechnic mixtures, shock pressure was found to decay in unreacting samples and intensify in reacting samples [64]. Velocity interferometry on shock initiated $TiH_{0.65}$+$KClO_4$ showed essentially no evidence of reaction in the first microsecond, but a very slight increase in material velocity was observed after 2-3 μs [71]. On the other hand, no evidence of reactions in pressure and material velocity profiles was seen on an impact-sensitive mixture of aluminium and potassium perchlorate [72]. Since reacting powder mixtures do not typically generate large pressure, material velocity, or volumetric changes, in-situ measurements present a significant challenge.

6.2.3 Shock Velocity

Another approach that makes use of pressure gauges consists of recording simultaneously pressure and shock velocity to obtain a shock Hugoniot data point. If reaction occurs within the shock pressure equilibration time scale (ns to μs), this data point can deviate from an estimated inert Hugoniot depending on the amount of material reacted. Using this method, no evidence of fast reactions was found for mixtures of 3Ni+Al, 2Al+Fe_2O_3, Mo+2Si, and equivolumetric Ni+Al (spherical) [3, 73, 74, 75]. On the other hand, in powder mixtures of 5Ti+3Si, Ni+Ti, and equivolumetric Ni+Al (flaked Ni and spherical Al), the measured Hugoniot data points deviated slightly from the estimated inert behavior [3, 52, 76, 75, 77].

However, the deviations were very small and within the range of uncertainty of the estimated inert Hugoniot. It was concluded that only a small amount of material has reacted near the shock wave.

Another method based on the assumption that fast reactions influence the shock velocity consists of tracking the trajectory of a shock wave in a long sample of powder mixture. If shock acceleration or steady-state propagation over a long distance was observed, the possibility of a reaction-supported shock exists. In Mn+S, only decaying shock waves were observed [20, 46]. Similar results were obtained in 5Ti+3Si, Ti+2B, 8Al+MoO_3, and 2Al+3CuO [39, 40]. High-speed video used in the experiments of [40] even showed that most of the reaction occurred on diffusion time scales (milliseconds to seconds). Shock acceleration in Zn+S was reported based on a sparse data set [21], but this result could not be reproduced in independent studies using a more reliable measuring technique in the same Zn+S mixture as well as in a Mn+S mixture [36].

In micron-sized, mechanically activated (via vibratory milling), aluminum-teflon mixtures initiated with very small explosive charges (10g), quasi-steady fronts with a velocity on the order of about 1000 m/s have been observed [44, 78, 79]. Due to the steadiness and speed of the fronts, the authors suggested the possibility of detonation. However, measured peak pressures were only on the order of hundreds of MPa, and such reaction front velocities could simply be the result of convective burning, as observed previously in nano-thermite mixtures where burning rates between 600 m/s and 1000 m/s are common [80]).

Although the shock velocity is relatively straightforward to measure, it does not provide direct observations of the reaction rate, and can be subject to interpretation. Previous work suggests that the bulk reaction is too slow to support the shock.

6.2.4 Light Emissions

Temperature and/or luminosity should provide a more direct means to experimentally determine the onset of reaction in highly exothermic mixtures. However, large local temperatures and strong light emissions can be observed in shocked powders (with or without gas in the pores) for many microseconds even in the absence of exothermic chemical reactions [81]. Nevertheless, optical measurements have shown that reaction onset often occurs within a few microseconds, although compared to inert simulants only a small difference in light intensity and temperature was observed in reactive mixtures. Horning et al. [82] monitored light emissions and temperature in shocked 2Al+Fe_2O_3 using a three-color pyrometer and an IR radiometer. They measured very high temperatures (>4000°C) that likely resulted from shocked gases in the pores of the sample, and they have not performed experiments with inert simulants for comparison.

Using a 4-color pyrometer, Boslough [83, 84] investigated the behavior of shocked pellets of nickel and aluminum powders. He also tested nickel powder alone as an inert simulant. Light intensity and temperature were found to decay more slowly in the reactive mixture, which could indicate that some local reactions were taking place. Furthermore, using the same pyrometer, Boslough [38] found bulk temperatures in shocked mixtures of aluminum and

hematite to be greater than that estimated with thermodynamic models, which suggests that some reactions must have taken place within the first 3 μs. Similarly to Boslough, Gryadunov et al. [85, 4] have observed greater light intensity in reactive mixtures of Ti+C than in an inert Ni+C stimulant, using a two-color pyrometer. The authors estimated the emitting surface to be 2-3% of the entire sample surface, which implies that only a very small fraction of the sample was initiated by the shock wave.

Batsanov [49] monitored light intensity and temperature in shocked mixtures of low-porosity (1-3%) Sn+S and inert SnS (8% porosity) using a two-channel pyrometer. The temperature in the inert mixture was lower and decayed faster than in the reactive one.

High-speed video recordings by Reeves et al. [87] have also revealed interesting features in the initiation of nanometric mixtures of Ni+Al powders compressed by a conical plunger. Their results seemed to show initiation of hot spots followed by growth of the initiation centers via a deflagration. At early times intense light appeared near the plunger and quickly disappeared; after 10 ms a bright area formed near the plunger propagated at a speed of approximately 8 cm/s away from the plunger. When the plunger velocity was increased [88], a bright luminous front propagating at a velocity of approximately 1000 m/s was observed, which suddenly stopped propagating after traveling for approximately 28 μs. This light probably resulted from shocked pores and ignition in the vicinity of the shock before it became too attenuated. The areas ignited by the shock remained luminous for slightly less than 49 μs.

6.2.5 Temperature via Thermocouples

Temperature measurements over a long period of time (tens of milliseconds or more) have been made with thermocouples. Thermocouples have a slow response and cannot resolve temperature on time scales shorter than milliseconds, but they can be useful in measuring the slow reactions that usually complete the consumption of the reactants. Using thermocouples, Batsanov et al. [89] found that reactions in Sn+S mixtures (10-30% porosity) contained in cylindrical ampoules had reached completion in less than 100 ms. In addition, Batsanov and Gurev [77] found that the bulk reactions in pre-heated (173°C) Sn+5S (50% porosity) shocked to 3.3 GPa were complete in 10 seconds. Thermocouple signals showed bulk reaction onset occurring 200 ms after the shock temperature jump in the work of Nabatov et al. [91] on Sn+S pressed to 4.3 g/cc and shocked to 16 GPa. These results imply that the bulk of the material is not initiated by the shock but consumed by a burning process after the sample pressure has been lowered to near ambient. The measured bulk reaction onset times may be indicative of the time required for the hot spots to coalesce.

6.3 Experimental Details

A specially-designed ampoule for recovery of shocked samples was used to investigate the initiation and burning properties of the reactive powders in this study. Pressures inside the ampoule during the shock-compression event was estimated using Finite-Element simulations, however dynamic measurements of the reaction progress were made using thermocou-

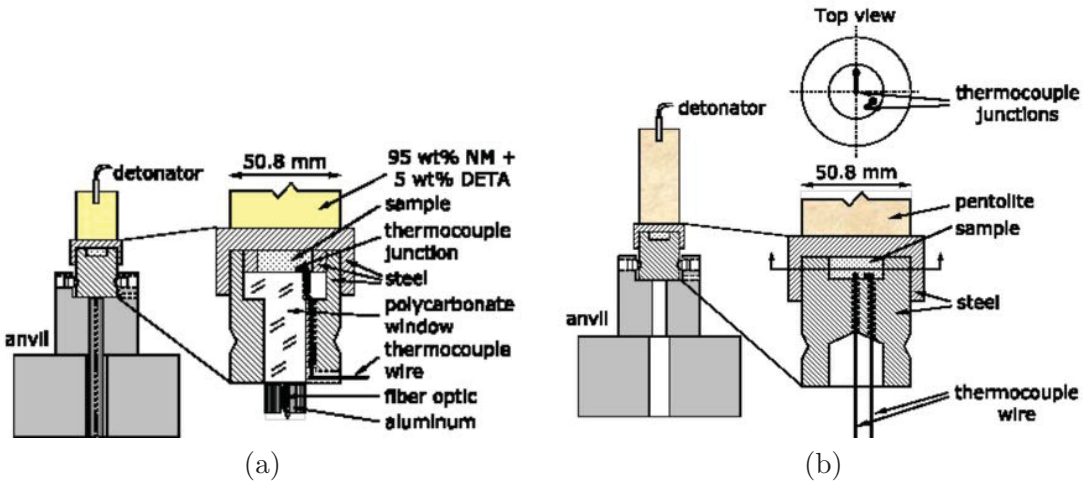

Figure 21: *Recovery capsule arrangement with a) optical diagnostics and thermocouples, and b) thermocouples alone.*

ples and pyrometry. The thermocouples consisted of K-type wire junction thermocouples embedded in the reactive mixture, and were designed to survive the shock phase of the loading in order to record reactions occurring at a later time. A 3-color pyrometer comprising photomultiplier tubes (PMT) was used to record light emissions simultaneously. Post-processing of the PMT signals was performed to infer the temperature. The raw PMT signals were also used as light intensity measurements. Finally, the post-trial samples were recovered for further analysis of the reaction products by visual inspection and Scanning Electron Microscopy images.

6.3.1 Recovery capsule

The experiments were conducted using the cylindrical configurations shown in Figure 21. The powder samples were hand-compacted (using a 25.4 mm diameter plastic rod struck firmly with a hammer) into a mild steel (hot-rolled) recovery capsule, similar to that of [47]. A strong shock wave was delivered to the sample by detonating a charge of high explosive in close contact with the test capsule. The test capsules were held rigidly in place in a heavy steel block/anvil using three strong set screws. After each experiment the sample remained sealed within the capsule, which was later cut open to allow post-shock analysis of the sample.

The cavity for the test powders was 25.4 mm in diameter. Cavities with a depth of 10 mm are shown in Figure 21a, but tests were also performed with cavity depths of 5.1 mm and 20.2 mm. The diameter of the bottom portion of the steel capsule that contains the test sample was 50.8 mm, while the outer diameter of the steel capsule cover was 63.5 mm. The thickness of the steel capsule cover between the sample and the explosive charge was 10 mm. Finally, the explosive charge diameter was 50.8 mm.

For the experiments that used thermocouples to monitor the reaction heat front (Fig. 21b),

the explosive charge was 450 g of commercial pentolite (Dyno Nobel Trojan Spartan 450, made with approximately equal amounts of PETN and TNT) with a thin layer of C4 (20g). The thin layer of C4 was used to fill small gaps between the base of the pentolite charge and the top of the test capsule, thus achieving a continuous mating between two so that spurious pressure spikes were minimized. For all experiments that included light detectors, the explosive charge was 130 g of a mixture of Nitromethane (NM) sensitized with 5wt% of Diethylenetriamine (DETA). The NM/DETA was contained in a PVC tube and sealed at its bottom with a thin Mylar sheet glued to the PVC with transparent silicone sealant.

In most experiments, 55 mm-diameter discs of acrylic, or polymethylmethacrylate (PMMA), were placed between the explosive and the steel capsule in order to control the shock pressure. A thicker disc attenuated the shock pressure before it reached the test sample.

The entire length of wire and fiber optic from the bottom of the test capsule to the exit port of the blast chamber was protected by passing it through a 12.7 mm hole in the anvil and using steel angle iron to cover the length of wire that linked the charge setup to the exit port. In addition, the wires and optic fibers were passed through a tygon tube for added protection.

It was found in this test series that all the samples either reacted fully or not at all. If the sample reacted, the steel capsule was to hot to handle by hand after the experiment while if it did not react, the capsule was only slightly warmer than room temperature. The capsule was retrieved after each experiment for analysis to determine more precisely the extent of reaction. In all experiments, visual inspection of the sample, as well as scraping of the sample with a screw driver were used to determine whether the sample was a compacted powder or a solid reaction product (products usually consisted of hard ceramics and/or alloys). In some cases, the sample was observed under SEM. The samples that contained sulfur were also placed on a hot plate and heated to approximately 200°C to see if any sulfur remained (sulfur melts at approximately 120°C).

The recovery method provides only limited information concerning the dynamic reaction mechanism or the reaction rate. Nevertheless, the evidence gathered using this technique suggests that the bulk of reactions occur via deflagrations, with the mechanical action of the shock being responsible only for initiation of the reactions in small zones (or hot spots).

In certain situations, a correlation between the threshold shock energy and autoignition enthalpy was observed [62, 63, 64], suggesting that temperature plays a key role in reaction initiation. Evidence that products melted and subsequently re-solidified during the reaction process was also obtained: many pores were typically found in an otherwise homogeneous matrix of product [58, 65, 66]. In contrast, in samples that remained unreacted after being shocked near the threshold energy, no remaining porosity was observed. These findings indicate that once initiated, exothermic reactions and large temperatures usually spread to the entire sample.

In addition, although the Ti-Si mixture can be readily initiated at low shock pressures, virtually no mixing of the reactants occurs near the threshold shock pressure for initiation

[59]. This suggests that little reactions and mixing are caused by the shock. Therefore, the bulk material must be consumed by a burning process rather than a mechanical initiation.

The results of [67, 68] on Ni-Al powders suggest that reactions are initiated in very small hot spots, which then grow or quench depending on different factors. The authors have observed in their recovered samples sparse and localized reaction spots in mostly unreacted zones whose bulk temperature (approximately 320°C) remained below alloying temperature. Thus, it appears that what they observed were quenched hot spots in the low-temperature regions of their samples (note that reactions do not self-propagate in Ni-Al mixtures that are not sufficiently pre-heated, due to their low heat release and large thermal conductivity).

6.3.2 Powder Sample Preparation

Both as-blended and mechanically activated mixtures were tested. The latter were prepared in inert argon or liquid hydrocarbon environments via the method of arrested reactive milling (ARM) using ball-milling machines. The ball-milling process was arrested just before self-ignition would occur (typically after 30-60 minutes, depending on the powder mixture). The ARM technique produces micron-sized particles containing both components of the mixture which are mixed at the nanometric scale (typically on the order of 100 nm). Although ARM mixtures contain particles as large or larger than as-blended mixtures, their burning speed is much greater due to the smaller segregation distances and greater contact area between the two components.

All the mixtures tested in this study are listed below:

- 5Ti + 3Si
- ARM 5Ti + 3Si
- Ti + Si
- ARM Ti + Si
- Ti + B
- ARM Ti + B
- Ti + 2B
- ARM Ti + 2B
- ARM Ni + Al
- 2Al + Bi_2O_3
- 2Al + 3PbO
- 8Al + $3Pb_3O_4$
- 4Al + Fe_2O_3
- ARM 4Al + Fe_2O_3
- ARM 8Al + MoO_3
- Mn + S
- Zn + S

The ARM powders were prepared by professor M. Radulescu's research team at the University of Ottawa, and professor E. Dreizin's research group at the New Jersey Institute of Technology. The as-blended mixtures were prepared by F.-X. Jetté and his collaborators at McGill University.

The micron-sized powders used to make the as-blended test mixtures are presented in Table 4. All powders were acquired from open commercial suppliers. The size specified by the supplier did not always agree with subsequent particle size measurements performed in the lab. For the pyrometry experiments, the Mn+S mixture tested was made with -325 mesh Mn, while all other Mn+S mixtures were made with the <10 μm Mn. The initial powder sizes for the ARM mixtures is not relevant since the mixing scale and actual particle size depend much more on the ARM process than on the starting powder morphology.

The powder mixtures were prepared by mixing the component powders in a bottle which was then rolled with a roller mill for several hours (>4) to uniformly mix the particles. The mixtures were then compacted into the test capsules for the as-blended samples, or processed in the ball-milling machine first before being compacted in the test capsules for the ARM mixtures. Finally, for mixtures of metal with sulfur, a high- density sample (>85% TMD) could be produced by heating the mixture until the sulfur component melted, and subsequently pouring the molten mixture into the steel capsule. This casting method is explained in more detail in [47].

Inert mixtures of WS_2 with S were prepared as an inert stimulant with mechanical properties similar to the Mn+S mixture. Because WS_2 is already a product of the reaction between W and S, no further reaction with S should result. Furthermore, since WS_2 has a density similar to Mn (7.5 g/cc for WS_2 vs 7.47 g/cc for Mn), a mixture of WS_2 and S can be made with similar mechanical properties to the Mn+S mixture if the volumetric content of S is similar in both mixture types.

Table 4: *Powders used for as-blended mixtures.*

Powder	**Specified Powder Size**
Al	3.5 - 15 μm
Al	-325 mesh
Bi_2O_3	N/A
PbO	-325 mesh
Pb_3O_4	N/A
Fe_2O_3	1-5 μm
Ti	-325 mesh
B	<5 μm
Si	-325mesh
Mn	<10 μm
Mn	-325 mesh
Zn	1-5 μm
WS_2	N/A
S	-325 mesh

6.4 Finite Element Modelling

In the absence of direct, in-situ pressure measurements in the samples, the pressure inside the capsule was calculated through Finite-Element simulations using LS-DYNA (Fig. 22). A Mie-Gruneisen equation of state was used along with the elastic-plastic-hydrodynamic material formulation for the test mixture. The numerical model consisted of a mixture Hugoniot (solid) using the component energy model [49]. More complex mixture rules such as the P-alpha model are also commonly used, however an examination of the relative accuracy shows the Batsanov model to be valid in spite of its simplicity [92]. The porosity was accounted for by using the porous mixture Hugoniot of Meyer [93]. The JWL equation of state was used for the explosives, with the parameters obtained from the output of thermodynamic equilibrium calculations using Cheetah [27].

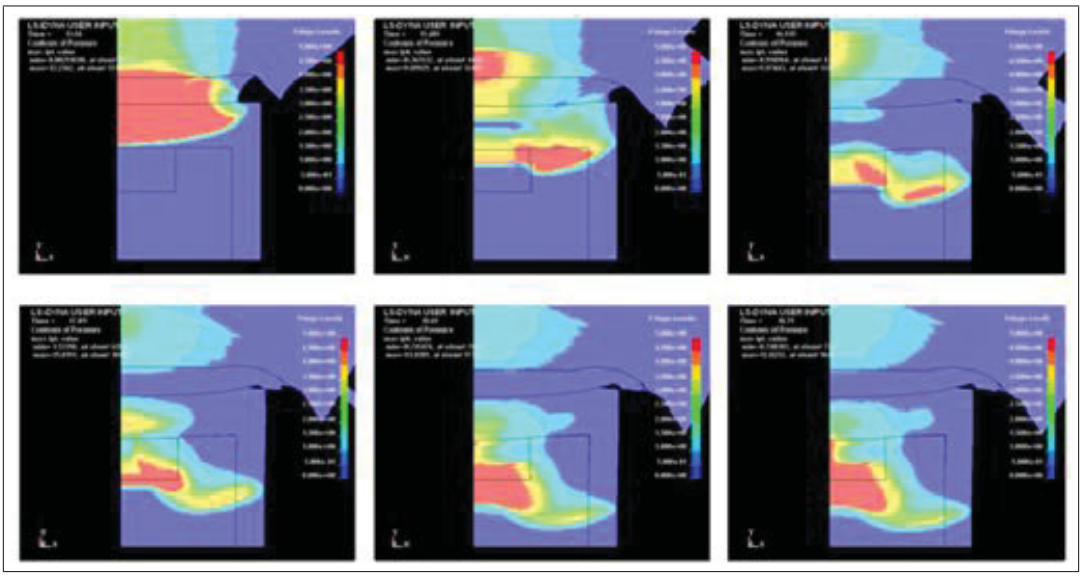

Figure 22: *Finite-Element simulation showing pressure contours for an encapsulated low-porosity Mn-S sample and an donor charge of 123.5g Nitromethane mixed with 6.5g Diethylenetriamine.*

The results show a highly non-uniform pressure field in the capsule due to multiple reflections, with a maximum pressure occurring at the bottom, in the centre. This maximum pressure was assumed to be the initiation pressure when interpreting the data in terms of shock initiation pressure limits.

6.5 Results and Discussion

The experimental results are discussed in three parts, focussing on the different diagnostic measurements. The first part discusses temperature measurements performed by pyrometry where a temperature was inferred from the reaction light. The second part discusses temperature measurements from embedded thermocouples in conjunction with simultaneous light

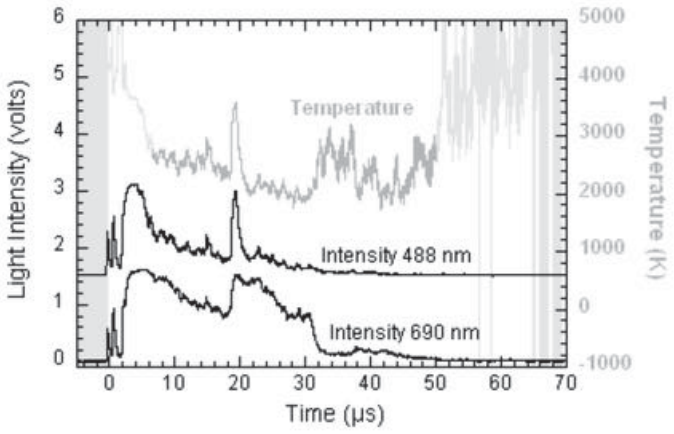

Figure 23: *Light intensity at two different wavelengths and temperature histories for a shocked Mn+S sample (93.3% TMD) for an incident shock of 5.3 GPa. This sample was recovered fully reacted.*

intensities measured by photomultiplier tubes (PMT). The third part discusses temperature results from embedded thermocouples in the absence of concurrent light measurements.

6.5.1 Pyrometry

The behavior of shocked samples at early times was studied using pyrometry. Tests were performed on dense (≈95% TMD) Mn+S with 0 mm PMMA attenuator (peak incident pressure in Mn+S sample ≈ 5.3 GPa). The -325 mesh Mn was used in those experiments. Photomultiplier tube (PMT) signals and the corresponding temperatures are shown in Figures 23 and 24. Time zero corresponds to the arrival of the shock wave as detected by the shock pin located at the bottom of the test sample. The same test was repeated with an inert WS_2+12.89S sample (≈92% TMD), and the signals are shown in Figure 25. The signals for the inert sample show that even with highly non-porous samples, light emissions are produced in the absence of reactions. These emissions produce an initial spike occurring very soon after shock arrival, then smaller peaks between 10 and 20 μs. The meaningful portion of the temperature signals (computed from the ratio of intensity signals that are neither saturated nor equal to the baseline signal) is highlighted with a darker color on the figures.

The light intensity signals with the inert stimulant (Fig. 25) are much weaker than those with reactive mixtures (Figs. 23 and 24), which implies that reaction onset occurs a few microseconds behind the shock wave. Furthermore, the temperature signal is less noisy for the reactive samples and shows a drop from an initially large value (near 5000 K), which suggests that reactions may be initiated by very hot spots. Temperature and light intensity decreased after approximately 30μs, as hot spots cooled down due to heat diffusion. Whether these hot spots quenched or grew cannot be ascertained from these signals as the sampling time was too short.

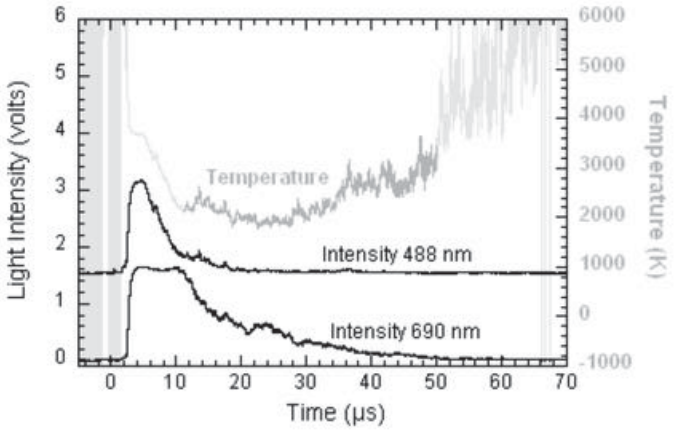

Figure 24: *Light intensity at two different wavelengths and temperature histories for a shocked Mn+S sample (95.9% TMD) for an incident shock of 5.3 GPa. This sample was recovered fully reacted.*

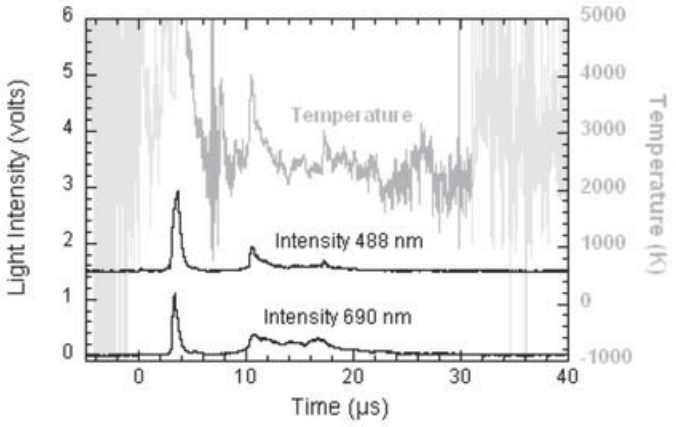

Figure 25: *Light intensity at two different wavelengths and temperature histories for a shocked WS_2+12.89S sample (92.1% TMD) for an incident shock of approximately 5.3 GPa.*

When thin discs (<6 mm) of PMMA are used to lower the pressure near 4.9 GPa, the signals for the reactive samples are similar to those for the inert simulant in Figure 25, and discussed by Jetté et. al. [50]. Thus, although the sample reacted in these tests (as confirmed by analyzing the recovered sample), reaction onset was not detected at early times. This suggests that either the reaction onset occurred after the recording time of a few tens of microseconds, or the number of hot spots ignited was too low, resulting in a light intensity too low to be detected by the PMT.

The light intensity observed can be compared to that from a measurement of the detonation front temperature in nitromethane made using the same pyrometer, with the same type and length of fiber optic whose viewing area is identical in both experiment types. The flame temperature (in ambient conditions) in the Mn+S powder mixture, based on pyrometric and spectrometric measurements, is on the order of 2000 K, while the detonation front in nitromethane has a temperature of 3600 K. If one assumes that both have a similar gray body emissivity, the ratio of light intensity for both reaction fronts is equal to $(\mathrm{T}_{NM}/\mathrm{T}_{Mn+S})_4 = 10.5$, which means that nitromethane detonation gives approximately 10.5 times the light intensity of burning Mn+S.

To prevent saturation of the photomultipliers, the gain was adjusted to be approximately one order of magnitude lower for the measurement of nitromethane detonation. The gain of the PMT was adjusted according to $dG/G = ndV/V$, where G is gain, n is number of dynodes (11 for the PMTs used in this work), and V is supply voltage. A supply voltage of 550 V was used for the nitromethane experiment and 700 V for the Mn+S experiments, producing a gain 14.2 times greater for the Mn+S experiments.

The light from the optic fibre passed through a collimator to straighten the light beam, then through an aperture before reaching the beam splitter that divides the light for the different PMTs. This aperture was set fully open for Mn+S shock initiation experiments, whereas it was set on the smallest opening (1.6 mm diameter) for measurements of nitromethane detonation temperature so that the area of the aperture was at least 16 times larger during the Mn+S shock initiation experiments.

Even though the light emitted by the Mn+S reaction should be only 10.5 times less than that from detonating NM, the pyrometer was set to be at least $16 \times 14.2 = 227$ times more sensitive in order to obtain good signal-to-noise ratio. If only the difference in black body emissions were accounted for (factor of 10.5), the amplitude of the signals (Figures 23) and 24, and 25 would be at least 20 times lower than shown. It is concluded that the luminous area in the Mn+S experiments must have been less than the sample area viewed. It was also found that a flame propagating in Mn+S would saturate the pyrometer if the aperture is kept fully open as in the shock initiation experiments. Overall, these observations indicate that only a relatively small portion of the emitted light is captured in the experiments shown in Figures 23, 24. Consequently, the pyrometry observations are consistent with reaction initiation taking place at a few local hot spots which slowly grow. Only the strongest pressure tested generated enough hot spots for light emissions to be detected within microseconds.

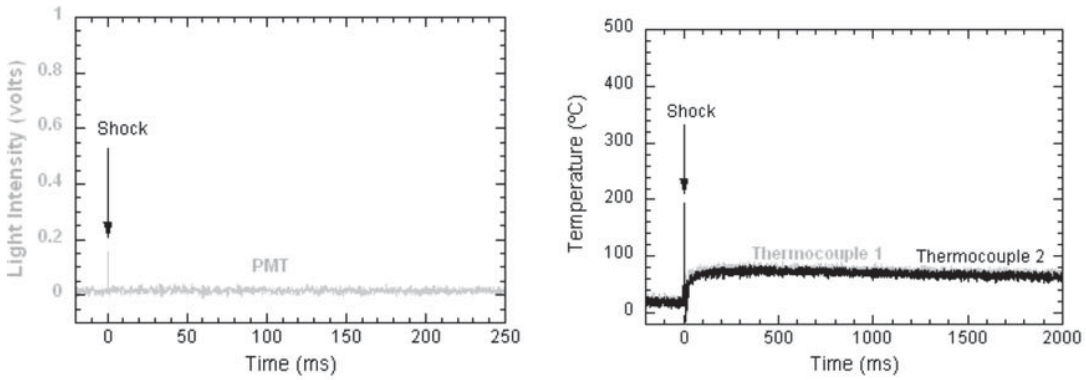

(a) (b)

Figure 26: *Light intensity and temperature histories for shocked samples that did not react: a) light intensity in Ti+Si sample (54.1% TMD) shocked to 3.3 GPa, b) temperature in Ti+2B sample (43.5% TMD) shocked to 2.1 GPa.*

6.5.2 Thermocouple and PMT light intensity

This section presents temperature signals obtained by converting the thermocouple voltages using the type K thermocouple calibration, along with light intensity signals. In Figure 26, typical signals obtained when the sample did not react are shown. Confirmation that the samples did not react was also obtained by examining the recovered samples. In all temperature and light intensity plots, time zero corresponds to the arrival of the shock wave at the bottom of the test sample, as indicated by a sharp jump in the thermocouple signal or by a light spike in the light intensity signals.

Because of the porosity of the samples, the shock wave caused a short-duration light flash, which produced to a spike in the light signals, even in the absence of reactions. This light most likely appeared as a result of shocked gases in the pores and local high temperatures, and thus decayed rapidly. Following this flash, no light was emitted by the non-reacting samples.

The shock wave also caused a step-like temperature jump in the mixtures, as detected by the thermocouples, even when no reactions occurred. This jump was typically on the order of 40-250°C, depending on sample depth and attenuator thickness. Because the shock that reached the bottom of the sample was weaker in longer samples or when thick PMMA attenuators were used, a smaller shock temperature jump was observed. For both reacting and non-reacting samples, the measured shock jumps were consistent with the increase in temperature predicted by methods for inert materials, such as that of [94]. Hence, there was no evidence of bulk reactions occurring in the shock jump time scale in non-reacting samples, and the temperature subsequently decayed slowly .

Figures 27 to 29 show typical light intensity and temperature signals in samples that reacted fully. In all reacting samples, temperature and light intensity increased significantly

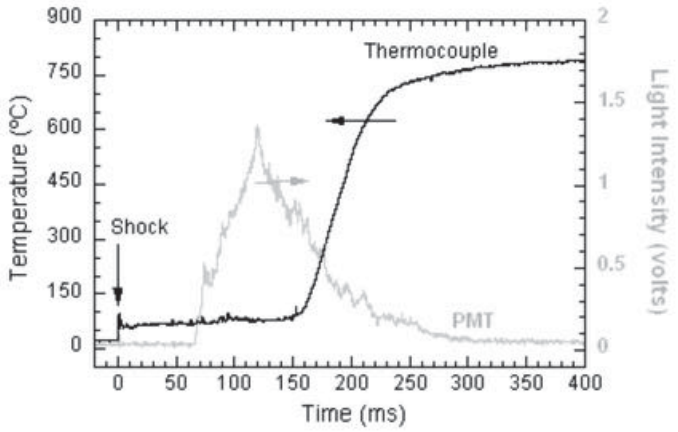

Figure 27: *Light intensity and temperature histories for a shocked 5Ti+3Si sample (49.8% TMD) for an incident shock of 2.2 GPa. The recovered sample was fully reacted.*

some time after the initial shock jump and spike. Intense light emissions were found to saturate the PMT in most experiments, and concurrent large temperatures increases were observed. These observations suggest the occurrence of exothermic reactions. Furthermore, the thermocouples signals tended towards very high equilibrium temperatures following the main reaction. This suggests a significant addition of energy that could not explained by shock heating alone, and indicates the occurence of bulk exothermicity.

Evidence of bulk reactions from temperature and light measurements was always associated with samples that reacted fully in post-trial sample analysis. Furthermore, in all tests where the thermocouples (TC) or PMT did not show evidence of bulk reaction for the duration of the experiment, the recovered samples were found to be nearly completely unreacted. No partial reaction was observed.

In unreacted cases, the thermocouples still functioned after the test, and were recovered in useable condition. The polycarbonate window and the fiber optic were also found nearly intact and still able to transmit light. In experiments that resulted in a reacted sample, the thermocouples were sometimes found damaged or open due to high reaction temperatures. However, thermocouples whose junction did not open due to melting of the wires still functioned. In these cases, the sample had fused with the polycarbonate window, but the window was still mostly transparent. The survival of the gauges in the harsh conditions provided reliable measurements of the strong light and high temperatures detected resulting from reactions, and care was taken to eliminate spurious behavior of the diagnostics.

As seen in Figures 26 to 28, light intensity began to increase slightly earlier than temperature. This may be because the thermocouples only responded to changes in bulk temperature in their vicinity while the the PMT responded to light emitted from any point over the entire sample surface. In cases where reaction would be initiated at a localized point a certain distance away from the thermocouple, the light would be detected immediately and the thermocouple would only respond when heat had time to diffuse to the thermocouple

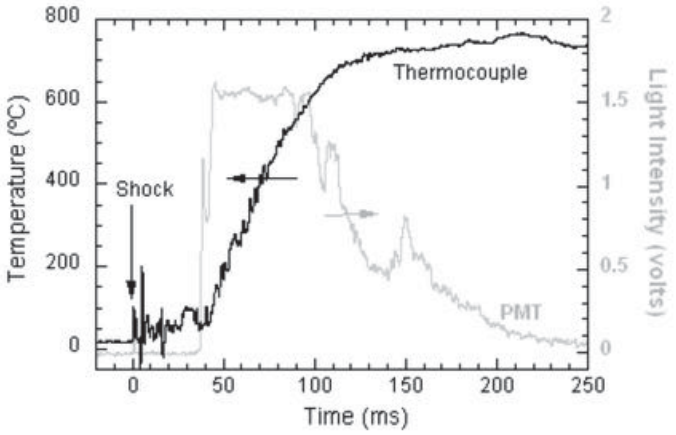

Figure 28: *Light intensity and temperature histories for a shocked ARM 5Ti+3Si sample (53.4% TMD) for an incident shock of 2.7 GPa. The recovered sample was fully reacted.*

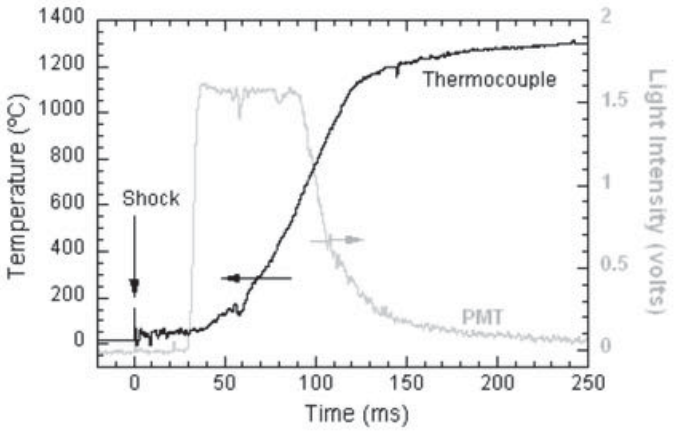

Figure 29: *Light intensity and temperature histories for a shocked ARM 5Ti+3Si sample (54.7% TMD) for an incident shock of 2.7 GPa. The recovered sample was fully reacted.*

location, causing a delayed response.

Due to the slow response time of the thermocouples and possible high thermal contact resistance between the thermocouple and the sample, the rise time and the peak temperature indicated by the thermocouples may not be exact. However, the moment the temperature begins to increase due to the onset of bulk temperature can be accurately found, and can serve as an indication of the bulk reaction onset time.

Both thermocouple and PMT data show that bulk reactions begin at least 30 ms after the shock had traversed the sample in 5Ti+3Si (Fig. 26) and ARM 5Ti+3Si (Figures 27 and 28). The reaction onset delays found for this test setup are defined as the time elapsed between arrival of the shock to the moment where light and temperature signals begin to increase beyond the levels due to the shock wave alone. By comparing Fig. 26 with Figures 27 and 28, the delay time is shorter in the ARM 5Ti+3Si than in the as-blended 5Ti+3Si. Because the difference is on the order of milliseconds, it can be concluded that the discrepancy is due to a difference in the burning rate rather than shock sensitivity, as shock pressure decays on the order of only a few hundred microseconds.

6.5.3 Thermocouples

The experiments involving titanium and silicon have shown that thermocouples were as reliable as light detectors in detecting bulk reaction onset delay time. Since test setups involving only thermocouples were simpler and more robust than those involving optical measurements, thermocouples were used to probe reaction onset in a large number of shocked reactive powder mixtures.

It was found that mixtures of fine aluminum (3.5 - 15 μm) mixed with metal oxides and ARM mixtures of aluminum mixed with metal oxides reacted much faster than the other SHS, thermite, and intermetallic mixtures tested. This is illustrated in Figures 30 and 31, which show typical results with SHS and ARM thermites, respectively. In Figure 30, bulk reaction onset delay in a Ti+2B mixture is almost 100 ms, while it is on the order of 10 ms for the ARM 4Al+Fe_2O_3 in Figure 31. The bulk reaction onset delay differs by an order of magnitude between the two mixtures used for this example. Their burning velocity also differs by one to two orders of magnitude [95]; the difference can be explained again in terms of a difference in burning velocity.

6.5.4 Flame speed measurements

A summary of the measured burning speeds is reported in Table 5. The methods used to obtain these results are described in more detail later in section 8.7, but are mentioned here as they provide valuable support for the following discussion of the initiation mechanisms. For each mixture, the result reported is a compilation of several tests with the indicated uncertainty representing the experimental scatter. Note that the ARM 4Al+Fe_2O_3 and ARM 8Al+MoO_3 mixtures produced a comparatively larger amount of gas, which was seen expanding from the edge of the glass cover as a very luminous cloud. As a result, burning speed in these mixtures may not be dependent only on diffusive mechanisms but also on

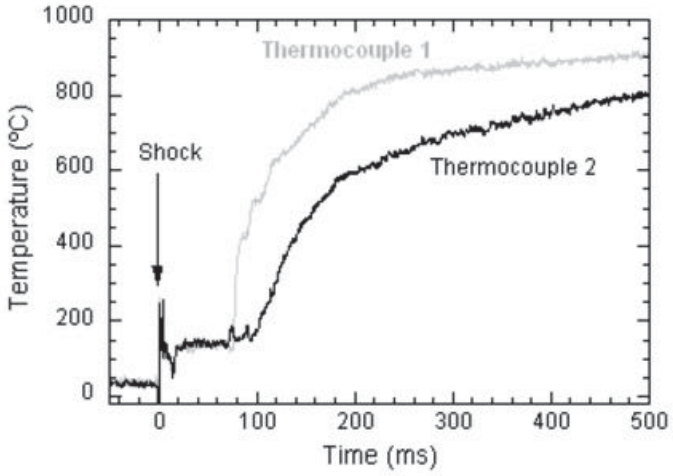

Figure 30: *Temperature histories for a shocked Ti+2B sample (39.6% TMD) for an incident shock of 4.2 GPa. The recovered sample was fully reacted.*

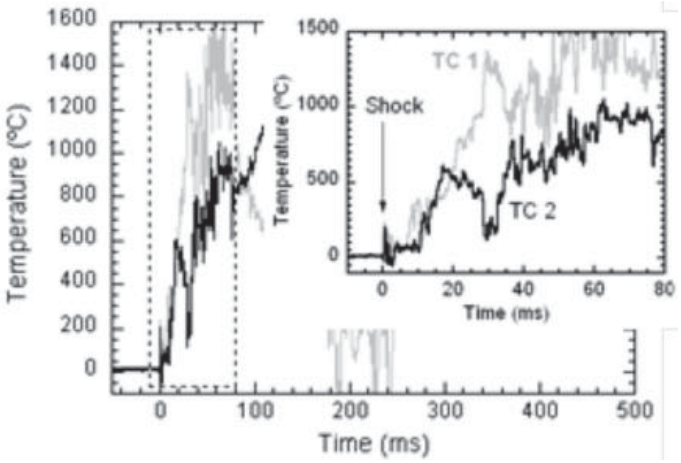

Figure 31: *Temperature histories for a shocked ARM 4Al+Fe_2O_3 sample (42.1% TMD) for an incident shock of 1.7 GPa. The recovered sample was fully reacted.*

Table 5: *Summary of burning speed measurements*

Mixture	Compaction (%TMD)	Burning speed (mm/s)
5Ti+3Si	50	16±5
ARM 5Ti+3Si	50	60±5
Ti+Si	35	14±1
ARM Ti+Si	30	13
Ti+2B	40	10±1
Ni+Al	50	23±2
ARM Ni+Al	50	44±4
$4Al+Fe_2O_3$	43	21±1
ARM $4Al+Fe_2O_3$	40	1600±1100
ARM $8Al+MoO_3$	30-50	6000±2500

convective mechanisms (fast burning speeds resulting from convective flow are discussed by Son et al.[96]). Furthermore, in ARM mixtures containing aluminum, the oxide layer surrounding the aluminum particles is likely removed, which could facilitate the initiation of the mixture by flowing hot gases.

6.6 General Discussion

The delay time before onset of bulk reaction was found to be mostly independent of incident shock pressure in all mixtures tested, and bulk reaction did not occur at all for weaker shocks. This should not be surprising since bulk reaction onset occurred milliseconds after the passage of the shock, at which time the shock pressures had long equilibrated to ambient conditions, i.e. after only a few hundred microseconds. This suggests that bulk reaction onset is not very dependent on pressure and shear once a minimum level sufficient for ignition is attained.

By comparing the various mixtures, it was found that bulk reaction onset delays were actually more dependent on the burning velocity of the mixtures. Indeed, there appears to be a correlation between a mixture's burning velocity and its bulk reaction onset delay time, as the delay time increases steadily as the reciprocal of the burning velocity increase (Fig. 32). It should be noted that diffusive burning in the shocked samples propagates in powders that are pre-compacted by shock compression before reaction occurs. The correlation in Figure 32 shows the reaction delay times as a function of the reciprocal of burning velocity in powder mixtures that were not shock-compacted. There is a strong increase in burning velocity with increasing initial powder density due to compaction, which is discussed in section 8.7 and is noted by Zhao et. al. [95].

The results are therefore consistent with a mechanism involving shock initiation of reactions locally in small zones (likely in the vicinity of pores), followed by the growth of these zones via diffusive and/or convective burning. This mechanism is analogous to that in high explosives whereby a small fraction of the explosive is initiated in hot spots, which then spread and grow via diffusive burning. In high explosives, burning velocities are strongly pressure dependent and reactions lead to a large volume of gas produced, hence pressure increases as a result of reaction, which in turn accelerates the reaction rate. In reactive powder mixtures, burning velocities may not depend on pressure to a large extent, and since gas production is small, bulk reaction rates are much slower in reactive powder mixtures

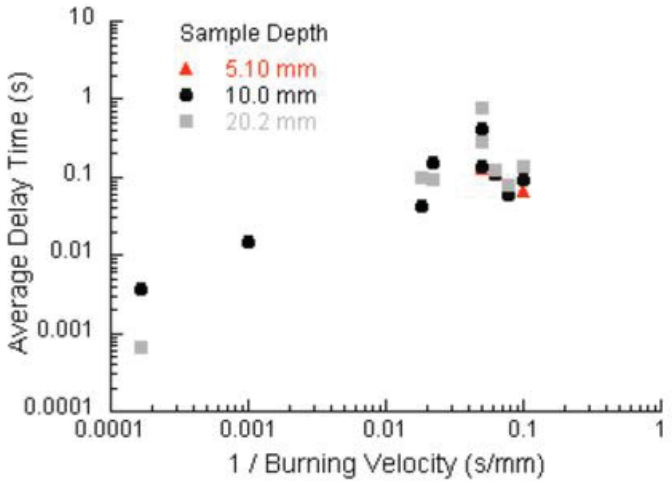

Figure 32: *Average bulk reaction onset delay times dependence on the mixtures burning velocity. Mixtures whose data is shown in plot (from lowest to highest burning velocity): Ti+2B, ARM Ti+Si, 5Ti+3Si, Ti+Si, 4Al+Fe_2O_3, ARM Ni+Al, ARM 5Ti+3Si, ARM 4Al+Fe_2O_3, ARM 8Al+MoO_3.*

than in high explosives.

A similar initiation mechanism was inferred in recent atomistic simulation work [97], where impedance mismatches within a layered Ni-Al composite led to significant thermal fluctuations within the sample following shock passage. Reactions in a sample shocked to pressures on the order of 171 GPa were found to initiate first in the hottest regions (hot spot temperatures were in excess of 5000 K), and spread away from the initiation center as a mass/heat diffusion wave. When voids were introduced into the model, even larger hot spot temperatures were generated (7000 K hotter), and reactions were initiated first in the areas surrounding the voids. Hence reactions initiate near hot spots and spread throughout the material through a diffusive (or convective) heat and mass transport mechanism.

Finally, it is also interesting to note that the delay times were found to be only weakly dependent on the sample depth in sensitive mixtures that could be initiated with very weak shocks. This suggests that in sensitive mixtures, the shock wave may initiate local reactions (hot spots) throughout the sample, so that the bulk reaction delay time represents the time required for those hot spots to merge. In less sensitive mixtures, bulk reaction delay was slightly more dependent on sample depth. This may be because the shock generally produces fewer hot spots, and there is a higher likelihood of igniting a single hot spot or a localized conglomeration of hot spots in a localized region of the powder sample. The time for the reaction to reach completion would then depend on propagation of the diffusive flame from a single or small number of locations throughout the rest of the sample.

6.7 Conclusions and Outcomes

Various mixtures of reactive powders contained in recovery capsules were subjected to shocks of different strengths while the bulk reaction onset was monitored using light detectors and/or in-situ thermocouples. In all mixtures that were initiated, reaction proceeded to completion and strong light emissions accompanied by large temperature changes were observed. Conversely, in samples that were not initiated, light and temperature signals were identical to those from baseline inert stimulant mixtures.

These results indicate that the initiation of reaction in these compositions may indeed be occurring on timescales compatible with the initial shock compression (i.e., microseconds). Fast-response pyrometry showed evidence of reaction-generated luminosity consistent with reaction (2000-3000 K) occurring within a microsecond of the shock. However, the intensity of this luminosity was more than one order of magnitude less than what would be expected from bulk reaction of the sample. Indeed, control experiments with inert simulants showed similar early time luminosity spikes, albeit at lower intensity than the reactive case. This suggests that the reaction initiation centers are qualitatively similar to luminous hot-spots observed in shock compression of inert powders.

The onset of bulk exothermic reaction was observed to occur on much longer timescales, typically milliseconds to hundreds of milliseconds. This result was consistently confirmed via two independent measurement techniques (in-situ thermocouples and photomultipliers). This phenomenon is consistent with diffusion-controlled flames propagating out from the shock-ignited initiation centers at burning rates typical of the reactive powder mixtures (centimeters per second).

These results can be interpreted in terms of phenomenological models of detonation initiation such as Ignition and Growth [98] developed for high explosives. In both explosives and the compositions studied here, the shock wave provides an ignition source at localization centers (pore collapse). The growth and merging of these centers is slow in the compositions studied in this paper, however, due to slow burning rates. Unlike molecular explosives, which have a pressure-dependent burning rate $r \sim p^n$ (n of order one or two), SHS, thermite, and intermetallic compositions have relatively pressure independent burning rates due to the low fraction of gas-phase products. As a result, the delay to bulk reaction is strongly dependent on the diffusive burn rate, and very weakly dependent on the shock pressure, although a minimum threshold pressure for initiation exists.

Though a relatively large number of different powder mixtures were tested in this study, definitive conclusions on the dependence of initiation pressure or delay time to bulk reaction on powder properties are difficult. The mechanisms of initiation are complex and appear to depend strongly on the reactivity and the microstructure of the mixture. However, due to the wide variations in microstructure from mixture to mixture, it is not useful to compare them, and the dependence of dynamic reaction properties on global powder properties such as packing density, particle size, or even material properties is best done on a case by case basis. Even comparison between mixtures with obvious microstructural variations within the same mixture such as ARM and as-blended mixture is not clear. For example, ARM

mixtures generally seem to react more quickly than their as-blended counterparts, with ignition delays in certain mixtures such as Al-Fe_2O_3 two orders of magnitude shorter when processed by ARM. However the trend is reversed in special cases such as Ti-B mixtures where delay to bulk reaction is surprisingly longer in ARM powders than as-blended ones. In general, combustion in powders is a highly multi-scale phenomenon, and it is likely that tests in much simpler configurations such as one-dimensional foils may be necessary to gain more insight on the detailed mechanisms.

7 Effect of Particle Morphology on Shock Sensitivity

7.1 Introduction

The present section presents an investigation of particle morphology on the shock initiation limits for gasless reactive systems. This work was performed in collaboration with D.L. Frost et al. at McGill University, and was published in [59].

Extensive experiments carried out over the past 50 years have shown that chemical reactions may be initiated in mixtures of a wide variety of metal powders with the impact of a shock wave (e.g., [99]). The precise mechanisms by which shock processing leads to chemical reaction are still under debate, but the micromechanical deformation and interactions between individual particles likely play an important role. In the present experimental study, the microstructural changes induced by shock loading of mixtures of titanium (Ti) and silicon (Si) powders is determined directly by microscopy and indirectly with thermal analysis. These changes are then compared with the critical shock strength for initiating chemical reactions in the powder mixture.

A number of research groups have investigated shock-induced reactions in Ti-Si mixtures. For example, Thadhani et al. [52] carried out an extensive study using three different-sized powder mixtures, denoted fine ($\sim$1 μm), medium ($\sim$10 μm), and coarse ($\sim$100 μm). They observed reactions only for the medium-sized particles, which experienced extensive plastic deformation and intimate mixing of both powders, instead of mere agglomeration (characteristic of the fine powder) or fracturing and entrapment of the Si particles within plastically deformed Ti particles (for the coarse powders). The authors concluded that the initiation of chemical reactions is controlled by mechanochemical processes rather than thermo-chemical effects.

Vreeland et al. [58] observed a significant increase in critical shock pressure to induce reactions when the density of a Ti-Si powder mixture increased from 51% to 60% TMD. These authors attributed this result to less contact area between the reactants resulting from a reduced ability for local shear deformation (i.e., turbulent mixing). Das et al. [100] also found that reducing the porosity reduced the reaction kinetics in shocked Ti-Si mixtures. Lee and Zhang [39] studied the initiation of reactions in Ti-Si contained within a cylindrical tube with porosities varying from 47–65%. Using a strong explosive booster, reaction of the mixture was initiated, but the reaction decoupled from the shock after several charge diameters.

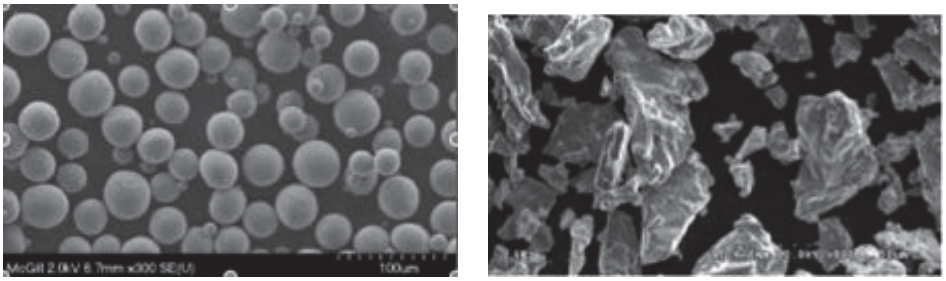

(a) (b)

Figure 33: *SEM photographs of a) spherical Ti particles and b) irregular Ti particles.*

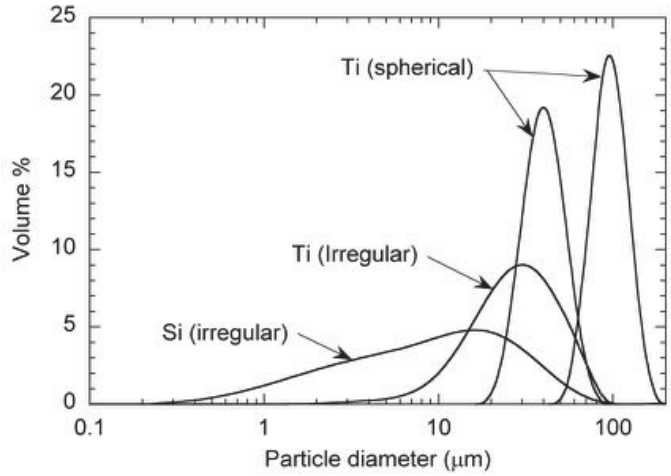

Figure 34: *Malvern particle size distributions, plotted on a volume percentage basis.*

In all of the previous studies, the titanium particles had an irregular morphology; in the present study, both spherical and irregular particles are used to determine the influence of morphology on the critical shock threshold for chemical reaction.

7.2 Experimental Details

Two different types of Ti powder were used, as shown in Fig. 33. The particle size distributions, measured with a Malvern system on a volume percentage basis, are shown in Fig. 34. Two different particle size ranges of the spherical Ti particles were used, 40±14 μm and 95±26 μm, on a volume-weighted basis. The irregular particles had broader size distributions with a volume weighted mean of 31 μm for the Ti powder (commercially denoted TI-101) and 15 μm for the Si powder (denoted Si-101). The powders, in an equimolar proportion Ti + Si, were mixed in a roller mill and then mechanically tamped to densities of 70±2%, 64±2%, or 51±4% TMD, for the 95 μm spherical, 40 μm spherical, and irregularly-shaped Ti powders, respectively.

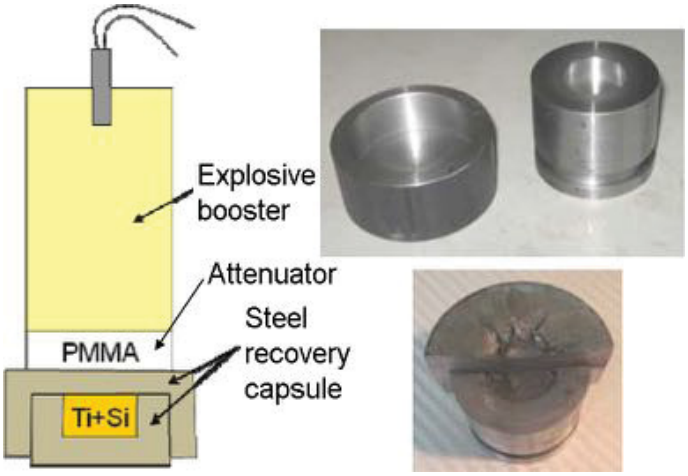

Figure 35: *Schematic of capsule design (not to scale) and photographs before and after a test (after the steel cover has been cut open). The sample diameter and depth are 25 mm and 10 mm, respectively. The outer diameter, inner diameter, and thickness of the steel capsule top are 75, 50, and 10 mm, respectively.*

The experiments were conducted using the cylindrical configuration shown in Fig. 35. The Ti-Si powders were placed in a mild steel recovery capsule. The reaction was initiated with a high explosive booster placed above PMMA disks of various thicknesses to attenuate the shock. Three types of booster charges were used: Tetryl, Pentolite (Orica Pentex AP), and Dyno D45 (Dyno Nobel). The capsule was clamped inside a large steel anvil (not shown in Fig. 35) for stability. After each test, the capsule was recovered and opened with a band saw.

7.3 Results and Discussion

Whether the sample reacted or not was evident by the temperature of the capsule after a test, visual inspection of the post-test sample, and from thermocouple measurements (reported elsewhere [51]). The samples containing the large spherical Ti particles (95 μm) did not react even if no PMMA attenuator disk was used. In this case, the shock pressure incident on the top surface of the powder samples was estimated, using the hydrocode LS-DYNA (the calculation procedure is described in [47]) to be about 23 GPa. In contrast, both of the smaller Ti particles (spherical and irregularly-shaped) exhibited a threshold attenuator thickness, and hence shock pressure, for reaction, as shown in Fig. 36. For the irregular Ti particles, the threshold shock pressure for reaction was 6.7$\pm$1.3 GPa, corresponding to a change in the PMMA attenuator thickness from 30.0 mm (no reaction) to 27.2 mm (reaction) with the Pentolite booster. From Fig. 36, it is apparent that within the scatter of the experimental results, the threshold shock pressure for reaction of the 40 μm spherical Ti particles, i.e., 6.8$\pm$2.2 GPa, was the same as for the irregular Ti particles.

Pre- and post-shock samples were prepared for analysis by encapsulating a sample of the

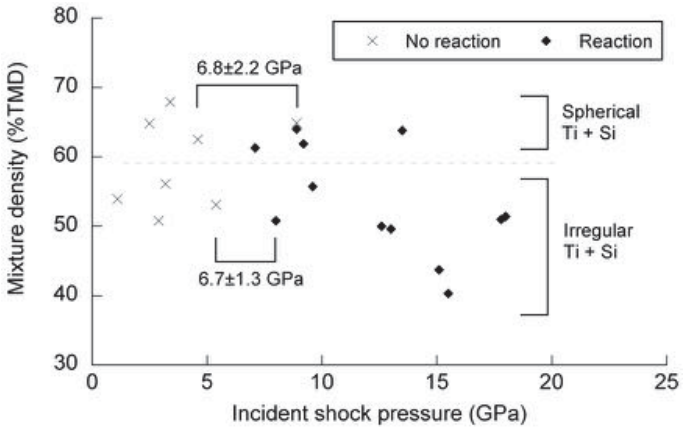

Figure 36: *Summary of mixture reactivity for 40 μm spherical Ti and irregularly-shaped Ti particles as a function of shock pressure incident on the powder.*

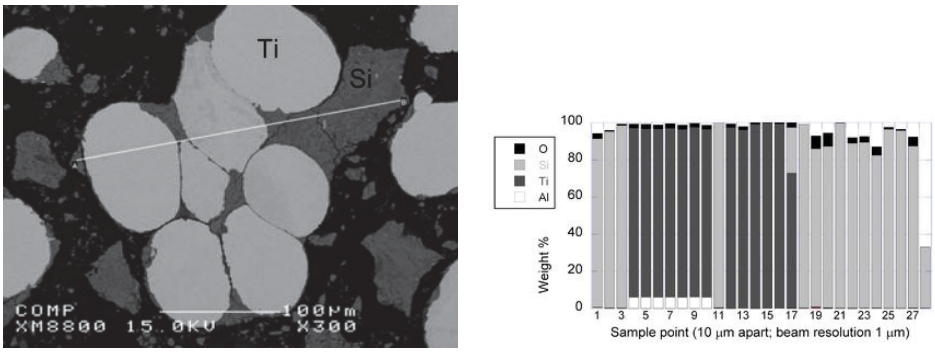

(a) (b)

Figure 37: *a) SEM image of shocked Ti-Si samples with 95 μm spherical Ti particles and b) corresponding backscatter analysis indicates that there is relatively little Ti-Si mixing (presence of Al is due to use of Al_2O_3 for polishing).*

powder in epoxy, then sectioning and polishing the sample to a mirror finish. SEM photographs for a mixture with the large Ti particles (95 μm) are shown in Fig. 37a for a shock loading of 23 GPa. The photographs show that while the large spherical Ti particles are deformed, there is little mixing with the Si particles. The Si particles are also agglomerated by the shock interaction. Micro-probe backscatter analysis was carried out to determine the atomic species at discrete locations, with 1 μm resolution, spaced 10 μm apart along the line shown in the photograph. The backscatter analysis in Fig. 37b also shows that there is very little mixing between the powders.

Differential thermal analysis (DTA) was carried out on the precursor and shocked sample shown in Fig. 37, and is shown in Fig. 38. The precursor sample exhibited an exothermic reaction near the melting point of Si, 1414°C (cf., the melting point of Ti of 1668°C). The shocked sample exhibited an exotherm about 80°C lower, or a temperature about 1334°C.

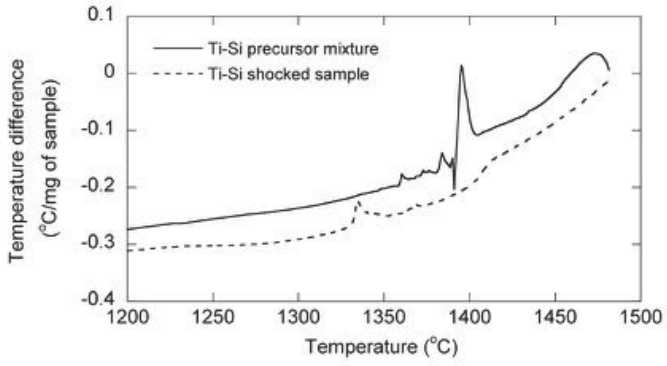

Figure 38: *DTA analysis of prescursor and shocked Ti-Si samples containing large Ti particles.*

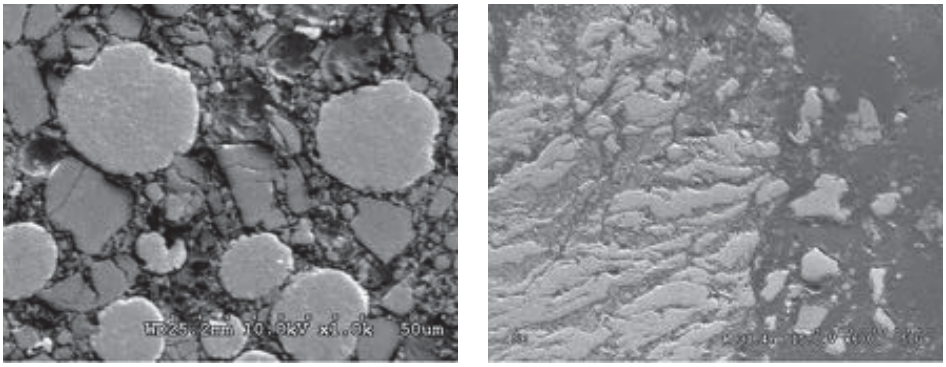

(a) (b)

Figure 39: *Post-test SEM photographs showing a) deformation of spherical 40μm Ti-Si mixture and b) irregularly-shaped Ti-Si mixture, shocked with a pressure level just below the reaction threshold.*

This is likely due to some mechanical alloying of the Ti and Si particles at the interface between the particles, as the melting point of the Ti-Si eutectic is 1332°C. The deformation of 40 μm spherical and irregular Ti-Si mixtures, shocked with a pressure just below the reaction threshold, are shown in Fig. 39. For the spherical particles, some fine-scale mixing occurs as the Si particles penetrate into the larger Ti particles. For the irregular Ti particles, the post-shock powder exhibits considerable deformation of the particles.

7.4 Conclusions and Outcomes

The critical shock pressure for initiating reactions in Ti-Si powder mixtures is dependent on particle size, but not on particle shape. Ti-Si mixtures with $\sim$100 μm Ti particles failed to react (with shock loading up to 23 GPa) in contrast with Ti particles with sizes of $\sim$10 μm. The reaction threshold was found to not be dependent on particle morphology for 30-40 μm

Ti particles. For both spherical and irregularly-shaped Ti particles, the critical incident shock strength for reaction initiation was found to be ∼7 GPa. Possible explanations for this remain speculative, but are generally related to factors influencing the shock-driven mixing of the particles and local heating. For example, particle morphology tends to influence large-scale shock-driven deformation, which has only a weak effect on reaction. It is likely that fine-scale mixing at the interfaces is a significant factor in the reaction sensitivity and rate. As a result, sensitivity is likely more related to material properties such as density, bulk modulus, stress-strain and strain rate behavior. For example, Ti is relatively ductile in comparison with Si, which is more brittle, harder (Mohs hardness of 7 compared with 6 for Ti), and less dense than Ti by a factor of 2. A first attempt to correlate shock sensitivity of powders with material properties is shown by Eakins et. al. [75]. In this work, the shock sensitivity is correlated with the difference between the shock impedance of the two powder constituents, which influences the relative velocity of the materials and the resulting interfacial mixing.

Another factor likely to influence shock sensitivity is temperature, or more specifically, heat generated by shock collapse of inter-particle pores. Shock compression of gases in the pores lead to local hot spots which provide initiation sites for the global reaction. The number density and size of pores depends strongly on particle size, which does influence the shock sensitivity of the mixtures.

While not conclusive, the results of this study support the necessity for mixing of the reactants down to a very small scale, as well as the presence of a large number of hot spots for initiation. This implies that increasing the small-scale interfacial mixing could provide a promising avenue for studying highly reactive gasless reactive systems. The shock sensitivity of powder mixtures thus appears to depend on a balance between creating a sufficient number of initiation sites by hot spot generation, and creating enough interfacial mixing to sustain the reaction. More systematic studies on the effects of material properties on shock initiation would provide more clarity on the phenomena involved. Such experiments are challenging as it is difficult to vary material properties systematically without simultaneously changing other properties such as reactivity of the ingredients. In addition, varying the particle size changes both the interfacial mixing and the number density of hot spots. Future studies on the dynamic modification of the microstructure in reactive powders may provide further elucidation of the reaction mechanisms, however this has proven feasible only through numerical simulations at this time [53, 95].

8 Mechanical Mixing of Gasless Reactive Materials

This section describes research efforts focussing on enhancing the mechanical mixing of the constituents of a gasless reactive mixture to achieve reactivity levels more conducive to explosive or detonation processes. Mechanical mixing to a very small scale offers a more conventional means of increasing the reaction rate of a two-component or three-component mixture, as it leads to a shorter diffusion distance between the ingredients, and consequently shorter timescales for flame propagation speeds. Ideal mixing would consist of molecular-

scale mixing as in a combustible gaseous mixture, however this is more difficult to achieve in solid-state reactive systems because of the lack of atomic mobility in a solid. Mixing components in the liquid phase opens the possibility of molecular-scale mixing, however the ignition temperature of solid mixtures is typically very close to the lowest melting temperature of the mixture components, and achieving liquefaction of all the components without initiating burning is a significant challenge. If there is a large difference in the melting temperature of the components, it is possible to mix in the liquid phase of one of the components, achieving a maximum contact surface between the liquified and solid components. This has been achieved in metal-sulfur mixtures due to the low melting temperature of the sulfur compared to that of the metallic component e.g. Mn-S [101]. A significant enhancement of the reactive properties of the mixture was observed, however, the limiting factor of the mixing scale was the size of the metallic powder which was micron-size. Smaller solid metallic particles could possibly further enhance the mixing.

In this section, a review of the historical approaches to achieving finer-scale mixing is given, leading to the approach of arrested milling used in the present project. This study was performed in collaboration with the research team of professor M.I. Radulescu of the University of Ottawa, and part of this work has been published [102].

8.1 Background

Since the discovery of Self-propagating High-temperature Synthesis (SHS) in the late 1960s in Russia by Merzhanov and co-workers [103], the heterogeneous flames in SHS of materials have been studied extensively. Reviews of the available experimental work can be found in [104, 105, 106, 107]. SHS modelling was mainly performed empirically, by extending the theory of laminar premixed gaseous flames with a reaction rate approximated by an Arrhenius law [108, 109]. It is only recently that a more realistic heterogeneous model for the flame structure was introduced by Makino [110]. Based on physical grounds, Makino applied spray-combustion theory [111] to model the diffusion-controlled structure of the SHS flame. Based on experimental evidence, Makino assumed that combustion occurs at the surface of the component with the highest melting temperature, while the other is molten in the reaction zone owing to heat diffusion from the products, and hence provides a perfect contact. In fact, the melting of one component in SHS combustion is assumed to be a required condition for the reactions to take place, a fact correlating with experiment. The heat diffusion from the hot products into the unreacted mixture provides the heat required to melt one of the components, facilitate the contact between the two components, and provide the thermal activation necessary to enhance the mass diffusion process in the liquid phase, which depends exponentially on temperature. The situation is thus perfectly analogous to that encountered in spray combustion. The consumption of the fuel droplets requires an oxidizer to arrive via diffusive processes to the surface of the fuel across the layer of products, where it would otherwise react with a much shorter time scale than the diffusive process itself. For this reason, the combustion rate in both systems is assumed to be diffusion controlled, and the material is assumed to react much faster once mixed, or for all practical purposes, at an infinite rate.

With the appropriate mass diffusivity, the theory proved to be very successful in capturing a great variety of SHS problems, such the flame propagation speed in the adiabatic condition, flame propagation and extinction under radiation heat loss conditions and finite charge effects, effects of bimodal particle distribution, the transition from steady to pulsating combustion and the initiation of the combustion wave by an external heat source. Comparison with a large database of experimental results substantiated the theory. Later developments of the theory were the extension to layered nano-scale systems [112], with equally good capture of the experimental data. It thus seems that the SHS combustion process is now well understood: the driving mechanism is through the heat diffusion from the high temperature products which serve to preheat the reactants and melt one of the components. The reactions are mass-diffusion controlled, and the rate is exponentially dependent on temperature through the exponential dependence of mass diffusivity on temperature. The particle size controls the reaction rate through the dependence of the reaction rate on the surface area of the un-molten particles being consumed at their surface.

8.1.1 SHS detonations: a convective-diffusive-reactive balance

The extension of the statistical model of Makino to the detonative combustion mode is not straightforward, as the compressible terms must be restored to account for the interplay between changes in kinetic energy and changes in internal and flow energy in the reaction zone, and hence the support of a shock wave. However, if one initially neglects the compressible aspects in the reaction zone (other than the leading shock), a convective-diffusive-reactive model can be constructed quite easily. Such a statistical 1D model would be quite appropriate and timely, and relevant to other combustion systems in gaseous detonations where diffusion limited phenomena also play an important role [113]. The physical picture would be a shock wave followed by an SHS deflagration, propagating by diffusive transport of heat. The absence of feedback of the compressibility on the reaction rates within the extended reaction zone structure can be argued on the basis of the smallness of temperature changes due to kinetic energy changes across the detonation wave (as compared to temperature changes due to chemical energy release).

Because the reactions are assumed to occur infinitely fast at the contact of the reacting materials (reactions are diffusion limited), one can readily apply the same formalism for evaluating the reaction rate and mass burning flux behind a shock wave, if one assumes a thermalized non-reacted state immediately behind the shock. This procedure, although not possible for conventional non-diffusive-limited systems, is clearly adequate in this situation, since the reactions are still diffusively controlled even in an infinitely fast reaction rate, by virtue of the heterogeneity. For this reason, the reactions would have a negligible rate near the shock, where temperature would be low, and have a much higher rate in the products, where the temperatures are highest, as described by the SHS deflagration model.

It would be instructive to extend the Makino theory for SHS combustion to a shock-preheated mixture, with the initial temperature corresponding to the shocked-state condition in the corresponding CJ detonation. If the mass burning flux derived from the Makino theory is compatible with the mass flux through the detonation wave, as computed from equilibrium calculations [28], than a self-sustaining detonation wave could be driven

by diffusively-controlled chemical reactions. Evidently, if the particle size approaches the atomic scale, the mixing rate would be sufficiently high such that the diffusively-controlled burning flux would eventually be able to cope with the flux required to maintain a detonative mode. It would be instructive to determine what the critical particle size would be needed to permit a diffusively controlled detonation wave. An estimate of the critical conditions is given in the next section.

8.1.2 Ignitability, self-sustenance and required particle size in diffusion-limited detonations

The conceptualization of a gasless detonation into a ZND-like structure described above, consisting of a leading shock, which serves to heat the mixture to a sufficiently high temperature to facilitate diffusion, followed by an extended heterogeneous zone in which reactions are limited by diffusion processes at the surface of the binary reactants, is an attractive thought experiment and one could determine the particle size that will permit the burning flux to cope with the convective nature of the wave. However, the ignitability and sustainment of the wave is also an important factor. From classical detonation theory, the parameter that governs whether a detonation can be ignited and remain self-sustained is the time scale of the reaction process. If the time scale is smaller than the time scale of blast decay inducing the convective motion, initiation is possible; likewise, if the reaction time scale is smaller than the time scale for lateral losses (radiative and gasdynamic cooling), the detonation can be self-sustained.

A detonability theory can in principle be formulated based on the Makino theory extended to the compressible regime. However, simple order of magnitude estimates can provide an estimate for the time scale for the chemical reactions. Bcause the time scale for reaction is expressed in terms of the required SHS deflagration wave speed and characteristic thermal diffusivity as (α_t/S_{SHS}^2), and the time scale of expansion waves propagating across the charge is simply the ratio of charge diameter to the acoustic speed (d/c), the critical charge radius can be written as:

$$d \approx \frac{\alpha_t c}{S_{SHS}^2} \tag{31}$$

Assuming the condition of matching burning flux is achieved across the wave and the mass velocity across the reaction zone is on the order of 10^2 m/s, roughly compatible with the estimates of [38], the critical charge diameter would be:

$$d \approx \frac{\alpha_t c}{S_{SHS}^2} \sim \frac{10^{-5}[m^2/s]10^3[m/s]}{10^4[m^2/s^2]} = 10^{-6}m \tag{32}$$

Clearly, the effect of the boundary would be negligible. In conclusion, *provided that the burning flux is sufficiently high*, the wave can propagate in micron-scale charges. The bottleneck indeed appears to be the requirement of a sufficiently high burning velocity, which can only be achieved if the particle size is very small. One can estimate the particle size for which such a high burning flux can be achieved, assuming that the burning flux scales are inversely proportional to the particle radius, as determined by Makino [114]. In

a Ti-C system, the burning speed is approximately 10^{-3} m/s for a particle radius of 10^{-5} m in a mixture initially at room temperature. To achieve the required burning rate at room temperature, the carbon particles would require an initial radius of 10^{-10}m. This is approximately the atomic dimension. Although the increase in temperature behind the shock enhances the mass diffusivity, a purely diffusion-controlled detonation wave would require initial powder dimensions on the order of the atomic size! One can thus conclude that the existence of detonation waves in heterogeneous powder mixtures depends exclusively on the propensity of the system to self-mix.

8.1.3 Mechanical mixing of reactive metals

Before treating the mechanical processes and mixing which can be obtained through the action of shock waves, it is instructive to investigate the available results in the field of mechanical alloying of reactive particles. Mechanical allowing, or more simply, ball milling, is a process by which two components in powder form are introduced in a vial along with a series of rebounding much larger balls. The vial is shaken or the balls agitated by rotating rods and the repeated ball collisions with the powders permits repeatedly welding, fracture and re-weld of the powder particles. Figure 40 shows a schematic representation the process. An excellent exhaustive review of the mechanical alloying process is given by Suryanarayana [115]. The mechanical events occurring during the ball milling process of two powders, where the materials are repeatedly exposed to high compression and shear is directly analogous to the mechanical loading via a rapid-compression of a porous mixture by a piston. Similar mechanisms would be occurring in a detonation wave, or during the shocking of the powders by a an external driving force.

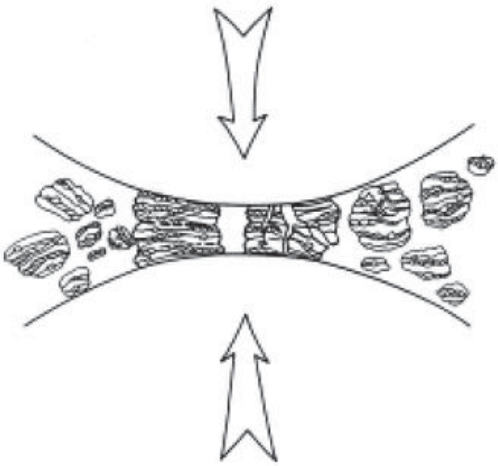

Figure 40: *Material deformation during ball collisions.*

Although an extensive range of phenomena do occur during the mechanical alloying process, the generic phenomenon, especially in a process involving a ductile and a brittle element, results in a lamellar structure, as shown schematically in Figure 41. This structure can

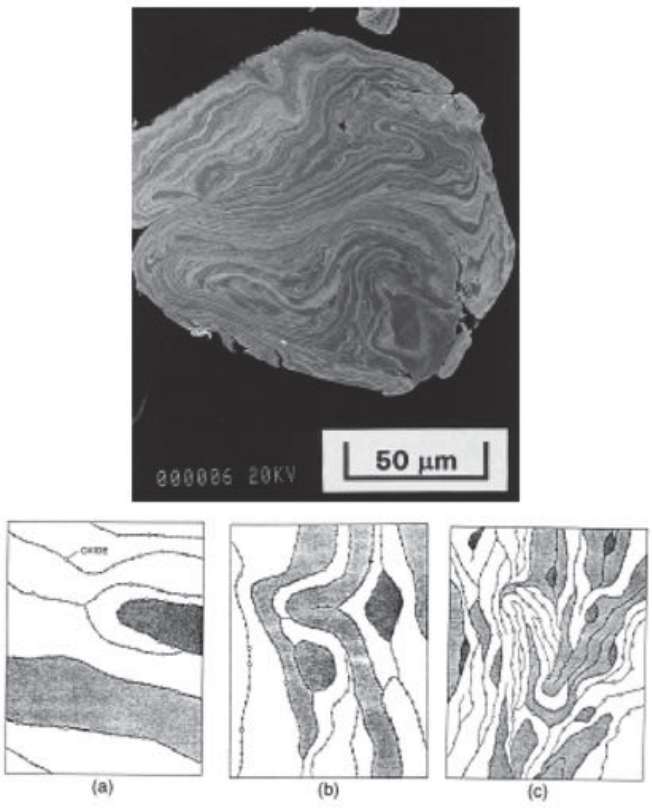

Figure 41: *Lamellar structure obtained during mechanical milling of Ag-Cu and sketch of the evolution of a lamellar structure for a ductile-brittle system.*

be deduced from scanning electron micrographs (SEM).Fine lamellae of decreasing size are observed with increasing mechanical milling time, during which nano-structure materials are formed.

These nano-structure materials, shown schematically in Figure 41, exhibit an increase in the number of defects, dislocations and increase grain surface area, hence an increased ability to inter-diffuse and react. The physics behind the creation of these nano-structure materials, which are universally observed during the mechanical activation processes, is still very poorly understood due to the inability to adequately probe the fine scale phenomena. Hellstern et al. [116] have attempted to describe the mechanism of formation of nanostructures from high resolution TEM observations involving the development of shear bands, containing high dislocation densities owing to the high deformation rates. The process is repeated itself until the minimum grain size possible is reached, often on the order of a few nanometers. The minimum grain size achievable is believed to be due to the competition between plastic deformation via dislocation motion and the recovery and recrystallization behaviour of the material [117]. Typically, smaller minimum grains are observed in systems with a high melting temperature and hardness. Molecular dynamic simulations of such mechanical events are discussed at the end of this review, as they are not restricted to the

mechanical alloying process alone, but also to the mechanical processes involving the action of shock waves.

When exothermic powders are milled, the mechanically-alloyed material exhibits a slow rise in temperature originating from the chemical reactions at the boundaries between the mixed powders. At these boundaries of the two materials, new intermediate phases could form, which act as barriers to the diffusion process between reactants. The slow increase in temperature is punctuated by a sudden increase in the temperature, marking a bulk ignition event and decomposition of the entire powder mixture into products. How the onset of bulk reaction correlates with the state of the mixture just prior to ignition is currently unclear, in spite of extensive experimentation [118]. The ignition phenomenon is likely a combination of the degree of mixing and size of the smallest grains achieved, which depends on the milling time, and the intensity of the ball collisions and localized compression and shears, which depend on the intensity of the milling process. Due to the difficulty of capturing the wealth of different phenomena occurring during the mechanical milling process, most activities to date have been purely empirical. An extensive overview of the chemical decomposition induced by mechanical alloying in given by Takacs [118].

An interesting range of experimental investigations discussed in the review of Takacs is the behaviour of incompletely mechanical alloyed mixtures in SHS ignition and propagation experiments. The idea is to stop the mechanical alloying process prior to the bulk ignition event then investigate the properties of an SHS deflagration wave through the partially alloyed mixture. This two-step process would be analogous to the problem of mechanical activation through shock waves followed by a diffusion controlled decomposition wave. Indeed, such experiments on SHS deflagration in pre-processed mixtures have shown that the reactivity of the powders is increased, i.e., the speed of the wave is higher and the ignition temperature decreased [119, 120, 121]. This simply falls within the predictions of current SHS phenomenology, although the authors of the mechanically activated SHS processes have not attempted any formal comparison with available models. This should be an important comparison to be made, in order to determine whether the mechanical activation merely reduces the size of the particles, or also promotes other non-equilibrium modifications to the materials themselves, as speculated by Anselmi-Tamburini et al. [120]. For example, Smolyakov attempted to incorporate the energy expenditure in the activation process to lower the activation energy of the diffusion-limited reactions, albeit in an ad-hoc approximate continuum model [122]. A systematic investigation of the effect of mechanical activation on SHS combustion characteristics would be extremely relevant to the problem of detonation waves, since the decomposition kinetics may be intimately coupled with the mechanical activation via shock waves.

8.2 Overview

The main objective of this investigation was to increase the speed of reaction kinetics using novel mechanical mixing techniques. Motivated by the strong dependence of diffusion-dominated burning velocity on mixing scale, techniques were developed to produced reactive materials mixed at a nanometer scale, i.e. nano-composites. Two methods were developed

to mix the reactants: cold rolling, and arrested milling. The cold rolling technique consisted of passing a stack of alternating foils of different reactive metals repeatedly through a rolling mill. The compressing action of the rollers reduced the thickness of the layers of reactive materials until micron and nanometer wide layers were obtained. The Arrested Milling (ARM) technique was also used to mix the reactive components down to a nano-scale level. An instrumented ball mill was used to monitor the temperature during milling to accurately determine the moment of onset of runaway reaction so that the milling could be stopped (arrested) before the milling process ignited the mixture. Although the ARM technique has been pioneered and developed in other laboratories such as the New Jersey Institute of Technology (NJIT), this capability did not exist in Canada. Researchers at the University of Ottawa have devoted their efforts into establishing a Canadian capability within the framework of the present TIF project. Facilities were built and a detailed study on the milling parameters such as milling time and inerting atmosphere was performed for a number of reactive mixtures. Once the procedure for obtaining nano-scale ARM powders was developed, the micro-structure was compared to ARM powders obtained from NJIT.

Event-Driven Molecular Dynamics (EDMD) was developed to model the milling process, calculate the energy distribution of the balls and infer the impact velocity, and frequency of the collisions. The intent was to use this information to determine the optimal parameters for ball milling to produce the finest possible scale of mixing.

Flame speed measurements were used to study the reactive behavior of the nano-composites. The combustion properties were investigated for mixtures of different porosities and micro-structures, as these parameters play a key role in the heat diffusion processes that dominate the reaction kinetics. The flame speed was measured for mixed powders of individual components, ARM powders, and cold-rolled foils. Changing the packing density of the powders provided a means of changing the rate of convective diffusion. Highly-porous materials contained a large volume of gas-filled voids between the particles which influenced the heat transport mechanism by producing a convective heat transfer through micro-jetting in the pores. As the porosity was decreased, the transport mechanism tended towards a conductive mode. By performing this flame speed study, the effects of micro-structure and the convective-diffusion mechanism on chemical kinetics was observed.

A mechanical press was used to achieve a wide range of porosities in the powder mixtures. Since minimal porosities are desirable for gasless detonation, very low porosities were achieved through two techniques. The first was to produce cold-rolled foils of alternating reactive metals. The foils consisted of thin samples of gasless reactive material with a lamellar microstructure and 100% TMD. The second techniques involved the development of a novel method of consolidating ARM powders using cold-gas spray deposition which projected the particles onto a substrate at high velocity to form a compacted structure with nearly zero porosity while maintaining the nano-scale mixed reactant structure within the grains.

Using mechanical mixing techniques to decrease the diffusion distance may provide a means of satisfying the third condition for gasless detonation, i.e. a sufficiently high reaction rate. This approach is based on the premise that ‘shock-assisted reaction’ is the dominant

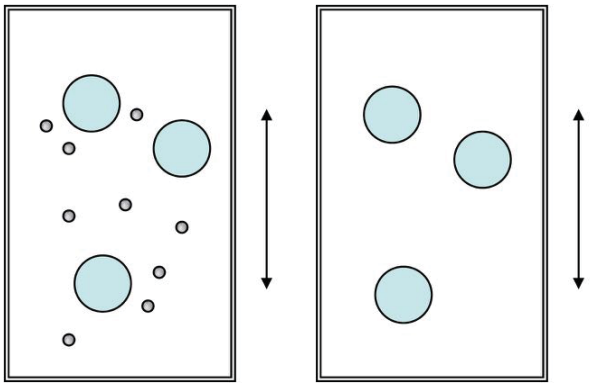

Figure 42: *Strategy for performing EDMD simulations of ball milling. The experiment consists of milling balls and reactive particles (a), while the simulation consists of hard spheres (b).*

mechanism of energy release in gasless reactive powders, and essentially increases the speed of these types of reactions. The ability to mix materials down to nanometer scales and lower opens the possibility of achieving an ultra-fast reaction process that at the limit of molecular-scale mixing (e.g. as in gases), may no longer depend on diffusion.

8.3 Event-Driven Molecular Dynamics

An Event-Driven Molecular Dynamics (EDMD) model was developed to model ball-milling in order to optimize the technique. The power of this modeling approach is in simulating the macroscopic behavior of systems containing a large number of particles by using simple collision rules to define the interactions between the particles. Ball-milling consists essentially of a number of particles in a container where energy is input into the system through motion of the container, causing inter-particle collisions. The simulations were developed with the objective of estimating the kinetic energy distribution of the particles and gaining insight into the characteristics of the collisions. The collision properties could then be related to milling parameters such as mixing scale.

8.3.1 Approach

The basic approach is to set up a simulation with a certain number of particles inside a container (Fig. 42). The shaking motion of the container constitutes the shaking motion of the mill. By measuring the collisions of the spheres inside the ball mill, a collisional frequency is obtained. By adjusting the coefficient of restitution of spheres in a simulation to match this frequency, the ball milling process is simulated. Using this simulation, the milling time and energy dissipated during the milling process can be estimated.

The event-driven model was set up with the following parameters:

— one collision at a time

— collisions of two objections only
— conservation of momentum and energy

The coefficient of restitution is given by:

$$\epsilon = -\frac{v_1 - v_2}{v_{01} - v_{02}} \tag{33}$$

where the subscripts 1 and 2 denote the two particles, and the subscript 0 denotes the condition before collision. The energy lost during the milling dose constitutes a source term in the energy equation.

8.3.2 Results and Discussion

As a spin-off application, EDMD was validated for the compaction of a dense hard disk medium by a moving piston. This application is relevant to shock propagation in granular hydrodynamics or in liquids [123]. This problem was solved analytically using the Helfand equation of state, and the analytical predictions were validated against molecular dynamics calculations using the EDMD technique, where the evolution of the system of colliding elements was be obtained analytically. With increasing compaction of the medium, it was shown that the compressibility changes substantially, with an isentropic exponent of $\gamma = 2$ in the dilute gas phase, and γ on the order of ten at higher compactions. This was shown to significantly affect the shock Hugoniot and shock jump conditions. Parametrization of the shock jump relations were obtained using the shock Mach number and piston speed. The important result that the temperature in the compressed medium depends to a very good approximation only on the square of the piston speed for all compaction levels was shown analytically and demonstrated numerically via the molecular dynamic calculations. This important result provides a very simple means to estimate the amount of energy injected into a hard particle system by surfaces generating strong shocks.

8.3.3 Conclusions and outcomes

The present study shows EDMD to be a promising approach to simulating hard particles dynamics interacting with walls and with each other. Although the original intent of developing EDMD was for optimizing the ball-milling process, the code has not been used for its original purpose yet. The code was written and tested on simple problems involving single and double ball dynamics in gases, but the application to metallic powders remains a future objective. Nevertheless the EDMD code is now functional and has yielded new results on the thermodynamic properties for compressed media which have applications to dense fluids such as strongly-shocked water.

Future improvements to the code include relaxing the assumption of elastic collisions, and research will be devoted to studying how the shock hydrodynamics are affected by the dissipative nature of granular flows or in reactive flows where collisions may be inelastic. The plastic deformation of powders inside a ball mill also constitutes a dissipative process, and should be modelled more accurately.

8.4 Ball Milling of Reactive Powders

Ball milling is a process by which powder materials are placed in a container or vial along with one or more hard spheres called grinding media. The vial is then subjected to vigorous motion, and the repeated collisions of the grinding media with the powder materials cause crushing and alloying of the powder particles. This process can be used to break powders up into finer-size particles. When different types of powder materials are subjected to ball milling, the process causes mechanical alloying and mixing at very small scales (microns or less), resulting in a material with a micro-structure in a metastable state.

To perform arrested milling, two or more reactive powders are placed in a ball mill or ball grinder. The powders are then milled. If the powders are allowed to mill continuously, there is a point where the powders will embark on a runaway reaction, rapidly reaching completion with the release of a large amount of chemical energy in the form of pressure and heat. If the process is stopped or arrested prior to this point, a reactive nano-composite powder is successfully formed. Various types of microstructures can result from arrested milling. If the milled powders are metals with one powder that is harder than the other, the harder powder breaks up and gets embedded inside a matrix of the softer powder. Milling of ductile metals can result in lamellar micro-structures with thin layers on the order of nanometers.

For each reactive powder system, the milling parameters must be carefully established experimentally. Some of the key parameters include the milling time, the starting size of the powder particles, number of balls, and amount of powder. Other parameters such as the presence of an inert atmosphere in the vial (e.g. argon), slow venting of the vial after the milling has been stopped, and the milling speed and direction, also play a role in the process. For particularly reactive systems staged milling can be used where the desired stoichiometry of the mixture is reached gradually where one of the ingredients is added at different stages of the milling process. There are a large number of parameters to adjust, and they vary from one mixture to the next, however the ultimate objective is usually the same: to achieve the finest scale mixing and the most uniform micro or nano-structure throughout the material.

8.4.1 Reactive ARM Mixtures

The gasless reactive mixtures investigated for arrested milling were:

— $5Ti + 3Si$
— $Al + Ni$
— $Ti + 2B$

ARM powders were also obtained from professor E. Dreizin at the New Jersey Institute of Technology (NJIT) for the following mixtures:

— $5Ti + 3Si$
— $4Al + Fe_2O_3$
— $Ti + B$
— $8Al + MoO_3$

h

(a) (b)

Figure 43: *a) Fritsch Pulverisette 7 Ball mill used for milling powders and b) instrumented vial.*

8.4.2 Experimental Details

The powders were milled inside a Fritsch Pulverisette 7 high-energy planetary ball-mill (Fig. 43a). The mill contains an instrumented vial for monitoring the pressure and temperature during the milling process (Fig. 43b). The powder and grinding balls are introduced into two milling vials. The vials are then placed diametrically opposite each other on a rotating disc inside the milling machine. Both the disc and the individual vials rotate, resulting in planetary motion of the vials about the axis of the disc. Rotation of the vial causes balls and powders to grind against each other along the vial wall, thus exerting a shearing force on the particles. Centrifugal forces due to the counter rotation of the disc accelerates balls against vial wall and each other generating impact forces.

The main parameters to adjust for each powder system are listed in Table 6. The ball to powder ratio of 20:1 is considered standard for planetary mills. Larger quantities of powder were produced in 12-g batches. The main parameter that must be determined individually for the mixtures is the milling time. This process is described below. The milling was generally performed in an inert Argon atmosphere, however certain mixtures were milled in air to enhance the reactive properties. For example, Ti-Si mixtures were found to reach runaway reaction at times an order of magnitude shorter in air than in Argon. This was due to an enhanced reaction with the Oxygen in the air. The particle size, size distribution, and morphology were determined mainly by the properties of the available powder, however the average size was typically below 20 μm. The milling temperature increased gradually

during the milling process due to dissipation heat from the collision and friction inside the vials, as well as partial alloying reactions. To prevent overheating, the milling process was stopped intermittently to allow the sample to cool before restarting the process.

Table 6: *Milling parameters for arrested milling of reactive powders.*

Parameter	Value	Comments
Ball to powder ratio (BPR)	20:1	• 30 hardened steel balls (10 mm) • 12 g powder
Milling speed	600 rpm	Maximum recommended speed for 30 balls
Milling time	minutes	Determined for each mixture
Milling atmosphere	Argon	
Starting size of powders	$< 20\mu$m (typ.)	• $< 1\mu$m for Boron • size distribution also important
Particle morphology		irregular, amorphous, spherical
Temperature	$< 60°$C	Controlled by intermittent milling
Rotation direction		• reversed every 2 min • mitigates powder adhesion to walls

The milling time was determined by identifying the point of runaway reaction through scoping tests. The reaction time was determined for each mixture by monitoring pressure and temperature within the milling vial. In argon, the vial temperature and pressure increased gradually during milling and at the point of reaction, a sharp increase was observed in both as shown in Figures 44a and 44b. In one case, the vial pressure decreased during the milling process, as shown in Figure 44c. This was observed for Ti-Si milled in air. This was attributed to reaction between the titanium and the oxygen in the air, and has been observed in past experiments [124]. The pressure decreases as the oxygen is consumed in the Ti-O_2 reaction, reducing the amount of gaseous oxygen in the vial. Arrested ball milled powders were produced by stopping the milling process slightly before (about 2 minutes) the determined time to reaction.

The milling time was established for the ARM mixtures investigated in this study. For Ti-Si in Argon, the reaction time was found to be approximately 36 minutes, thus the milling was arrested at 34 minutes. For Aluminum and Nickel powders, the reaction time was found to be 54 minutes. For Ti-B, no runaway reaction was observed, even after 10 hours of milling.

8.4.3 Results and Discussion

The ARM powders were examined under a Scanning Electron Microscope (SEM) to observe the microstructure and mixing scale of the reactive components. Element mapping was performed through X-ray Diffraction (XRD) and image processing techniques to identify the materials in the images and measure the relative proportions of each.

For Ti-Si mixtures, the ARM powders had a finely mixed microstructure with lamellar

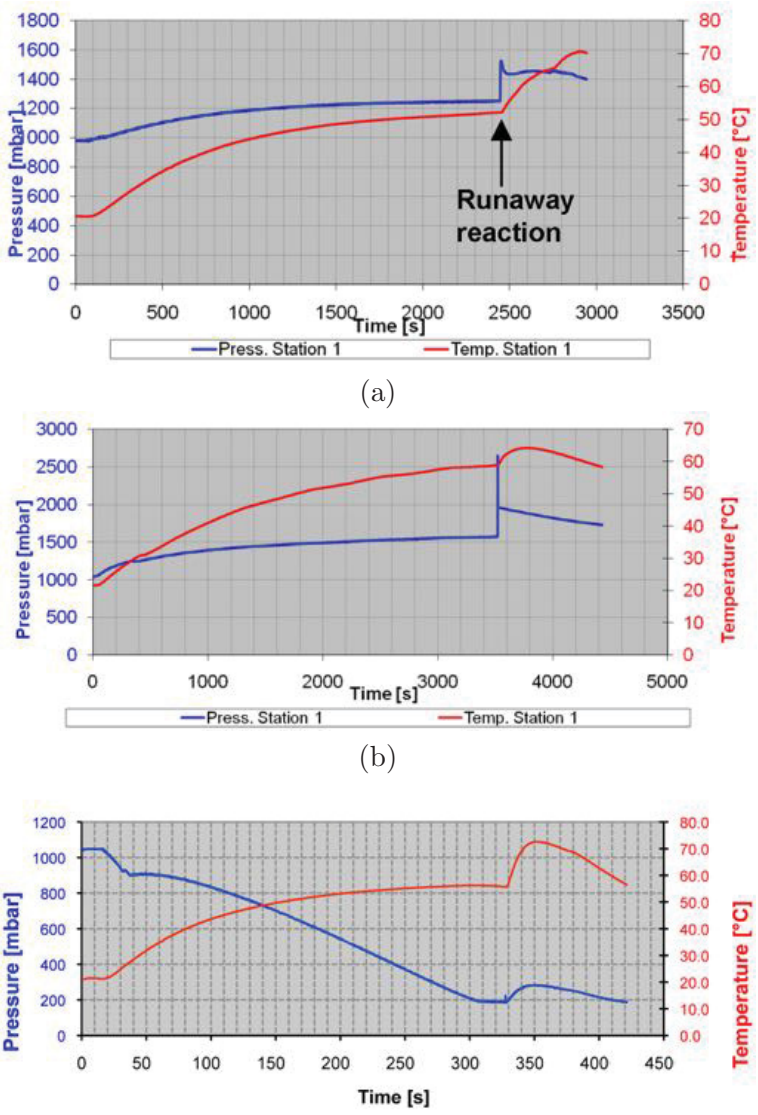

Figure 44: *Milling time to runaway reaction for a) 5Ti+3Si in an Argon atmosphere, b) Al-Ni in an Argon atmosphere, and c) 5Ti+3Si in an air atmosphere.*

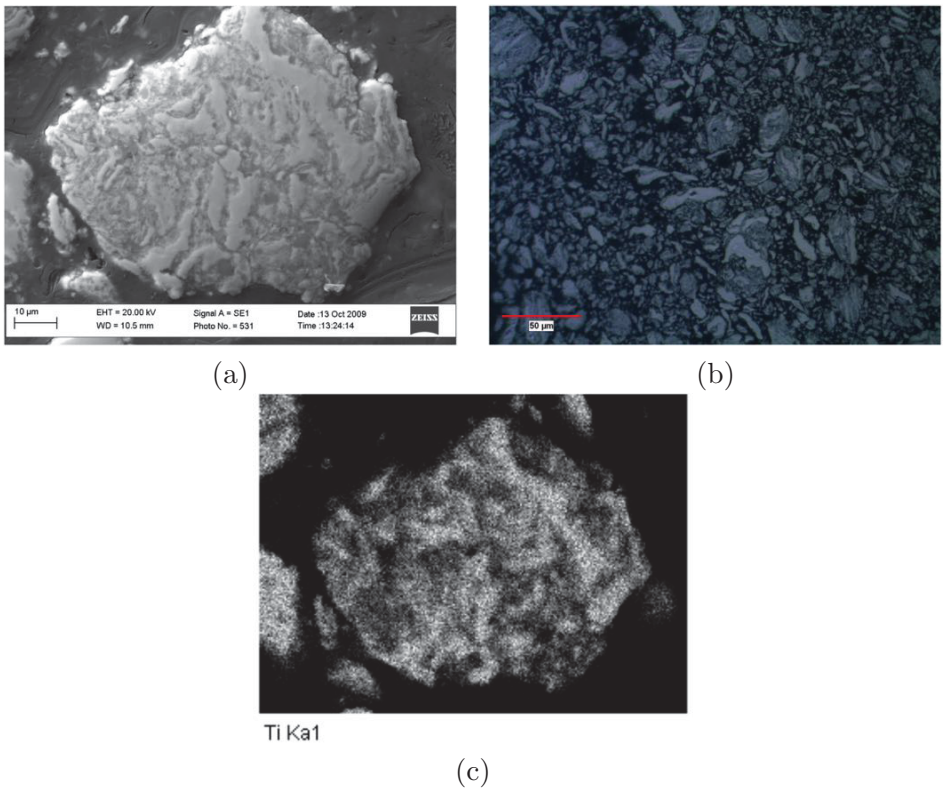

Figure 45: *SEM image of an ARM powder of 5Ti+3Si milled at a) 600 rpm, and b) 400 rpm. The element mapping of Ti is shown in (c).*

features, as shown in Figure 45a. The average size of the particles of ARM powder was about 20 μm, but some large agglomerated particles larger than 100 μm were also found. The microstructure for an ARM 5Ti+3Si powder milled at 400 rpm for 110 min instead of 600 rpm at 34 min is shown in Figure 45b. Lower milling speeds allow for longer milling times and seem to yield smaller particles although the lamellar structure within the particles does not change. Figure 45c shows the element mapping image for the powder. The image shows the location of the Titanium within the ARM powder microstructure. The other elements such as Silicon blend into the black background in the image.

The Ni-Al mixtures also yielded ARM powders with finely-mixed components (Fig. 46), however there was much more variability in the microstructure. It is believed the variability is due to cold welding of the aluminum, as there was excessive adhesion of aluminum to the walls of the vial. This resulted in a large variation of stoichiometry within the powder, as well as ARM particles of a large diameter, typically above 1 mm in diameter. Powder particles that did not undergo excessive cold welding or adhere to vial walls exhibited a very refined lamellar microstructure. It was found that cold welding could be mitigated by withholding a portion of the stoichiometric balance of Aluminum from the initial milling stage. Milling is paused after 35 minutes, and the balance of Aluminum is introduced. The ARM powder is then milled to completion.

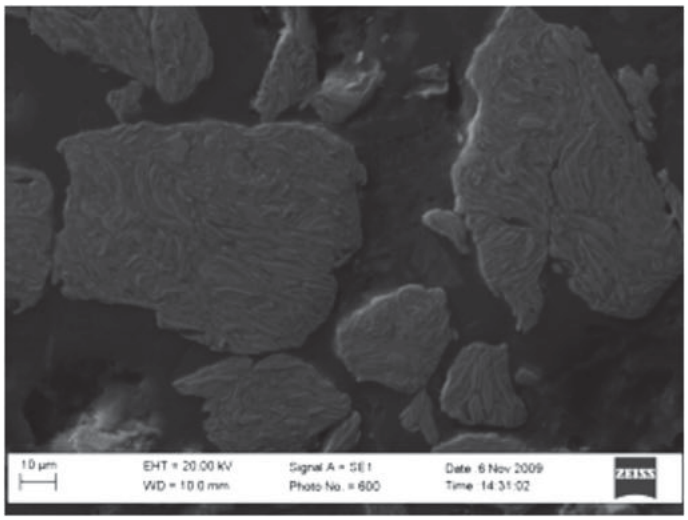

Figure 46: *SEM image of an ARM powder of Ni+Al.*

The Ti-B mixture yielded an ARM powder with a very different microstructure. Instead of being lamellar, the microstructure comprised small boron particles embedded within the titanium particles, as well as a very homogeneous distribution of elements throughout the ARM particles (Fig. 47). This is likely due to the amorphous state of the boron and the sub-micron size of the particles. The large disparity in the particle size of the titanium (20 μm) and the boron led to particles of the latter being blended into the deforming titanium in a manner akin to raisins being kneaded into dough. The element mapping images confirm the homogeneity of the mixing, as uniformly-distributed dots of boron (Fig. 47b) appear against a titanium background (Fig. 47c). Contrary to published literature, mechanically-activated reaction during ball milling did not occur, even after 10 hours of milling. However, a spontaneous reaction did occur when the vial was opened and the contents were exposed to air. In order to avoid this, the vial was opened in an inert Argon atmosphere and allowed to cool before letting the powder very gradually come into contact with air.

The microstructure of ARM powders produced by E. Dreizin at NJIT was also examined by SEM and element mapping XRD (Fig. 48). For the Ti-B powder, the microstructure is similar to that obtained in the present study, but lower concentrations of boron were found (Fig. 48a). The Ti-Si powders seem to show much less mixing than those in the present study, with silicon particles surrounding the larger titanium particles (Fig. 48b). The Al-Fe_2O_3 powders showed a homogeneous distribution of elements with occasional larger unmixed particles(Fig. 48c). The Al-MoO_3 powders showed a very homogeneous distribution of elements within the 20 μm particles (Fig. 48d).

8.4.4 Conclusions and Outcomes

Arrested milling facilities were set up and ARM procedures were successfully established for a number of reactive powders. Analysis of the microstructure showed very fine mixing

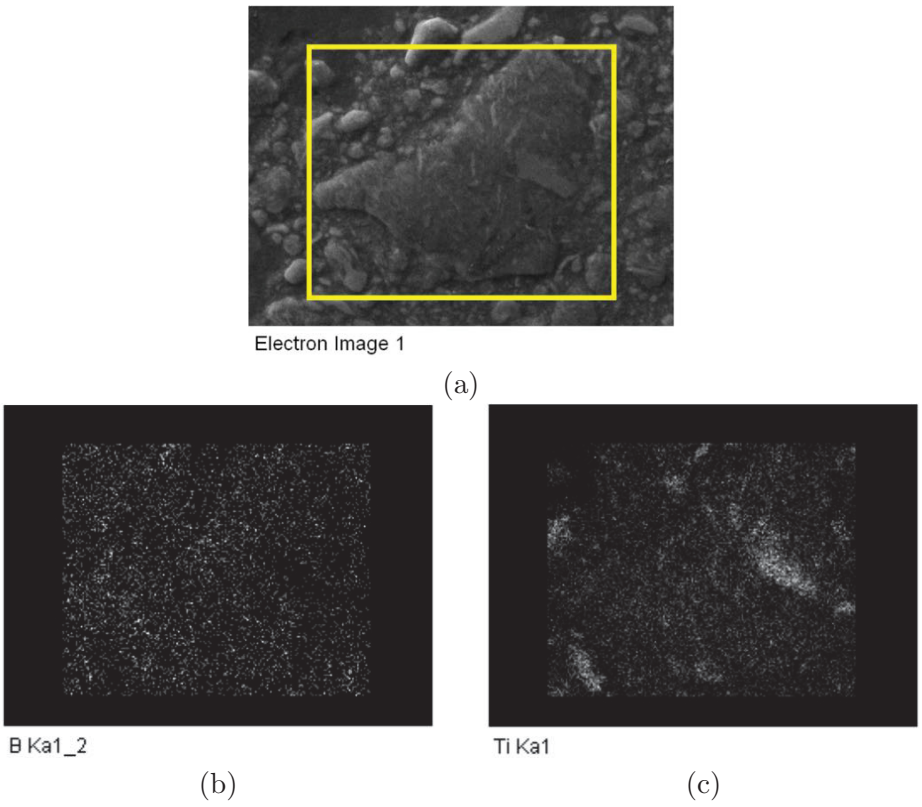

Figure 47: *SEM images of a) an ARM powder of Ti + 2B. The element mapping is shown for b) boron, and c) titanium.*

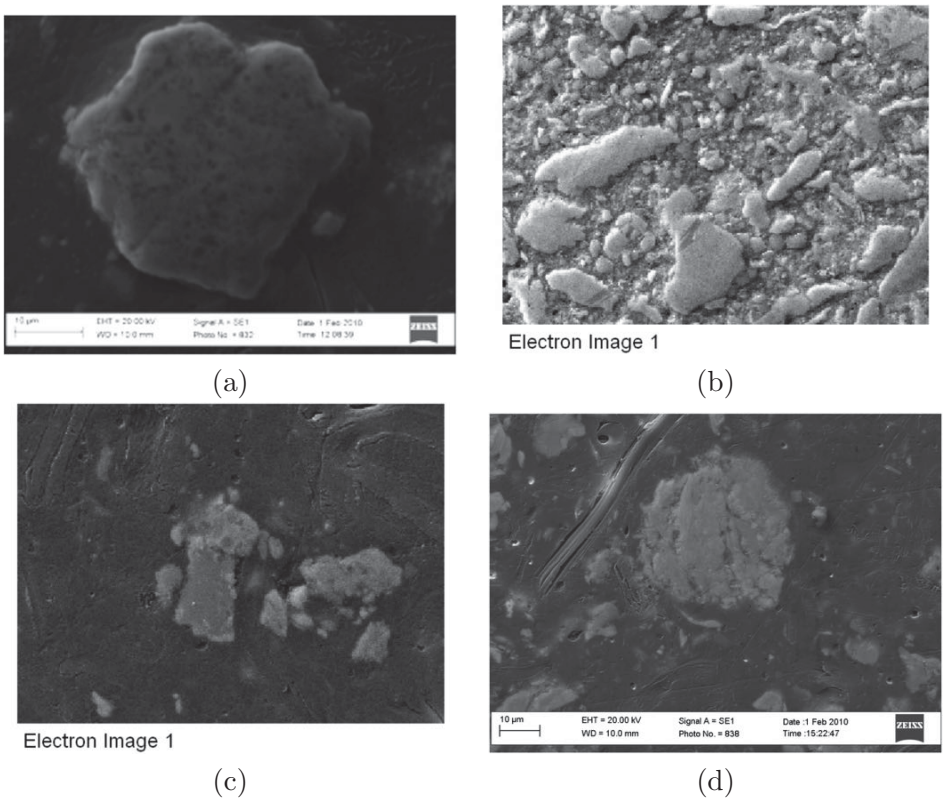

Figure 48: *SEM images of ARM powders produced at the NJIT: a) Ti + 2B, b) 5Ti + 3Si, c) 4Al + Fe_2O_3, and d) 8Al + MoO_3.*

at a sub-micron scale consisting of thin lamellar structures or sub-micron particles of one material embedded in the other. Comparison of the microstructure with ARM powders from a well-established expert in the field (NJIT) showed comparable, if not better homogeneity of the mixing.

In spite of nano-scale mixing being achieved, the overall uniformity of the mixing is still heterogeneous, with occasional larger unmixed particles embedded within the well-mixed ones. The optimal ball-milling parameters for obtaining the smallest-scale, most uniform mixtures, have yet to be achieved, and it is clear that much work remains in improving the process. The fact that ARM powders can be produced, comparable in quality to those from a well-established research center at NJIT shows that a high-level Canadian capability for ARM reactive powders has been established.

The milling parameters and microstructures of the mixtures used in this study were found to vary over a wide range, which is an indication of the extensive effort required to optimize the ARM process for each mixture. Due the wide variations in material properties, reactivity, particle size and morphology of the reactants, optimization of ARM procedures represent an ongoing effort, with plans to scale the process to larger amounts in the future.

8.5 Multi-layer Reactive Foils

To study the combustion behaviour of a simple reactive nano-composite with no porosity (100% TMD), aluminum and nickel foils were layered through a repeated cold rolling process to produce multi-layer samples. This process is not feasible for producing large samples of reactive material, and may not be applicable to materials with unfavorable material properties such as brittle materials. However the simplicity of the technique makes it attractive for laboratory studies, as the only equipment required are foils of reactive material and a roller.

The reactive foils also have the attractive feature of having no porosity, which is advantageous for detonation propagation. The relatively simple, quasi one-dimensional microstructure also allows for detailed studies of the reaction mechanisms both experimentally and numerically along the material interfaces.

8.5.1 Experimental Details

Aluminum foil with a purity of 99% was purchased from Lebow Company. The foil was 12.5 μm thick. Nickel foil with a purity of 99.9% was obtained from Alfa Aesar and a thickness of 25 μm. The foil was cut into squares of approximately 2.5 cm. To achieve a molar ratio of Al:Ni of 1:1, 3 layers for Aluminum foil was used for every layer of Nickel foil. The foil was stacked until its thickness was approximately 1mm. This stack of foil was placed between two sheets of stainless steel 1.1 mm thick. The two stainless steel sheets were clamped together using locking pliers and placed into a Durston 90 mm flat rolling mill (Fig. 49). The sample was rolled several times until its length had doubled. The sample was then folded in two and the process was repeated. Samples were folded either 15 or 20 times. Each time the sample was folded was called a rolling pass.

8.5.2 Results and Discussion

Foil samples were extremely difficult to produce. The stacked foil did not coalesce quickly into a solid mass. After five rolling passes, or folds, samples would appear solid, but after another rolling pass would flake considerably. During each pass the stainless steel sheets that surrounded the sample would deform considerably. Every attempt was made to keep them flat and they were periodically straightened or replaced. Every attempt was made to retain all pieces of flaked foil and reinsert them into the sample. Some flakes were lost but were not significant in number or weight. After fifteen rolling passes the sample contained many well formed layers. Layers formed during rolling are fairly regular in thickness. They do not compare in regularity to those produced by vapour deposition but are clearly more regular than the layers present in the ARM powders tested. The nickel is also clearly deformed into layers which did not occur consistently in the ARM powders. After twenty rolling passes the samples shows significant de-bonding of layers (Fig. 50). Layers however are regular and relatively even, and similar to the pattern seen in the fifteen rolling pass sample. XRD analysis showed that the cold rolled samples retained the 1:1 molar ratio of Al:Ni of the starting materials, thus maintaining the starting stoichiometry.

Figure 49: *Durston rolling mill.*

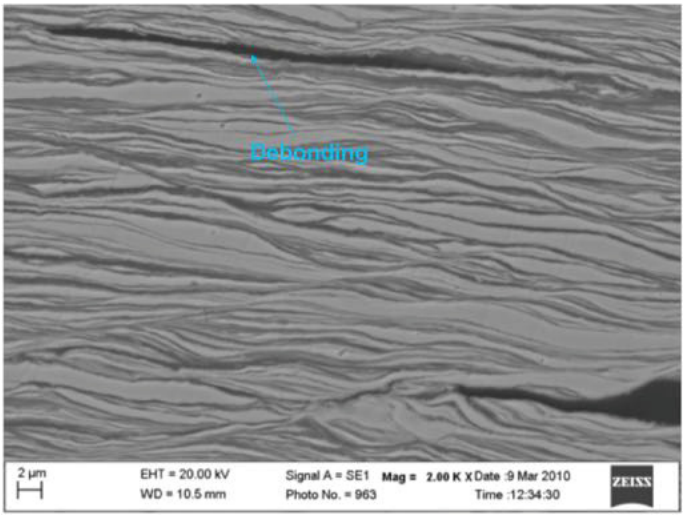

Figure 50: *SEM image of cold rolled Al:Ni foil individual layers after 20 rolling passes.*

8.5.3 Conclusions and Outcomes

A simple cold-rolling procedure was tried, but a number of practical problems made the procedure undesirable. However, one of the main advantages of this technique was that the stoichiometry of the reactants was maintained and uniform. One of the biggest disadvantages was de-bonding of the layers.

8.6 Cold-gas Deposition of Reactive Powders

Cold-gas spray deposition is a coating technique where powder materials are introduced into a supersonic flow and accelerated onto a substrate. Upon impact with the substrate surface, the particles of the powder deform and mate with the substrate material in a tightly-bound arrangement due to irregularities at the interface which provides an interlocking configuration to ensure adhesion. Due to the high velocity of the particles at impact, sufficient deformation occurs such that very few voids form in the coating material.

By using this technique with ARM powders, a bulk material with finely mixed reactive materials can be produced with little or no voids. Although the technique is typically used to produce thin coatings on substrate materials such as aluminum, by performing multiple passes with the cold-gas spray nozzle, a thicker bulk material can be produced.

The application of this technique to ARM powders is at a very exploratory stage, and will not be discussed in detail. However, a preliminary trial with ARM Al-Ni powder proved successful in producing a bulk nano-composite material. One factor of concern was that the high-velocity impact of the ARM powders with the substrate would ignite the particles, but due to the low impact sensitivity of the powders this did not occur.

This novel application of cold-gas spray technology to reactive materials opens many possibilities of new energetic materials and applications such as micro-shock devices and reactive projectiles or armour. It represents a promising area for further investigation.

8.7 Burning Rates of Mechanically-Mixed Powders

This section describes a preliminary investigation of the reaction rates in mechanically-mixed powders. The consists of a study of the flame propagation characteristics of manually-mixed powder mixtures, ARM powders, and densely-compacted powders. The characteristics of the flame propagation in the powders were observed, and insight was gained on the effects of powder properties such as composition, mixing scale, porosity, and reactivity.

The flame speeds were measured in a number of powder mixtures using optical diagnostic techniques. The main parameters varied were the powder packing density and the microstructure of the materials, i.e. loose reactive powder mixtures as opposed to nano-scale mixed ARM powders.

As the reaction kinetics are a key parameter in detonation processes, a rapid reaction rate constitutes a condition for the existence of gasless detonation in a charge of a practical size.

8.7.1 Reactive Powders Tested

The reactive powders tested consist of:

- Titanium-Air
- Titanium-Silicon
- Titanium-Silicon (ARM)
- Titanium-Boron
- Titanium-Boron (ARM)
- Aluminum-Nickel
- Aluminum-Nickel (ARM)
- Aluminum-Nickel (foil)
- Aluminum-Nickel (spray-deposited)
- Aluminum-Molybdenum trioxide (ARM)
- Aluminum-Iron Oxide (ARM)

All the powders were in loose form and were packed into an apparatus for measuring the flame front velocity. For mixtures not designated as "ARM", the powder ingredients were separate and were manually mixed by stirring them together before compacting them in the test apparatus. The foil and spray-deposited materials were maximally dense (≈100% TMD), i.e. they were consolidated pieces of reactive material, and were tested alone without placing them in a container or apparatus.

8.7.2 Burning Modes

The propagation of flames in reactive powders has been studied in the area of SHS. When SHS reactions are initialized, various modes of combustion can occur and change the dynamics of the wave front propagation. When stationary flame regimes break down, the steady-state propagation of the combustion front gives way to various modes of unsteady propagation. The modes of propagation have been classified into five modes [125]

The first mode is steady flame propagation (ordered steady propagation). This mode occurs when the reaction front is planar and is advancing towards the un-reacted portion of the mix at a constant velocity, which normally leads to a more uniform structure of the wave front. The combustion front consists of a narrow zone which separates the reactants and the products of the reaction.

The second mode is pulsating combustion (ordered unsteady propagation). The combustion rate is periodically exited and the reaction wave travels in a pulsating (periodic oscillations) manner which results in a laminated structure. This lamination is due to the presence of cracks in the specimen due to mechanical/thermal stresses caused by thermal gradients along the direction of the reaction, and locally on the plane of the reaction wave.

The third mode is spinning combustion (ordered unsteady propagation). The propagation of the reaction wave is characterized by the spinning movement of a hot spot at the surface of the sample, along the sample length (towards the unburned section of sample), or by the movement of a spinning hot plane. In the first case, the hot spot progresses along the side of the sample and the exterior trails merge together in the volume as the reaction

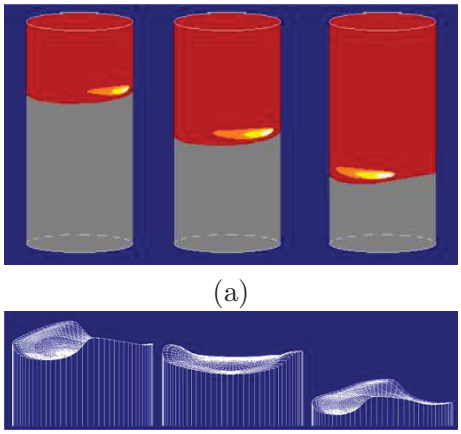

(a)

(b)

Figure 51: *Schematic representation of a) a spinning hot spot combustion front, and b) a spinning plane combustion front.*

progresses (Fig. 51a). In the case of a hot plane, the reaction occurs at the same time over the volume of the sample and the plane of reaction spins along the sample length as it progresses (Fig. 51b).

The fourth mode is the limit burning regime (disordered unsteady propagation), where one part of the reaction front follows one side of the sample and then bifurcates from it to later merge with another incoming trail.

The fifth and final mode is multispot combustion (disordered unsteady propagation) occurs when the combustion rate oscillates aperiodically and when hot spots migrate randomly in the combustion front.

8.7.3 Experimental Details

A steel channel was constructed using 1020 mild steel (Fig. 52). The overall dimensions of the channel were 32 mm by 140 mm. A slot was milled 5mm deep and 5 mm wide with a length of 100 mm (Fig. 52a). A corresponding punch of matching dimensions was constructed to facilitate the packing of the channel (Fig. 52a). It was desired to have samples of varying packing density. To fill the channel, a portion powder was poured in, and the excess was levelled off. The powder was then compacted by hand by placing the punch section of the apparatus into the channel and using body weight to compress the content. This process was repeated until the channel was full, typically in four steps. Packing densities of approximately 45% TMD were achieved in this manner. For denser compaction, samples were compressed using a 2-Ton arbour press (Fig. 53). The channel was again filled in four stages, but the arbour press was used to tap and compact the sample, achieving densities of up to 55% TMD. For even denser compacted samples, a 20-ton press was used, achieving packing densities of up to 76% TMD.

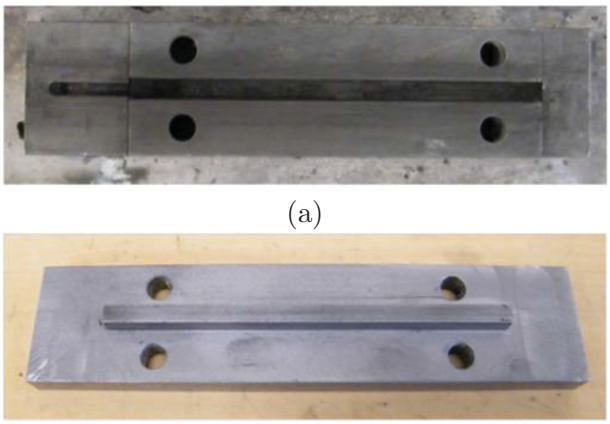

(a)

(b)

Figure 52: *Apparatus for conducting flame speed measurements. Shown are a) the base containing the channel for the sample material, and b) the punch for compacting the powder in the channel.*

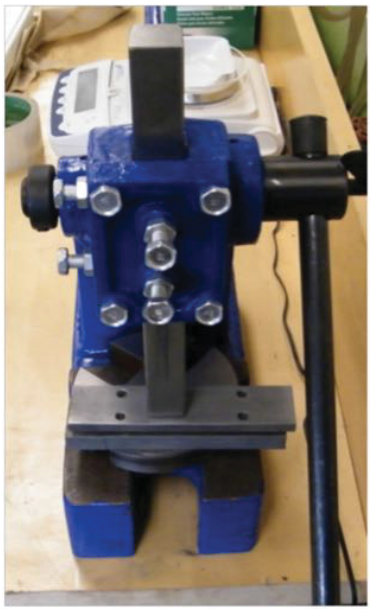

Figure 53: *2-Ton arbour press used to compact the powder in the channel.*

At one end of the channel is a 2.5 mm by 2.5 mm by 20 mm slot used to ignite the main sample. This smaller slot was filled with powder just prior to sample testing, and was more convenient to ignite than the main powder sample. It was designed to function as a fuze to carry an SHS flame front to the main sample and ignite it. The ignition powder was ignited with a small hand-held isobutane (C_4H_{10}) torch.

After the channel was packed with powder it was placed under a Casio EX-F1 high speed camera. The camera is capable of recording video at 1200 fps. This speed was verified to $\pm$ 0.5 fps ($\pm$ 0.00083 sec.) using a high speed timer and spark generator. The camera was set to F10.8 with a shutter speed of 1/40000 seconds and was approximately 1.5 m above the sample. The camera zoom was adjusted so that the sample holder filled the entire filmed area to achieve maximize image resolution.

This camera setup was also used to observe the burning rate of reactive samples in other configurations, including reactive metallic foils and powders compacted using cold-gas spray deposition. For 100% TMD ARM powder prepared using a cold-gas spray deposition, the aluminum block substrate onto which the powder was deposited was first milled to a thin layer about 1 mm thick. This was done to minimize the thermal mass of the substrate and allow the compacted powder to be ignited by raising its temperature with the isobutane flame. Without milling the substrate, the powder could not be ignited due to excessive heat transfer into the substrate.

To record video imagery of the burning process, the sample was placed onto a block of concrete under the camera. The camera was triggered and the sample ignited. After the sample had completed burning, an image was taken of the setup to show how the powder moved during the reaction. After the reaction, the sample was allowed to cool for approximately 20 minutes. After this time, the sample was removed and retained for possible future analysis of reaction product constituents. The channel was cleaned with a scraper, acetone and lint free cloths to prepare it for a new test. To prevent sparks and material from being ejected from the channel during burning, a glass plate was placed over the powder-filled channel to maintain visibility of the burning process for certain tests. The glass cover plate also limited the exposure of the powder to the surrounding air, which could have an effect on the flame front propagation in certain systems.

8.7.4 Results and Discussion

Baseline tests on burning pure titanium powder were also conducted. Titanium powder consisting of 20-μm particles were packed into the channel. Upon ignition, the oxidation reaction between the titanium and the air in the inter-particle pores propagated along the channel.

The propagation mode of the flame was found to be steady, with a planar front propagating at a nearly constant speed (Fig. 54). Even though steadiness was observed almost throughout the reaction, the stability of the propagation wave was not always constant. The plane of the reaction front did not always follow the channel in a perpendicular manner. The rocking motion of the propagation front could mean that the mode of propagation of the

Figure 54: *High-speed video of flame propagation in Ti-air powder mixtures.*

reaction front is in spinning mode (ordered unsteady propagation). The average flame speed was found to be 6.92 mm/s.

For the Ti-Si system, multiple modes of flame propagation were observed, depending on the type of powders used and the exposure to surrounding air. For samples of manually-mixed Ti and Si powders, the mode of propagation was a steady flame front. The flame front displayed a planar zone of reaction advancing at a constant velocity (Figure 55a). The flame front is seen to progress from right to left in successive video frames. Sometimes the stability of the wave front was perturbed and the steady mode of propagation became unsteady for a fraction of time of the reaction. This appeared as a momentary jump in the flame speed. The flame would resume steady propagation after the jump.

ARM powders were tested and the mode of propagation of the reaction wave was more chaotic and violent than with the unmilled powders. During the reaction, volatile particles were ejected from the channel and ignited un-reacted powders in front of the initial reaction wave (Figure 55b). If the ejection of the particles is neglected and analysis of the progression of a reaction wave is done for a newly created hot spot, the mode of propagation of that spot can be considered steady for a short period of time, after which the propagation front becomes unstable again and multiple disordered unsteady propagation modes can be observed.

To limit the exposure of the un-reacted powders to the oxygen in the air, a thick glass cover

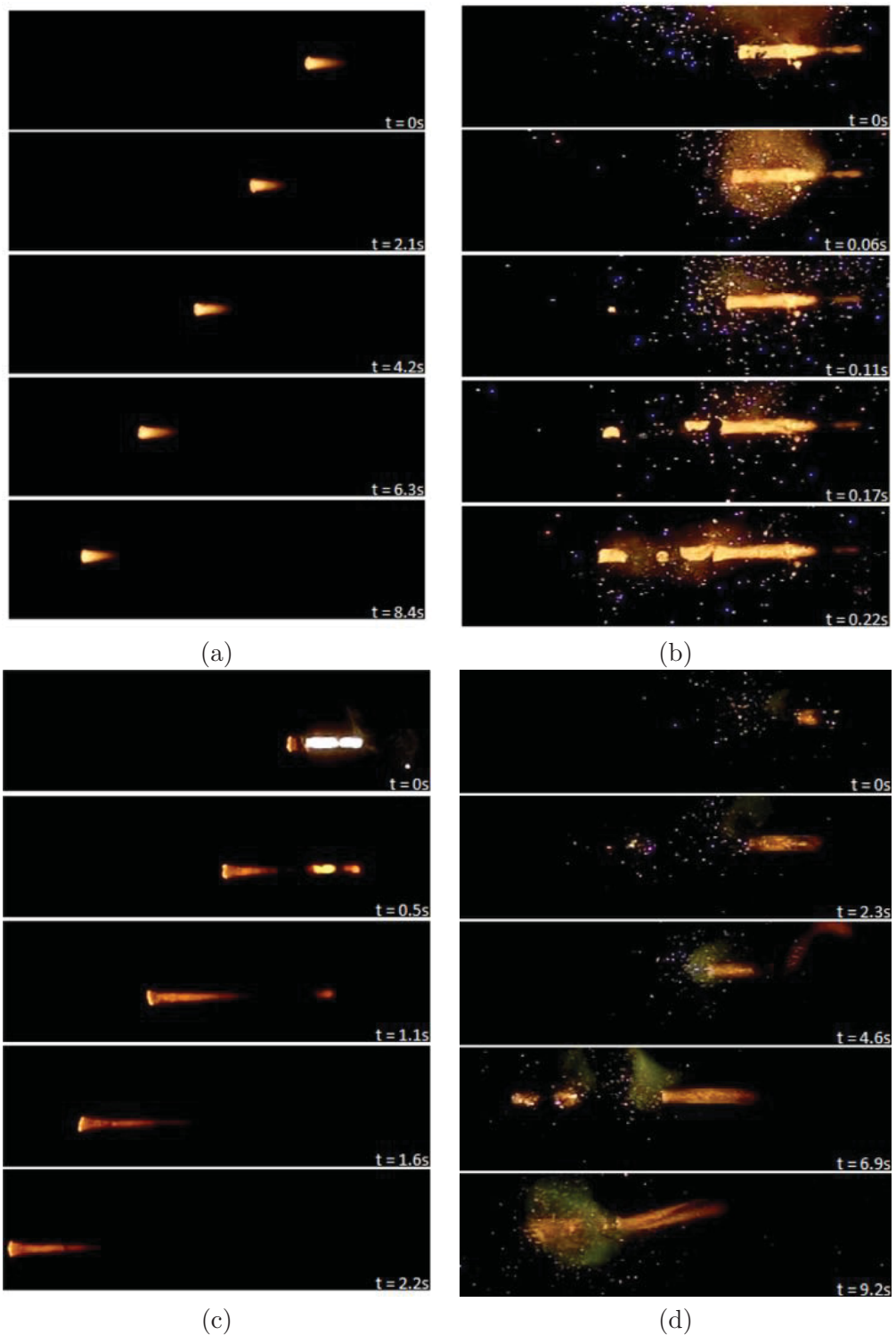

Figure 55: *High-speed video frames of flame front propagating in 5Ti+3Si powder mixture: a) a steady flame in a loose powder mixture without a glass cover, b) an unsteady flame in an ARM powder without a glass cover, c) a spinning flame in ARM powder with a glass cover plate, and d) a pulsating flame for NJIT ARM powder without a glass cover.*

was placed over the channel. This measure also prevented any particles from being ejected from the channel. Video footage of the reaction of ARM powders under a thick glass cover showed less chaotic mode of flame propagation, however the wave exhibited some unstable behaviour. The plane of the reaction front did not always follow the axis of the channel. A rocking side-to-side motion was observed, which could indicate a spinning mode of propagation of the reaction front (ordered unsteady propagation). Figure 55c shows the rocking (or spinning) motion of the reaction front.

Tests were performed with 5Ti+3Si ARM powder from NJIT. When the channel was uncovered and the powder was exposed to air a pulsating mode of propagation was observed (Figure 55d). This mode was identified not only from video records of the propagation, but from the appearance of the combustion products. The products had a periodic laminated structure which was not observed after other modes of propagation. As a result of the channel being open, particles were ejected in all directions, occasionally igniting new reaction sites in front of the initial propagating flame front. Another feature was the appearance of a greenish vapour near the flame front. The cause of this vapour is unknown, but may be caused by impurities in the powder or residual substances left by the hexane in which the powder was shipped. Hexane was used to passivate the powder, and was removed prior to testing by air drying and exposing the powder to a vacuum.

When a glass cover was placed on the channel to limit the exposure of the powders to the air and limit the launching of hot particles, the mode changed from pulsating to spinning combustion. Inspection of the combustion products after the tests confirmed the spinning mode as they no longer showed a laminated structure.

The results of the flame speed measurements as a function of % TMD (packing density) are shown in Figure 56. Due to fluctuations in the propagation speed, the average speed over the entire channel is shown. The flame speed in mixed Ti-Si powders is found to increase with increasing packing density (Fig. 56a). This is expected since the energy density of the material, and subsequently the flame temperature, increases with packing density. The ARM powders showed an increase in flame speed by a factor of approximately five, which supports the assumption that decreasing the diffusion distance increases the reaction kinetics. The ARM powder from NJIT did not show a significant increase in the flame speed. This is consistent with observations in SEM images that the Ti and Si did not appear well mixed (Fig. 48b).

For the Ti-B system, only two powder configurations were tested: compacted mixtures of manually-mixed powders and NJIT ARM powders, both in an open channel exposed to air. For the manually-mixed powders, the mode of propagation of the flame front was irregular, fluctuating from one mode to another. Steady propagation was observed for short periods of time when the flame front displayed a planar zone of reaction advancing at a constant velocity. The reaction wave sometimes spontaneously switched to a disordered unsteady mode (multispot). In other tests, the steady propagation switched from a steady mode to an ordered unsteady mode (spinning). Figure 57a shows the wave front being disturbed after 1.5 seconds, then returning to a more planar wave at 4.6 seconds after transitioning through the spinning mode of propagation at 3.1 seconds.

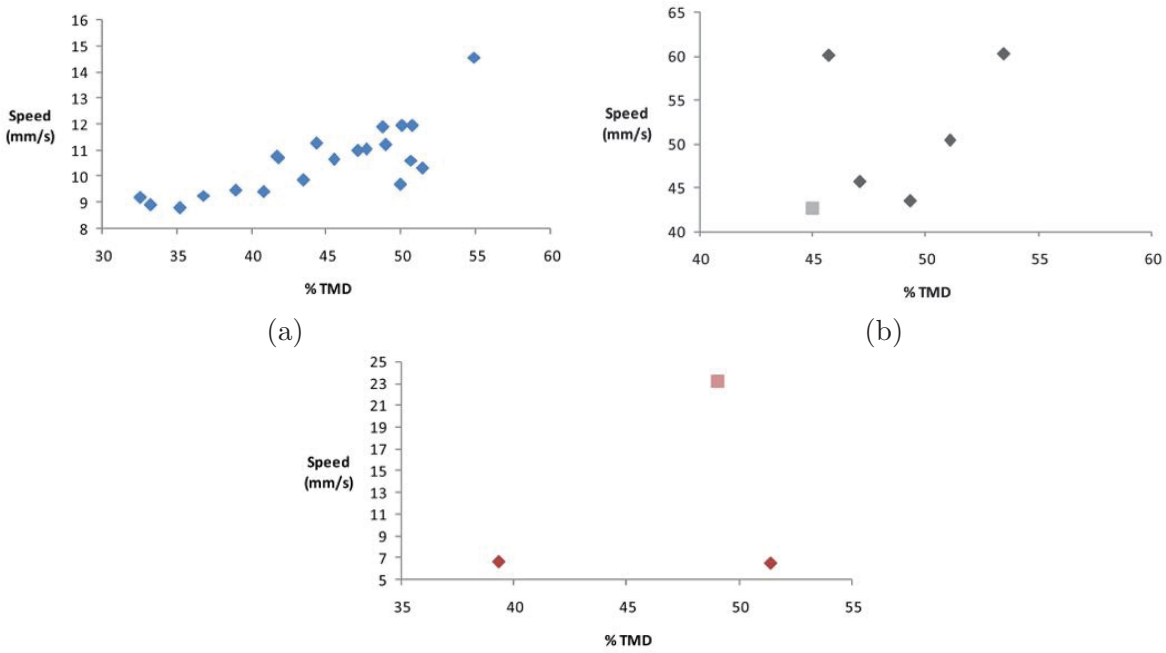

Figure 56: *The dependence of flame speed in 5Ti+3Si powder mixtures on % TMD for a) loose powders, b) ARM powders, and c) NJIT ARM powders.*

In experiments performed with NJIT ARM Ti-B powders, a pulsating mode of propagation was observed. This was confirmed by both the video records and post-trial examination of the reaction products. The final products had a typical laminated structure associated with pulsating propagation. Because the experiments were performed in an open channel, particles were ejected and initiated new reaction spots ahead of the initial flame front (Fig. 57b). As for NJIT ARM Ti-Si powders, green vapor, presumably from the burning of residual impurities, was observed near the flame front.

The flame speed was found to vary between 5 mm/s and 17 mm/s (Fig. 58). A weak increase in flame speed with increasing packing density was observed in manually-mixed powders (Fig. 58a), while NJIT ARM powder showed no clear dependence for the limited amount of data obtained (Fig. 58b). The flame speed in the NJIT ARM powder appeared to be lower than the manually-mixed powder by a factor of approximately two, which is the opposite to the trend observed in the Ti-Si powders (Fig. 56). This was unexpected since the ARM powder should have been mixed at a finer scale than the manually-mixed powders.

For the Al-Ni system, manually-mixed and ARM powders were tested over a wide range of packing densities. The loose powders were packed through a number of packing methods (cf. 8.7.3) to achieve packing densities from 35% to 100%. For manually-mixed powders, samples were tested with TMDs between 35% and 54%. To achieve 35% TMD, the powders were deposited in the test channel with no compaction. For higher packing densities,

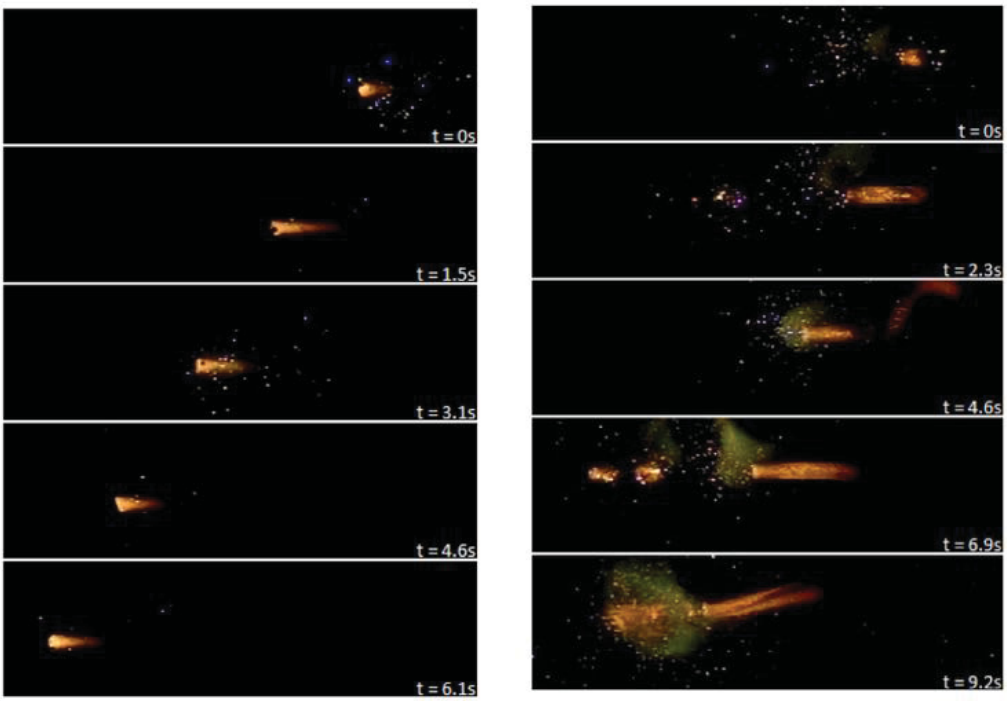

(a) (b)

Figure 57: *High-speed video of flame propagation in Ti+2B powder mixtures on % TMD for a) manually-mixed powders, and b) NJIT ARM powders.*

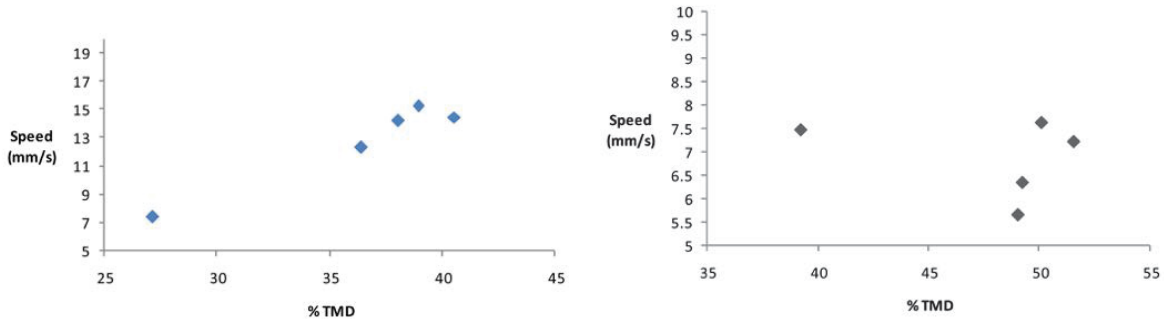

(a) (b)

Figure 58: *The dependence of flame speed in Ti+2B powder mixtures on % TMD for a) manually-mixed powders, and b) NJIT ARM powders.*

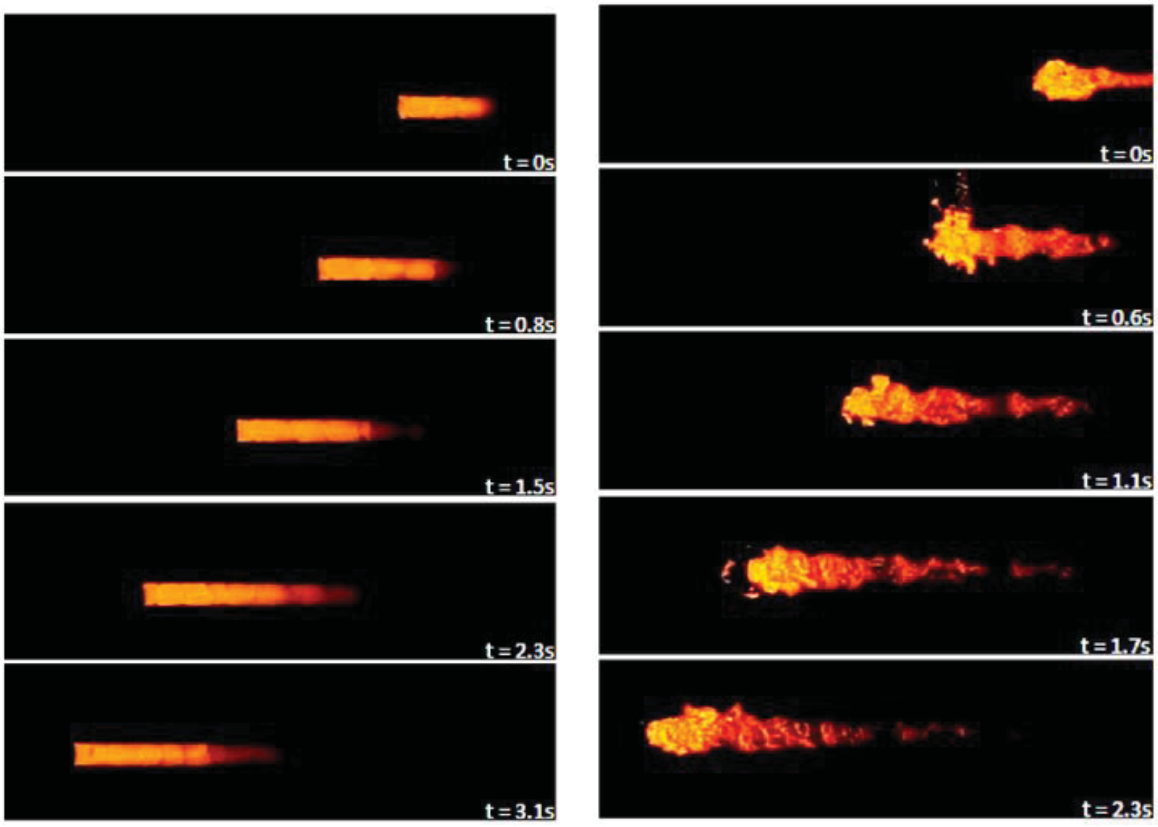

(a) (b)

Figure 59: *Video images of flame propagation in Al-Ni powder mixtures for a) manually-mixed, and b) ARM powders.*

the powders were compacted using the punch and arbour press to tap and compress the powder. The ARM powders were packed at densities from 45% to 76% TMD using the same techniques, however, 100% TMD powder was packed using cold-gas spray deposition (cf. 8.6). The glass cover was not used for any of the tests, thus the powder in the channel was exposed to air.

For the manually-mixed powders, the flame front was steady, planar and propagated in a very even and regular manner (Fig. 59). Some sparks were noted but did not ignite the sample at other locations. The burned sample stayed inside the channel and its final size was comparable to the packed reactant powder. The SHS products were, for the most part, solid and in one large piece (Fig. 60). Some samples did crack and break when being removed from the channel.

For ARM Al-Ni powders, the propagation was more violent and chaotic. Hot particles were randomly ejected from the channel, igniting the powders in front of the combustion wave (Fig. 59b). The reaction front was never planar, and the migration of hot spots occurred randomly. The mode of propagation was multispot combustion, i.e. disordered

Figure 60: *Burned sample of Al-Ni after combustion.*

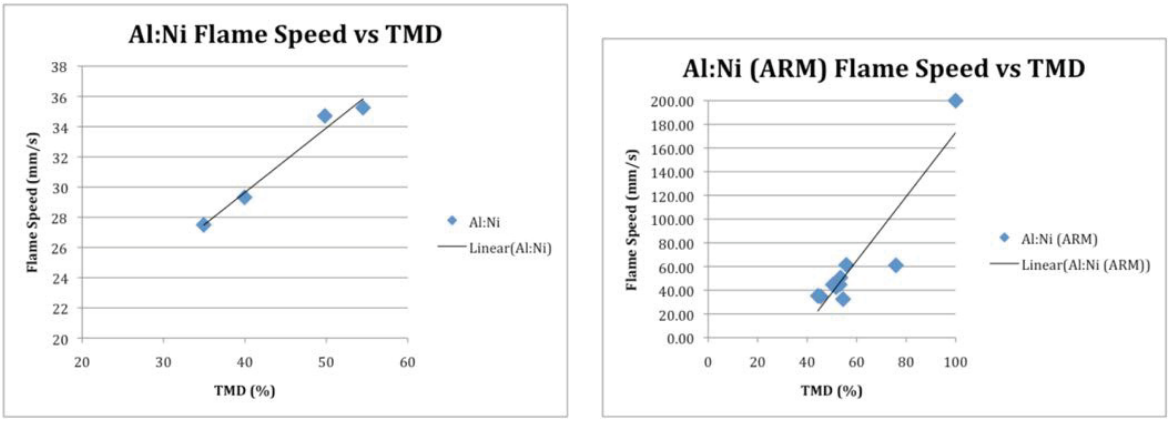

(a) (b)

Figure 61: *The dependence of flame speed in Al-Ni powder mixtures on % TMD for a) manually-mixed powders, and b) ARM powders.*

and unsteady.

The flame speed in Al-Ni powders were found to increase with powder compaction. Manually-mixed powders exhibited lower flame speeds than ARM powders for comparable packing densities (Fig. 61), but both powders showed an increasing trend of flame speed with compaction, as illustrated by the linear fits. The 100% TMD ARM powder obtained through spray-deposition and the foils showed the highest average velocity at ≈200 mm/s. The chaotic nature of the propagation, even in maximally-dense reactive material points to a dependence of the flame speed on uniformity of the mixture. It is likely the flame propagated rapidly through the finely-mixed regions, and slowed down when larger poorly-mixed regions were encountered.

For the Al-Fe_2O_3 system, only NJIT ARM powders were investigated. The sample was tested with no glass cover on the channel, and therefore exposed to ambient air. When ignited, the violent reaction created a cloud of particles that ejected powders outside of the channel (Fig. 62a). After the reaction no powder was left inside of the channel. It was possible to witness an aperiodic release of gas as the reaction progressed towards the un-reacted portion of the powders. This mode of propagation could not be identified using an SHS reaction mode.

When a glass cover was put over the channel, limiting exposure to air, the reaction was

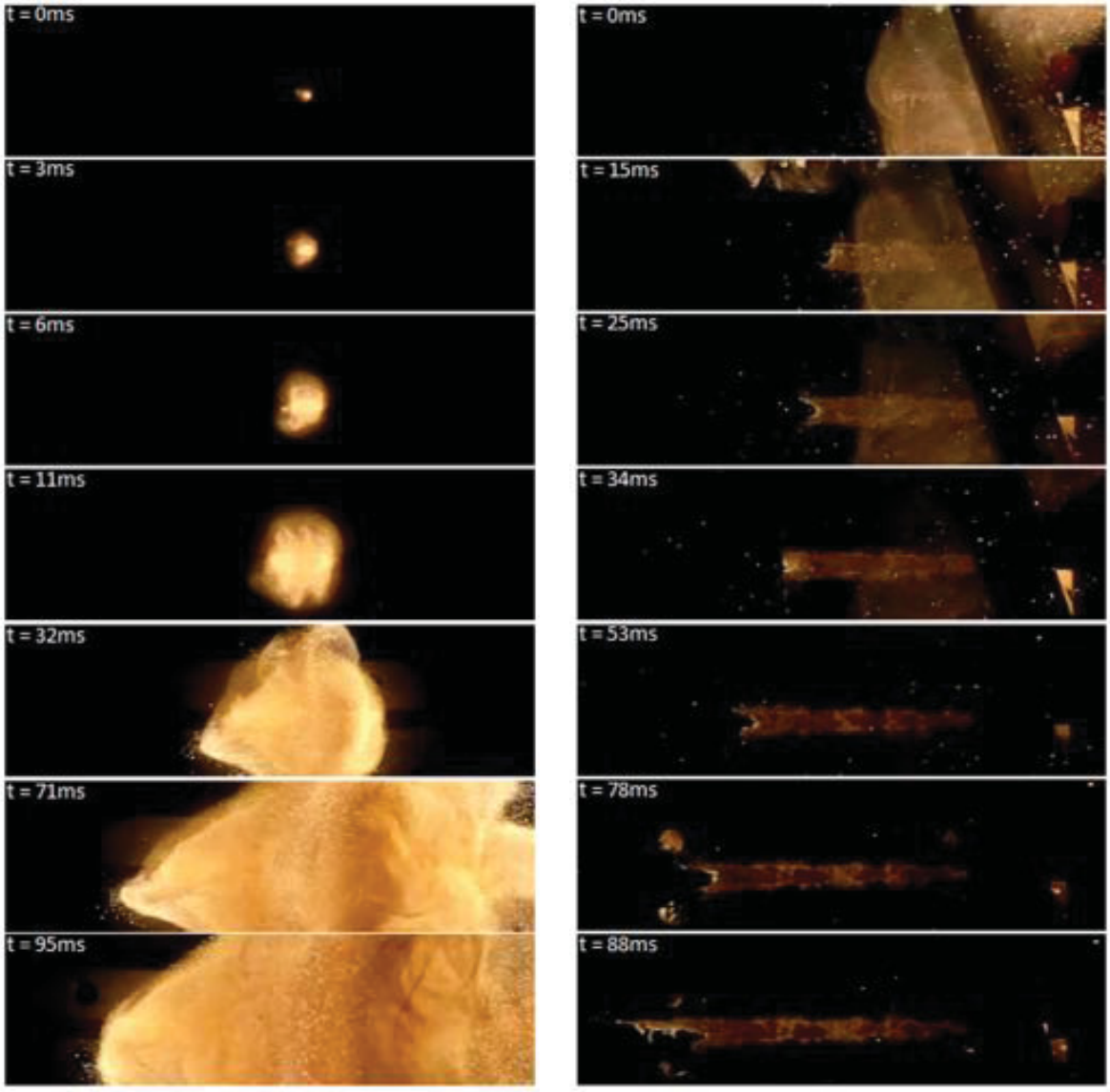

(a) (b)

Figure 62: *Video images of flame propagation in Al-Fe_2O_3 ARM powder from NJIT. Reaction in a) an uncovered channel, and b) a glass-covered channel are shown.*

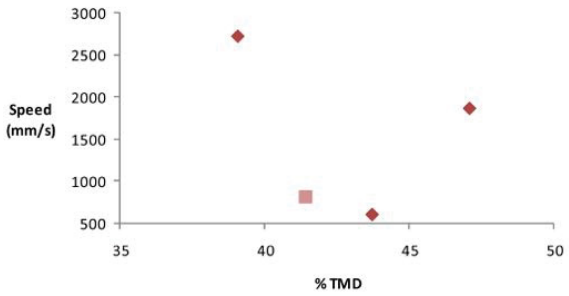

Figure 63: *Dependence of the flame speed in Al-Fe_2O_3 ARM powder from NJIT on packing density.*

more directional and coherent. Classification according to SHS combustion modes was then possible. The flame front was observed to progress towards the un-reacted powders in a disordered unsteady propagation, in a limit burning mode (Fig. 62b). The flame front moved along the edges of the channel faster than in the centre. The edge trails later bifurcate and merge with the incoming centre trail.

The flame speed was up to two orders of magnitude higher than the previous powders tested, with a maximum speed of 2700 mm/s being observed (Fig. 63). The flame propagation was chaotic, and a wide scatter in the speeds was found over a range from 500 mm/s to 2700 mm/s. The data was insufficient to identify a dependence on packing density. This system appears to be highly reactive, and gaseous reaction products (FeO) are believed to contribute to the convective-diffusive mechanisms that drive the combustion wave.

For the Al-MoO_3 system, a violent reaction was observed similar to that in the Al-Fe_2O_3 system. Without a glass cover, the reaction ejected hot particles in all directions, leaving no products in the channel after the combustion event (Fig. 64a). The reaction wave could again only be classified according to an SHS combustion mode after a cover was placed over the channel (Fig. 64b). The flame front was never planar, and a random movement of hot spots was observed. The mode of propagation was neither steady nor ordered but could be considered as a disordered unsteady propagation referred to as multispot combustion.

The flame speed was high, reaching maximum values near 8500 mm/s (Fig. 65). A wide range of speeds from 4000 mm/s to 8500 mm/s was observed, though no clear dependence on packing density could be discerned from the limited data. The 8Al+MoO_3 stoichiometry has been reported as a gasless reaction, however the high reactivity of the mixtures may be driven by the heated air in the inter-particle pores.

8.7.5 Conclusions and Outcomes

In this study, burning phenomena were observed for a number of mechanically-mixed, low-gas reactive ingredients. ARM methods were successfully developed to produce solid reactive composites with a lamellar microstructure and even sub-micron mixing scales. The

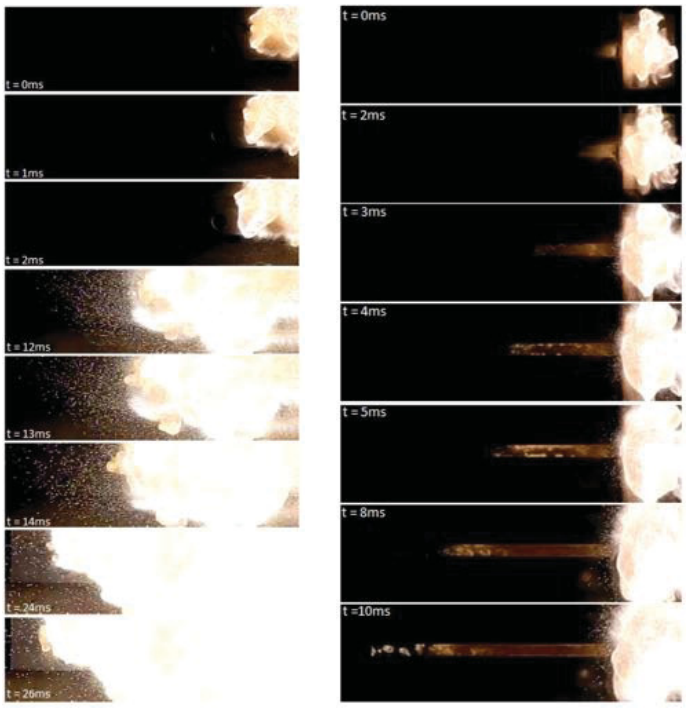

(a) (b)

Figure 64: *High-speed video of flame propagation in NJIT ARM powders of Al-MoO_3 a) without a cover, and b) with a glass cover.*

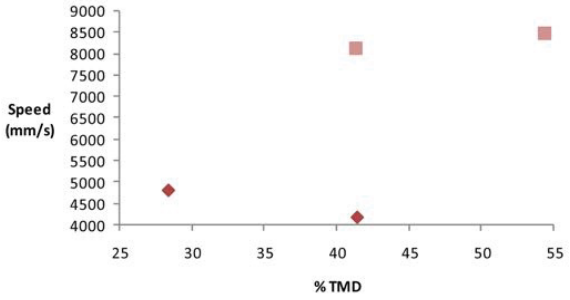

Figure 65: *Dependence of the flame speed in Al-MoO_3 ARM powder from NJIT on packing density.*

micro-structure is highly irregular, and optimization of the ball-milling technique is necessary to achieve a more uniform mixing. In addition, maximally-dense reactive composites were achieved using cold rolling of foils, as well as cold-gas spray deposition techniques. The latter innovative technique remains to be developed and investigated, however preliminary results are very promising.

The flame speed was measured through high-speed video imaging. ARM powders were found to burn more rapidly than their unmilled counterparts. The flame speed was also found to increase with increasing packing density. The flame propagation was found to be highly irregular and chaotic, with steady flames being the exception more than the rule. The preliminary results suggest that unsteadiness in the reaction waves is influenced by non-uniformities in the microstructure, and the presence of gas or air contributing to the convective-diffusive heat transfer processes. The most energetic mixtures were found to be the Al-Fe_2O_3 and Al-MoO_3 systems.

ARM techniques were shown to be a viable method of decreasing the mixing scale and increasing the diffusion-driven reaction of gasless reactive composite mixtures. In addition, the dependence of burn rate on packing density provides another mechanism of increasing the reaction rate. Investigating and optimizing ARM techniques, combined with methods of consolidating powders into low-porosity composites are promising directions in achieving highly energetic gasless reactive materials.

9 Overall Summary and Assessment of Outcomes

The original approach to achieve gasless detonation in this project was to start with powder mixtures described in Russian papers claiming the discovery of the phenomenon. In these papers, a new energy release mechanism named"super-diffusion" was postulated to explain the observed detonation waves. A second approach to achieving gasless detonation was also initiated based on new techniques of mechanically pre-mixing reactive materials to drastically increase diffusion-driven reaction rates. Theoretical analyses of gasless detonation were also performed in several areas.

Simple Hugoniot analyses and impedance-matching methods were used to theoretically evaluate the performance of gasless detonation in terms of shock transmission into metal targets. It was found that gasless detonations could indeed exist within a very narrow range of conditions, but that low porosity was necessary to achieve the condition of volume expansion. Finite-Element (FE) modeling was also performed on the compacted powder mixtures, and material models for various mixtures of metals and chalcogenides were implemented into the LS-DYNA code. These models were based on Batsanov's method of estimating Hugoniots of mixtures [49] and Meyer's porous media model [93]. These models were used successfully to estimate shock pressures of the powders before the onset of reaction. Finally, a substantial effort was placed in thermo-chemical equilibrium calculations of gasless systems.

While seeking to theoretically analyze the behaviour and performance of reactive solids,

it was found that a knowledge gap existed for performing thermo-chemical equilibrium calculations on materials that react in the solid or liquid phase. Since equilibrium calculations are a fundamental and important step in estimating the performance of energetic materials, it was necessary to develop new tools for analyzing condensed phase reaction products at high pressures and temperatures. Calculation methods known as CALPHAD techniques were used for the first time in Chapman Jouguet detonation calculations via the FACTSAGE code, which specializes in complex phase transitions and equilibrium states of metals and solids. A rigorous shock physics formulation had to be developed to extend FACTSAGE thermo-chemical equilibrium results to high pressures so that they could apply to detonation states. With these models, a capability was developed to not only calculate the combustion properties of condensed-phase reactions at detonation conditions, but also optimize and design new mixtures. However, the accuracy of these models depends on the stability of the combustion products and availability of high-pressure thermodynamic data for relevant reaction species in the condensed phase. Reactive systems with highly complex reactions that exhibit a strong and unknown pressure dependence remain a challenge to be addressed in future efforts.

For the experimental research effort, attempts were first made to reproduce existing gasless detonation results. After carefully reproducing the Russian experiments, it was found that detonation waves did not occur, but that the Russian observations were likely misinterpretations of fluctuations of decaying shocks due to variations in the material properties of the powder mixtures. These Russian mixtures thus failed to achieve the two main conditions necessary for detonation: very fast reaction rates, and volume expansion to drive the shock. Further investigation of other reactive mixtures with different reactivity, particle morphology, and packing density were also investigated. Experiments showed that very fast reactions on a detonation timescale (microseconds) could indeed be achieved, however these reactions were insufficient to sustain a full detonation wave. The fast microsecond-scale reactions were found to decouple from the leading shock wave [39, 40], leading to a gradual decay of the wave. Rapid reactions were also observed by Jetté et al. [50, 36] and were described as hot spots. Only a small portion of the material was observed to react rapidly, however, and the bulk of the chemical energy release was found to occur at much later times, tens of milliseconds after the shock had passed and decayed. The timescale of the bulk energy release, or exothermicity, was found to be 2-3 orders of magnitude longer than the microsecond shock timescale, and was found to be consistent with diffusion-driven combustion. In all the mixtures tested in this study, the small fraction of chemical energy released at the shock front was found to be insufficient to sustain a detonation wave.

An excellent review of the state of reactive shock synthesis was recently given by Eakins and Thadhani [53]. The concepts of 'shock-induced reaction' and 'shock-assisted reaction' were restated with supporting evidence from large-scale simulations of the inter-particle interactions under shock compression. Within the framework of the present project, the fast reactions observed can be categorized as 'shock-induced', and the bulk exothermicity can be categorized as 'shock-assisted'. Eakins and Thadhani proposed a method of representing mixtures in terms of their difference in acoustic impedance and yield strength which identifies combinations most likely to undergo 'shock-induced reactions'. In this represen-

tation, the Ti-Si system appears as one of the most suitable, yet extensive testing in the present work have shown that the 'shock-induced reactions' are still insufficient to support detonation. This suggests that additional factors such as volume expansion and reaction kinetics should be considered to achieve detonation.

With these discoveries and the realization that the Russian literature was unlikely to lead to a gasless detonation capability, emphasis in this project was switched to the back-up approach in the TIF proposal of mechanically-mixed materials.

The approach of using mechanically-mixed materials was based on conventional diffusion theory to drive the reaction rather than a new energy release mechanism, however the rapid reactions necessary for detonation were to be achieved through mixing to a nano-scale level. It was necessary to develop novel techniques to achieve nano-scale mixing of the reactive constituents in the composite materials. Arrested Ball-Milling and foil-rolling techniques were developed in collaboration with the University of Ottawa to achieve nano-composite reactive materials for the first time in Canada. To date, an increase of burning velocity by a factor of three has been observed in the nano-composites. While not yet sufficient to sustain detonation, this approach shows promise in achieving the required condition of very fast reaction, and further optimization of the mixing process to improve uniformity and further reduce the mixing scale may provide the desired results. Research using a relatively new metal-coating technique known as cold-gas spray deposition was developed to achieve very low porosity in the nano-composite materials. As a result, a novel reactive nano-composite with zero porosity was successfully synthesized for the first time.

One of the main successes of this project is the development of nano-composite synthesis methods, and achieving an increase in the reaction rate to approach conditions for gasless detonation. Another success is the development of new embedded gauge techniques for measurements inside solid reactive materials (metallic powders). Finally, new computational methods were developed to perform thermo-chemical equilibrium calculations on gasless reactive systems. These methods not only allow one to estimate the performance of reactive materials in condensed phase, but also optimize and design new mixtures.

This project has generated and published new knowledge on gasless reactive systems, and has developed in-house capabilities for computational and experimental research on novel energetic materials. The research activities within this program have led to scientific documentation in the open literature, and information on the program has been requested by and delivered to two U.S. organizations: DTRA (W. Wilson) and Advanced Energetics Research (K. Kim). The gasless reactive expertise developed at DRDC was used as leverage in obtaining reactive ball-milled materials from the New Jersey Institute of Technology through an existing MOU with the U.S. The capabilities developed in this project have successfully produced a new reactive nano-composite material with potential applications in S&T areas where the tunability of the energy release could be an advantage.

10 Way Ahead

A promising area has emerged from the present TIF project: reactive nano-composite materials. To investigate this topic, an infrastructure for the synthesis of new reactive nano-composites covering a wide range of porosities and reactivity has been built at the University of Ottawa. A future project in this area should focus on optimizing the Arrested-Milling and Cold-gas Spray Deposition processes to achieve more uniform mixing at the nanometer scale or smaller. The mechanisms of diffusion-driven combustion in reactive nano-composites should be investigated to determine the properties the energy-release mechanisms in order to achieve the desired performance of these materials. In addition, a computational capability for equilibrium calculations of gasless or low-gas reactive systems has been developed using the CALPHAD techniques implemented in FACTSAGE. This approach can be used to estimate the performance of selected inter-metallic and thermite mixtures, and can be used to enhanced new reactive systems. This CALPHAD-based approach could also be further developed to perform mixture optimizations accounting for composition changes along the shock Hugoniot. Because the potential applications of reactive nano-composites is wide, it is recommended that linkages be made with research groups and end-users in terminal effects, biological effects (e.g. human injury), novel energy sources, and emerging functional materials. Through these linkages, the research directions outlined above can be pursued through DND programs with collaboration with academia, though industrial partners must be sought for technology exploitation.

A 2010 TIF proposal was submitted on novel reactive nano-composite materials, where the plan was to investigate and develop the tunability of the energy release of this class of energetic materials. The main objectives of the project were to optimize the techniques for processing reactive nano-composite materials and investigate the energy release properties. The enhanced FACTSAGE code was to be used to estimate the performance of these new materials, as well as design and optimize new mixtures. This proposal will not be funded in 2011, and new avenues of funding are being sought.

The new features in FACTSAGE also make it suitable for calculating shock properties of a wide range of alloys of interest to the CF such as Nickel-Aluminum-Bronze or 350WT steel used in naval platforms. Another proposal to use FACTSAGE as part of a set of non-destructive evaluation tools for naval materials is planned for a future date.

Finally, further development of reactive nano-composite materials is planned for joint cellular research with the Casualty Management Section and nano-materials research with the Hazard Protection Section. It is recommended that some of the capabilities developed within this project through academia be transferred to DRDC Suffield, such as the arrested ball-milling technique. In addition, this area of research should be further consolidated within the Military Engineering Section, and new research and Defence S&T opportunites should be explored through linkages with the Casualty Management Section Hazard Protection Section.

Acknowledgements

The author would like to acknowledge his many collaborators whose published and unpublished work appear in this report. Paul Thibault spearheaded the equilibrium calculations through collaborations with James Gottlieb at UTIAS and Aimen Gheribi and Arthur Pelton at the Polytechnique de Montréal. The shock initiation studies were performed at McGill University by François-Xavier Jetté, Sam Goroshin, David Frost, and Andrew Higgins and their teams of students. The investigation of mechanically-mixed powders was performed at the University of Ottawa by Matei Radulescu, Michel Nganbe, and Bertrand Jodoin with Yannick Charron-Tousignant, Jason Van Dyke, Brian Barrett and their teams of students. The author would also like to thank the trials support personnel at DRDC Suffield including Brian Eichelbaum, Kiril Mudri, Mark Churcher, Geoff Paulgaard, University of Calgary COOP student Geoff Buckley-Herd, University of Saskatchewan student Mario Mudri, as well as the FOS, with the always excellent support of the ESEG. The ARM powders provided by professor E. Dreizin at NJIT are gratefully acknowledged. Last but not least, the author would like to acknowledge the support of colleagues Fan Zhang, James Huang, John Anderson, Louis Gagné, Pat Lambert, for their support and valuable discussions, as well as the constant encouragement and guidance of the DRDC Suffield Chief Scientist, Kent Harding.

References

[1] Thadhani, N.N. (1994) , Shock-induced and shock-assisted solid-state chemical reactions in powder mixtures, *J.Appl.Phys.*, 76(4), pp. 2129-2138.

[2] Batsanov, SS. , Effect of high dynamic pressure on the structure of solids, *Propellants, Explosives, Pyrotechnics, 12pp. 206-208* (1987)

[3] Graham, RA, Anderson, M.U., Horie, Y., You, S.-K., Holman, G.T. *Shock Waves 3, p. 79* (1993)

[4] Gryadunov, AN, Shteinberg, AS, Dobler, EA, Gorel'skii, VA, Zelepugin, S. "Ignition and Development of a Chemical Reaction of Titanium and Carbon Under Shock Loading", *International Journal of Self-Propagating High-Temperature Synthesis, 3(3), pp. 253-260* (1995)

[5] Wong, F.C.H., Gottlieb, J.J. and Lussier, L.-S., "Chemical Equilibrium Analysis of Combustion Products of Constant Volume", *Defence R&D Canada Valcartier, Technical Report, DRDC Valcartier TR 2003-375* (2003)

[6] Bale B. et al. *Calphad 28, p. 189* (2002)

[7] Bale C. et al. *Calphad 33, p. 295* (2009)

[8] Saunders, N., Miodownik, A. P. "CALPHAD, Calculation of Phase Diagrams, A Comprehensive Guide", *Pergamon Materials Series, Vol 1 Ed. R W Cahn* (1998)

[9] Schoenitz, M, Ward, T, Dreizin, EL. "Preparation of Energetic Metastable Nano-Composite Materials by Arrested Reactive Milling", *Mat.Res.Soc.Symp.Proc., 800pp. AA2.6.1-AA2.6.6* (2004)

[10] Altshuler, A.M. "Detonation Waves of Transfomations in Energetic Materials: An Assessment of Soviet Research", *Technical Research Corporation* (1990)

[11] ZND, Inc. "Assessment of Self-Propagating High-Temperature Synthesis (SHS)", *ZND Inc.* (1996)

[12] Radulescu, M.I. "Detonative combustion in gasless SHS systems - A literature review", *DRDC Suffield Contractor Report* (2008)

[13] Graham, R.A., Morosin, B., Dodson, B.W. "The Chemistry of Shock Compression: A Bibliography", *Sandia Report, Sandia National Laboratories Sandia National Laboratories* (1983)

[14] Graham, RA, Morosin, B, Venturini, EL, Beauchamp, EK, Hammetter, WF. "Shock-Induced Modification of Inorganic Powders", *Emergent Process Methods for High Technology Ceramics, 17, pp. 719-733* (1984)

[15] Graham, R.A. "Shock Compression Chemistry in Materials Synthesis and Processing", *National Academy Press 1984 National Materials Advisory Board National Research Council* (1985)

[16] Graham, RA, Morosin, B, Horie, Y, Venturini, EL, Boslough, MB, Carr, MJ, Williamson, DL. "Chemical Synthesis Under High Pressure Shock Loading", *Shock Waves in Condensed Matter, pp. 693-711* (1985)

[17] Graham, R.A. "Shock compression of solids as a physical-chemical-mechanical proces", *in Shock Compression of Condensed Matter -1987, S.C. Schmidt and N.C. Holmes eds., North Holland, 11* (1988)

[18] Thadhani, NN. "Shock Induced Chemical Reactions and Synthesis of Materials", *Progress in Materials Science, 37pp. 117-226* (1993)

[19] Eakins, D, Thadhani, NN. "Discrete particle simulation of shock wave propagation in a binary Ni+Al powder mixture", *Journal of Applied Physics, 101(5), pp. 043508-1-043508-11* (2007)

[20] Jiang, J, Goroshin, S, Lee, JHS. "Shock Wave Induced Chemical Reaction in Mn+S Mixture", *Shock Compression of Condensed Matter - 1997, pp. 655-658* (1998)

[21] Gur'ev, DL, Gordopolov, YA, Batsanov, SS, Fortov, VE. "Solid-State Detonation in the Zinc-Sulfur System", *Appl.Phys.Lett., 88, pp. 1-9* (2006)

[22] Gur'ev, DL, Gordopolov, Y, Batsanov, SS. "Solid-State Synthesis of ZnTe in Shock Waves", *Combustion, Explosion, and Shock Waves, 42(1), pp. 116-123* (2006)

[23] Suceska, M. "Working Capacity of Explosives", *in "Test Methods for Explosives", Springer Verlag New York Inc, Chapter 5, pp. 203-206* (1995)

[24] Shiryaev, A.A. "Thermodynamic of SHS: modern approach", *Int. J. of SHS, 4(4), pp. 351-362* (downloaded 16 October 2010)

[25] Shiryaev, A.A. "Program for Thermodynamics Equilibrium Calculations THERMO", *www.shiranat.chat.ru* (downloaded 16 October 2010)

[26] www.outotec.com/hsc "Chemical Reaction and Equilibrium Software HSC Chemistry - thermochemical software", *Outotec research Oy, Information Center, P.O. Box 69 (Kupartie 10, 28330 Pori), Fin - 28101 Pori, Finland* (downloaded 16 October 2010)

[27] Fried, L.E., Howard, W.M., Souers, P.C., Vitello, P.A. "Cheetah 3.0 User's Manual", *LLNL Report, Energetic Materials Center, Lawrence Livermore National Laboratory* (2001)

[28] Bennett, LS, Horie, Y. "Shock Induced inorganic reactions and condensed phase detonations", *Shock Waves, 4, pp. 127-136* (1994)

[29] McBride, B.J., Gordon, S. "Computer Program for Calculation of Complex Chemical Equilibrium Compositions and Applications: II Users Manual and Program Description", *NASA RP-1311, NASA Reference Publication National Aeronautics and Space Administration Lewis Research Center* (1996)

[30] Saunders, N, Guo, Z, Li, X, Miodownik, AP, Schill, J-P. "Using JMatPro to Model Materials Properties and Behavior", *JOM, pp. 60-65* (2003)

[31] Thibault, P.A. "Detonation and performance modelling", *Presented at the 2nd Workshop on Gasless Detonation, Montreal, QC, Canada* (2009, 15 May)

[32] Thibault, P.A. "A Review of Equation of State Models, Chemical Equilibrium Calculations and CERV Code Requirements for SHS Detonation Modelling", *Time Scales Scientific Ltd. report, DRDC Suffield CR* (2009)

[33] Gheribi, A., Pelton A., Thibault, P.A., Lee, J.J. "Thermodynamics approach to identify the condition on the gasless detonation", *Paper in preparation for submission to Phys. Rev.* (2010)

[34] Merzhanov, AG, Gordopolov, Y, Trofimov, VS. "On the Possibility of Gasless Detonation in Condensed Systems", *Shock Waves, 5pp. 157-159* (1996)

[35] Gordopolov, Yu.A., Trofimov, V.S., Merzhanov, A.G. "The possibility of gasless detonation in condensed systems", *Physics - Doklady, 40(3), pp. 115-117* (1995)

[36] Jetté, FX, Goroshin, S, Higgins, AJ, Lee, JJ. "Experimental investigation of gasless detonation in metal-sulfur compositions", *Combustion, Explosion, and Shock Waves, 45(2), pp. 211-217* (2009)

[37] Merzhanov, A.G. and Rogachev, A.S. and Mukasyan, A.S. and Khusid, B.M. "Macrokinetics of Structural Transformation During the Gasless Combustion of a Titanium and Carbon Powder Mixture *Combustion, Explosion, and Shock Waves, 26(1), pp. 92-102*, (1990).

[38] Boslough, M.B. "A Thermochemical Model for Shock-Induced Reactions (heat detonations) *J.Chem.Phys., 92(3), pp. 1839-1848*, (1990).

[39] Lee, JJ, Zhang, F. "Shock-induced reactions in cylindrical charges of titanium-silicon powder mixtures", *Shock Compression of Condensed Matter - 2007, Part 2pp. 1045-1048* (2007)

[40] Lee, JJ, Zhang, F. "Initiation of reactive waves in metallic powder mixtures using a high-explosive booster", *Shock Compression of Condensed Matter - 2009, Part 2, pp. 890-900* (2009)

[41] Batsanov, S.S., Gordopolov, Yu.A. "Solid-state detonation velocity limits", *Combustion, Explosion, and Shock Waves, 43(5), pp. 587-589* (2007)

[42] Bolkhovitinov, L.G., Batsanov, S.S. "Theory of solid-state detonation", *Combustion, Explosion, and Shock Waves, 43(2), pp. 219221* (2007)

[43] Batsanov, SS. "An additive method for calculation of the sound velocity in porous metals", *Inorganic Materials, 43(10), pp. 1070-1072* (2007)

[44] Dolgoborodov, A.Yu., Makhov, M.N., Kolbanev, I. V., Streletskii, I.N., Fortov, V. E. "Detonation in an aluminum–Teflon mixture", *JETP Lett., 81, No. 7, 311 314* (2005)

[45] Mock (Jr.), W., Holt, W.H. "Impact initiation of rods of pressed polytetrafluoroethylene (PTFE) and aluminum powders", *Proc. of the APS Shock Compression of Condensed Matter, pp. 10971100* (2005)

[46] Lee, JHS, Goroshin, S, Yoshinaka, A, Romano, M, Jiang, J, Hooten, I, Zhang, F. "Attempts to initiate detonations in metal-sulphur mixtures", *Shock Compression of Condensed Matter -1999, 2, pp. 775-778* (2000)

[47] Jetté, FX, Goroshin, S, Higgins, AJ. "Shock Reactivity of Non-Porous Mixtures of Manganese and Sulfur", *Shock Compression of Condensed Matter, pp. 1033-1036* (2007)

[48] Oelze, ML, O'Brien, J,W.D., Darmody, RG. "Measurement of Attenuation and Speed of Sound in Soils", *Soil Sci.Soc.Am.J., 66pp. 788-796* (2002)

[49] Batsanov, SS. "Effects of Explosions on Materials - Modification and Synthesis Under High-Pressure Shock Compaction", *Springer-Verlag, New York* (1994)

[50] Jetté, FX, Goroshin, S, Higgins, AJ. "Time-Resolved Temperature Measurements of Shock Initiation in a Manganese-Sulfur Mixture", *Shock Compression of Condensed Matter, 955 pp. 1037-1040* (2007)

[51] Jetté, FX, Goroshin, S, Higgins, AJ, Frost, DL, Lee, JJ. "Time-Resolved Temperature Measurements of Shock Initiation in Heterogeneous Exothermic Mixtures", *16th APS - Shock Compression of Condensed Matter, Topical Group Meeting, pp.* (2009)

[52] Thadhani, NN, Graham, RA, Royal, T, Dunbar, E, Anderson, MU, Holman, GT. "Shock-induced chemical reactions in titanium-silicon powder mixtures of different morphologies: Time-resolved pressure measurements and materials analysis", *J.Appl.Phys., 82(3), pp. 1113-1128* (1997)

[53] Eakins, DE, Thadhani, NN. "Shock compression of reactive powder mixtures", *International Materials Reviews, 54(4), pp. 181-213* (2009)

[54] Trott, WM, Knudson, MD, Chhabildas, LC, Asay, JR. "Measurements of spatially resolved velocity variations in shock compressed heterogeneous materials using a line-imaging velocity interferometer", *Shock Compression of Condensed Matter -1999, pp. 993* (2000)

[55] Jetté, F.-X., Higgins, A.J., Goroshin, S., Frost, D.L., Charron-Tousignant, Y., Radulescu, M.I., Lee, J.J. "In-situ measurements of the onset of bulk exothermicity in shock initiation of reactive powder mixtures", *Journal of Applied Physics, 109, pp. 084905* (2011)

[56] Song, I, Thadhani, NN. "Effects of Shock Processing Parameters on Synthesis of Nickel Aluminides", *Shock Compression of Condensed Matter - 1989, pp. 499-502* (1990)

[57] Dunbar, E., Thadhani, N.N., Graham, R.A. *Journal of Materials Science 28, p. 2903* (1993)

[58] Vreeland, J, Montilla, KL, Mutz, AH. "Shock wave initiation of the Ti5Si3 reaction in elemental powders", *J.Appl.Phys., 82(6), pp. 2840-2844* (1997)

[59] Frost, D.L., Jetté, F.-X., Goroshin, S., Higgins, A.J., Lee, J.J. "Effect of Particle Morphology on Critical Conditions for Shock-Initiated Reactions in Titanium-Silicon Powder Mixtures", *16th APS - Shock Compression of Condensed Matter, Topical Group Meeting, pp.* (2009)

[60] Das, K., and Bandyopadhyay, A., Gupta, Y.G., *AIP Conference Proceedings, p. 1094* (2004)

[61] Bandyopadhyay, A., Das, K., Gupta, Y.G. *AIP Conference Proceedings, p. 1026* (2004)

[62] Hardt, A.P. "Shock Initiation of Thermite", *Proceedings of the 13th International Pyrotechnics Seminar, p. 425* (1988)

[63] Krueger, BR, Vreeland, J. "A Hugoniot theory for solid and powder mixtures", *J. Appl. Phys., 69(2), pp. 710-716* (1991)

[64] Lee, I., Finnegan, S.A. *Journal of Thermal Analysis 50, p. 707* (1997)

[65] Yu, L.H., Meyers, M.A. "New Evidence Concerning The Shock-Induced Chemical Reaction Mechanism in a Ni/Al Mixture", *Journal of Materials Science 26, p. 601* (1991)

[66] Hardt, A.P., McHugh, S.L., Weinland, S.L. "Shock Initiation of Thermite", *Proceedings of the 11th International Pyrotechnics Seminar, p. 255* (1986)

[67] Horie, Y., Graham, R.A., Simonsen, I.K. "Shock Compaction of Ceramic Powders in Reactive Mixtures", *Materials Letters 3, p. 354* (1985)

[68] Simonsen, I.K., Horie, Y., Graham, R.A., Carr, M. "Shock Wave Effects in the Ti-C SHS System", *Materials Letters 5, p. 75* (1987)

[69] Bennett, LS, Sorrell, FY, Simonsen, IK, Horie, Y, Iyer, KR. "Ultrafast chemical reactions between nickel and aluminum powders during shock loading", *Appl.Phys.Lett., 61(5), pp. 520-521* (1992)

[70] Yang, Y, Gould, RD, Horie, Y, Iyer, KR. "New Evidence Concerning The Shock-Induced Chemical Reaction Mechanism in a Ni/Al Mixture", *10th Biennial Intl.Conf.of the APS Topcial Group on Shock Compression of Condensed Matter, pp. 1-4* (1997)

[71] Sheffield, S.A., Schwarz, A.C. "Shock Waves in Dense Hard Disk Fluids", *Proc. 8th International Pyrotechnics Seminar, p. 972* (1982)

[72] Walley, SM, Balzer, JE, Proud, W.G., Field, JE. "Response of thermites to dynamic high pressure and shear", *Proceedings R.Society Lond.A., 456pp. 1483-1503* (2000)

[73] Holman, G.T., Graham, RA, Anderson, M.U. *AIP Conference Proceedings, p. 1119* (1994)

[74] Vandersall, K.S., Thadhani, N.N. "Shock-Induced Ultrafast SHS Reactions", *J. Appl. Phys. 94, p. 1575* (2003)

[75] Eakins, D, Thadhani, NN. *J. Appl. Phys. 100, 113521-1* (2006)

[76] Xu, X, Thadhani, NN. "Investigation of shock-induced reaction behavior of as-blended and ball-milled Ni+Ti powder mixtures using time-resolved stress measurements", *Journal of Applied Physics, 96(4), pp. 2000-2009* (2004)

[77] Batsanov, S.S., Doronin, G.S., Klochkov, S.V., Teut, A.I. *Combustion Explosion, Shock Waves 22, p. 765* (1986)

[78] Dolgoborodov, A.Yu., Streletskii, A.N., Makhov, M.N., Kolbanev, I.V., Fortov, V.E. "Explosive Compositions Based on the Mechanoactivated Metal-Oxidizer Mixtures", *Russian Journal of Physical Chemistry, 1(6), pp. 606-611* (2007)

[79] Dolgoborodov, A.Yu., Streletskii, AN, Kolbanev, I.V., Makhov, M.N. *14th International Symposium on Detonation, in press* (2010)

[80] Bockmon, B.S., Pantoya, M.L., Son, S.F., Asay, B.W. *41st Aerospace Sciences Meeting and Exhibit of the AIAA* (2003)

[81] Matytsin, A.I., Popov, S.T. *Fiz. Gor. I Vzryva 23, p. 126* (1986)

[82] Horning, H.C., Kury, J.W., Simpson, R.L., Helm, F.H., Von Holle, W.G. *Proc. of the 11th International Pyrotechnics Seminar, p. 699* (1986)

[83] Boslough, M.B., Graham, R.A. *Chemical Physics Letters 121, p. 446* (1985)

[84] Boslough, M.B. *Int. J. Impact Engng, 5, p. 173* (1987)

[85] Gryadunov, AN, Shteinberg, AS, Dobler, EA. "Initiation of a Chemical Reaction in a Titanium-Carbon Powder Mixture by High-Velocity Impact", *Proceedings of the Russian Academy of Sciences, 321(5), pp. 855-858* (1992)

[86] Batsanov, SS, Gogulya, MF, Brazhnikov, MA, Simakov, GV, Maksimov, II. "Behavior of the Reacting System Sn + S IN Shock Waves", *Combustion, Explosion, and Shock Waves, 30(3), pp. 361-365* (1994)

[87] Reeves, R.V., White, J.D.E., Mukasyan, A.M., Son, S.F. *AIP Conference Proceedings, p. 466* (2009)

[88] Reeves, R.V., White, J.D.E., Mukasyan, A.M., Son, S.F. *Private Communication* (2010).

[89] Batsanov, S.S., Shestakova, N.A., Stupnikov, V.P., Litvak, G.S., Nigmatullina, V.M. *Doklady Akademii Nauk SSSR, 185, p.174* (1969)

[90] Batsanov, S.S., Gurev, D.G. *Combustion Explosion, Shock Waves 23, p. 236* (1986)

[91] Nabatov, S.S., Shubitidze, S.O., Yakushev, V.V. *Combustion, Explosion, and Shock Waves, 26, p. 732* (1991)

[92] Petel, E. E., Jetté, F.-X. "Comparison of methods for calculating the shock hugoniot of mixtures", *Shock Waves, 20, pp.73-83* (2010)

[93] Meyers, M.A. "Dynamic behavior of materials", *John Wiley & Sons, Inc,* (1994)

[94] Walsh, J.M., Christian, R.H. *Phys. Rev. 97, p. 1544* (1955)

[95] Zhao, S., Germann, T.C., Strachan, A. *Journal of Chemical Physics,125, 164717-1* (2006)

[96] Son, S.F., Asay, B.W., Foley, T.J. Yetter, R.A. Wu, M.H., and Risha, G.A. *J. Propul. Power 23, 715* (2007)

[97] Lee, E.L., Tarver, C.M. *Physics of Fluids 23, p. 2362* 1980)

[98] Zaug, J.M., Young, C. E., Long, G.T., Maienschein, J.L., Glascoe, E.A., Hansen, D.W., Wardell, J.E., Black, C.K., Sykora, G.B. *AIP Conference Proceedings, p. 420* (2009)

[99] Gordopolov, Yu.A., Batsanov, S.S. Trofimov, V.S. "chapter in: Shock Wave Science and Technology Ref. Library: Heterogenous Detonations', *ed. F. Zhang* (2009)

[100] Das, K., Gupta, Y.G., and Bandyopadhyay, A. *Mat. Sci. & Eng. A, 426, p. 147* (2006)

[101] Goroshin, S, Mizera, A, Frost, DL, Lee, JHS. "Metal-Sulfur Combustion", *Twenty-Sixth Symposium (Int'l) on Combustion/The Combustion Institute, pp. 1883-11889* (1996)

[102] Bacciochini, A, Radulescu, MI, Charron-Tousignant, Y, Van Dyke, J, Nganbe, M, Yandouzi, M, Lee, JJ, and Jodoin, B "Enhanced reactivity of mechanically-activated nano-scale gasless reactive materials consolidated by coldspray *Surface and Coatings Technology, 206, pp. 4343-4348*, (2012).

[103] Merzhanov, A.G., Borovoinskaya, I.P. "Self-propagating high-temperature synthesis of refractory inorganic componds", *Doklady Akademii Nauk SSSR, 204(2), pp.366-369* (1972)

[104] Frankhouser, W.L., Brendley, K.W., Kieszek, M.C., Sullivan, S.T. "Gasless Combustion Synthesis of Refractory Compounds", *Collection of Papers from McGill on: SHS and Shock Induced Solid Phase Reactions, Noyes Publications,* (1983)

[105] Munir, Z.A., Anseimi-Tamburini, U. "The Synthesis of High-Temperature Materials by Combustion", *Materials Science Reports Collection of Papers from McGill on: SHS and Shock Induced Solid Phase Reactions,* (1989)

[106] Merzhanov, AG, Mukas'yan, AS, Rogachev, AS, Sychev, AE, Hwang, S, Varma, A. "Combustion-Front Microstructure in Heterogeneous Gasless Media (Using as an example The 5Ti + 3Si System)", *Combustion, Explosion, and Shock Waves, 32(6), pp. 655-666* (1997)

[107] Varma, A., Lebrat, J.-P. "Combustion synthesis of advanced materials", *Chemical Engineering Science 47(9-11), pp. 2179-2194*

[108] Merzhanov, A.G., Khajkin, B.I. "Theory of combustion waves in homogeneous media", *Progress in Energy and Combustion Science 14, pp. 1-98* (1988)

[109] Margolis, S. B. "The transition to nonsteady deflagration in gasless combustion", *Progress in Energy and Combustion Science 17, pp. 135-162* (1991)

[110] Makino, A. "Fundamental aspects of the heterogeneous flame in the self-propagating high-temperature synthesis (SHS) process", *Progress in Energy and Combustion Science, 27pp. 1-74* (2001)

[111] Law, C.K. "Combustion Physics" *Cambridge* (2006)

[112] Makino, A. "Heterogeneous flame propagation in the self-propagating, high temperature, synthesis (SHS) process in multi-layer foils: theory and experimental comparisons", *Combustion and Flame 134, pp. 273-288* (2003)

[113] Radulescu, M.I., Sharpe, G.J., Law, C.K., Lee, J.H.S. "The hydrodynamic structure of unstable gaseous detonations", *Journal of Fluid Mechanics 580, pp. 31-81* (2007)

[114] Makino, A., Araki, N., Kuwabara, T. "Flammability limits, dilution limits and effect of particle-size on burning velocity in combustion synthesis of TiC", *JSME International Journal Series B-Fluids And Thermal Engineering 37(3), pp. 576-582* (1994)

[115] Suryanarayana, C. "Mechanical alloying and milling", *Progress in Materials Science, 46, pp. 1-184* (2001)

[116] Hellstern, E., Fecht, H.J., Garland, C., Johnson, W.L. "Multicomponent ultrafine microstructures", *McCandlish LE, Polk DE, Siegel RW, Kear BH, editors, vol. 132., Pittsburgh, PA: Mater. Res. Soc, 1989. pp. 137-142* (1989)

[117] Eckert, J., Holzer, J.C., Krill, C.E., Johnson, W.L. "Structural and thermodynamic properties of nanocrystalline fcc metals prepared by mechanical attrition", *Journal of Materials Research 7(7), pp. 1751-1761* (1992)

[118] Takacs, L. "Self-sustaining reactions induced by ball milling", *Progress in Materials Science, 47pp. 355-414* (2002)

[119] Lagerbom, J., Tiainen, T., Lehtonen, M., Lintula, P. "Effect of partial mechanical alloying on the self-propagating high-temperature synthesis of Ni3Si", *Journal of Materials Science 34(7), pp.1477-1482* (1999)

[120] Anselmi-Tamburini, U, Maglia, F, Spinolo, G, Doppiu, S, Monagheddu, M, Cocco, G. "Self-Propagating Reactions in the Ti-Si System: A SHS-MASHS Comparative Study", *Journal of Materials Synthesis and Processing, 8(5/6), pp. 377-383* (2000)

[121] Vyushkova, B.V., Levashov, E.A., Ermilov, A.G., Pityulin, A.N., Borovinskaya, I.P., Egorychev, K.N. "Characteristics of the effect of preliminary mechanical activation of a batch on parameters of the self-propagating high-temperature synthesis process, structure, and properties of multicomponent cermet shtm-5", *Combustion Explosion and Shock Waves 30(5), pp. 630-634* (1994)

[122] Smolyakov, V.K. "Combustion of mechanically activated heterogeneous systems", *Combustion, Explosion, and Shock Waves, 41(3), pp. 319-325* (2005)

[123] Sirmas, N., Tudorache, M., Barahona, J., Radulescu, M. I. "Shock Waves in Dense Hard Disk Fluids", *in review for Shock Waves* (2010)

[124] Krueger, BR, Mutz, AH, Vreeland, J. "Shock-Induced and Self-Propagating High-Temperature Synthesis Reactions in Two Powder Mixtures: 5:3 Atomic Ratio Ti/Si and 1:1 Atomic Ratio Ni/Si", *Metallurgical Transactions A, 23App. 55-58* (1992)

[125] Merzhanov, AG. "Fluid Dynamics Phenomena in the Processes of Self-Propagating High-Temperature Synthesis", *Combust.Sci.and Tech. Collection of Papers from McGill on: SHS and Shock Induced Solid Phase Reactions, 105pp. 295-325* (1995)

This page intentionally left blank.

DOCUMENT CONTROL DATA

(Security classification of title, body of abstract and indexing annotation must be entered when document is classified)

1. ORIGINATOR (The name and address of the organization preparing the document. Organizations for whom the document was prepared, e.g. Centre sponsoring a contractor's report, or tasking agency, are entered in section 8.)

   Defence R&D Canada – Suffield
   Box 4000, Station Main, Medicine Hat, Alberta,
   Canada T1A 8K6

2. SECURITY CLASSIFICATION (Overall security classification of the document including special warning terms if applicable.)

   UNCLASSIFIED
   (NON-CONTROLLED GOODS)
   DMC A
   REVIEW: GCEC June 2010

3. TITLE (The complete document title as indicated on the title page. Its classification should be indicated by the appropriate abbreviation (S, C or U) in parentheses after the title.)

   Investigation of Gasless Detonation

4. AUTHORS (Last name, followed by initials – ranks, titles, etc. not to be used.)

   Lee, J.J.

5. DATE OF PUBLICATION (Month and year of publication of document.)	6a. NO. OF PAGES (Total containing information. Include Annexes, Appendices, etc.)	6b. NO. OF REFS (Total cited in document.)
December 2012	136	125

7. DESCRIPTIVE NOTES (The category of the document, e.g. technical report, technical note or memorandum. If appropriate, enter the type of report, e.g. interim, progress, summary, annual or final. Give the inclusive dates when a specific reporting period is covered.)

   Technical Report

8. SPONSORING ACTIVITY (The name of the department project office or laboratory sponsoring the research and development – include address.)

   Defence R&D Canada – Suffield
   Box 4000, Station Main, Medicine Hat, Alberta, Canada T1A 8K6

9a. PROJECT NO. (The applicable research and development project number under which the document was written. Please specify whether project or grant.)	9b. GRANT OR CONTRACT NO. (If appropriate, the applicable number under which the document was written.)

10a. ORIGINATOR'S DOCUMENT NUMBER (The official document number by which the document is identified by the originating activity. This number must be unique to this document.)	10b. OTHER DOCUMENT NO(s). (Any other numbers which may be assigned this document either by the originator or by the sponsor.)
DRDC Suffield TR 2012-142	

11. DOCUMENT AVAILABILITY (Any limitations on further dissemination of the document, other than those imposed by security classification.)

   (X) Unlimited distribution
   ( ) Defence departments and defence contractors; further distribution only as approved
   ( ) Defence departments and Canadian defence contractors; further distribution only as approved
   ( ) Government departments and agencies; further distribution only as approved
   ( ) Defence departments; further distribution only as approved
   ( ) Other (please specify):

12. DOCUMENT ANNOUNCEMENT (Any limitation to the bibliographic announcement of this document. This will normally correspond to the Document Availability (11). However, where further distribution (beyond the audience specified in (11)) is possible, a wider announcement audience may be selected.)

   Unlimited

13. ABSTRACT

This report describes the body of work produced in the Technology Investment Fund (TIF) project titled “Gasless Detonation - A Novel System For Energy Release And Terminal Effects”. The main objectives of the project were to establish the properties and explosive performance of a new mode of energy release known as gasless detonation. Theoretical and experimental studies were performed on gasless reactive mixtures to investigate shock-initiated reactions in these systems. Ultimately, gasless detonation was not achieved in this project, however several practical and scientific results were produced as a result of the increased understanding of gasless reactive systems. On the theoretical side, a rigor-ous assessment of the conditions for gasless detonation and an estimation of its explosive performance was performed. This assessment included the new use of Calculation of Phase Diagrams (CALPHAD) techniques for performing thermo-chemical calculations of detona-tion properties in low-gas reactive mixtures. On the experimental side, there were many outcomes. The Russian claims of gasless detonation were disproved through attempts to duplicate their experiments. The limits of shock-initiated combustion were found for many gasless reactive systems, as well as their dependence on mixture reactivity and morphology. Mechanisms of reactive wave propagation were elucidated, and a dual propagation mode was observed where a small portion of the mixture reacts rapidly within microseconds, fol-lowed by a slower bulk reaction where the remaining majority of the energy is released. A back-up hypothesis to achieve gasless detonation was also investigated. This effort involved developing methods to synthesize very dense gasless reactive mixtures by combining the Arrested-Milling (ARM) technique with Cold-Gas Dynamic Spray (CGDS) deposition. A new reactive nano-composite material mixed down to a nano-scale level was achieved with nearly 100% Theoretical Maximum Density. This synthesis method was developed for a number of reactive mixtures, and accelerated flame speeds were observed for the new ma-terials. This approach yielded promising results and constitutes a future research direction in the advanced energetics program.

Le présent rapport décrit le travail effectué dans le cadre du projet du Fonds d’investissement technologique (FIT) intitulé « Gasless Detonation - A Novel System For Energy Release And Terminal Effects ». Les principaux objectifs de ce projet étaient d’établir les propriétés et le rendement explosif d’un nouveau mode de libération d’énergie appelé « détonation sans dégagement de gaz ». Des études théoriques et expérimentales ont été effectuées sur des mélanges réactifs sans gaz, afin d’étudier les réactions produites par des chocs dans ces systèmes. Finalement, aucune détonation sans dégagement de gaz n’a été produite dans le cadre du projet, mais un certain nombre de résultats pratiques et scientifiques ont été obtenus grâce à la compréhension accrue des systèmes réactifs sans gaz. Sur le plan théorique, une évaluation rigoureuse des conditions pour une détonation sans dégagement de gaz et une estimation de son rendement explosif a été effectuée. Cette évaluation comprenait la nouvelle utilisation de techniques de calcul de diagrammes de phase (CALPHAD) pour effectuer des calculs thermochimiques des propriétés de détonation dans des mélanges réactifs à faible taux de gaz. Sur le plan expérimental, il y a eu un de nombreux résultats. Les allégations russes de réussite de détonations sans dégagement de gaz ont été réfutées au moyen de tentatives de reproduction des expériences russes. Les limites de combustion produite par des chocs ont été découvertes pour un certain nombre de systèmes réactifs sans gaz, ainsi que leur dépendance à la réactivité et à la morphologie du mélange. Des mécanismes de propagation d’ondes réactives ont été élucidés, et un mode de double propagation a été observé. Dans ce mode, une petite partie du mélange réagit rapidement en quelques microsecondes, ce qui est suivi par une réaction en masse plus lente où la majorité restante de l’énergie est libérée. Une autre hypothèse a également été étudiée relativement à l’obtention d’une détonation sans dégagement de gaz. Cet effort comprenait la mise au point de méthodes visant à synthétiser des mélanges réactifs sans gaz très denses en combinant le procédé ARM (de l’anglais « Arrested-Milling ») avec un dépôt par pulvérisation dynamique à froid en phase gazeuse (CGDS). Une nouvelle matière nanocomposite réactive mélangée jusqu’à une échelle nanométrique a été obtenue avec une densité théorique maximale de près de 100 %. Cette méthode de synthèse a été mise au point pour un certain nombre de mélanges réactifs, et des vitesses de flamme accélérées ont été observées pour les nouvelles matières. Cette approche a produit des résultats prometteurs et constitue une orientation future des recherches dans le cadre du programme de matières énergétiques avancées.

14.

KEYWORDS, DESCRIPTORS or IDENTIFIERS

Gasless Detonation; ntermetallic; Thermite; Nano-thermite

Defence R&D Canada

Canada's Leader in Defence
and National Security
Science and Technology

R & D pour la défense Canada

Chef de file au Canada en matière
de science et de technologie pour
la défense et la sécurité nationale

www.drdc-rddc.gc.ca